MOFs for Mercury Detection

Subjects: Materials Science, Composites | Chemistry, Analytical

Contributor: Muthaiah Shellaiah

The advantages of metal organic frameworks (MOFs) are: existence of porosity to adsorb specific analyte, improved aqueous solubility, exceptional photophysical and chemical properties. MOFs are noted as exceptional candidates towards the detection and removal of specific analytes, particular for the detection/removal of environmental contaminants, such as heavy metal ions, toxic anions, hazardous gases, explosives, etc. Among heavy metal ions, mercury has been noted as a global hazard because of its high toxicity in the elemental (Hg0), divalent cationic (Hg2+), and methyl mercury (CH3Hg+) forms. To secure the environment and living organisms, many countries have imposed stringent regulations to monitor mercury at all costs. Regarding the detection/removal requirements of mercury, researchers have proposed and reported all kinds of MOFs-based luminescent/non-luminescent probes towards mercury.This review provides valuable information about the MOFs which have been engaged in detection and removal of elemental mercury and Hg2+ ions. Moreover, the involved mechanisms or adsorption isotherms related to sensors or removal studies are clarified for the readers. Finally, advantages and limitations of MOFs in mercury detection/removal are described together with future scopes.

Hg2+ CH3Hg+ elemental mercury MOFs luminescent detection adsorption isotherms real analysis non-luminescent probes organic linkers metal nodes

1. Introduction

Due to the harmful and hazardous effects on ecosystem, detection/removal of mercury in different states, such as elemental, ionic, and organometallic (like methyl mercury), is in high demand and has attracted intense research interest [1][2][3][4][5]. Accumulated mercury in environmental water often sedimented and converted as toxic methylmercury, which entered the food cycle and caused serious diseases in living beings as stated next [6]. Accumulation of mercury in human body may lead to various health issues, such as brain damage, central nervous syndromes, Minamata disease, cognitive and motion disorders, etc. [7][8][9] Therefore, U.S. Environmental Protection Agency (EPA) regulated an allowable maximum level of mercury of 2 ppb (10 nM) in the drinking water and 3 ppm (1.5 μM) in fish tissue [10][11]. Moreover, Agency for Toxic Substances and Disease Registry (ATSDR) of the U. S. Department of Health and Human Service has set a highest allowable mercury concentration of 625 ppb in normal soil [1][2][3][4][5][6][7][8][9][10][11][12][13]. Till now the development of innovative tactics towards detection and removal of mercury are still the main focus of many research groups [12][13]. In this light, luminescent approaches comprising of nanoprobes, small molecules, supramolecular assemblies, aggregation induced emission, and covalent or metal organic frameworks (COFs/MOFs) are seemingly impressive with respect to their applicability, such as in vitro/vivo imaging studies [14][15][16][17][18][19]. However, design and development of metal organic frameworks (MOFs)-based probes towards specific analytes discrimination are highly anticipated with real time applications [20][21][22][23][24] due to the following advantages: existence of porosity to adsorb specific analyte, improved aqueous solubility, exceptional photophysical and chemical properties.

In fact, the majority of the MOFs are composed of organic ligand and metal nodes with certain porosity and tend to form different micro/nano-structures, such as particles, cubes, rods, spheres, etc. [25][26][27][28][29] Moreover, they also find their applications in multiple opto-electronics, photovoltaics, electronics, solar cells, light emitting devices (LEDs), field effect transistors (FETs), DNA detection, bio-analysis, real time detection/removal of specific analytes, etc. [30][31][32][33] In sensory studies, they can behave as single, dual, and non-emissive materials, which tend to provide diverse responses upon interaction with guest analytes [34]. Moreover, the MOFs may display luminescent responses when interact with guest analytes via one-dimension (1D) (wavelength change and intensity alteration) or two-dimension (2D) (ratiometric variation combined with 1D responses) signals [21][35]. However, by tuning the functional organic units mediated responses, MOFs can be utilized in numerous sensory applications, such as pH sensors, virus and antibiotic detection, metal ions recognition, anions detection, volatile explosives quantification, etc. [36][37][38][39][40][41] Similarly, by modulating the functional units in MOFs, capture and removal of specific analytes can be achieved and become an effective approach for toxic analyte removal [42][43][44][45][46]. In this track, studies on detection and removal of highly toxic mercury and its analogous can find inspiring and exceptional applicability towards the environmental and health safety [47].

So far, diverse MOFs have been demonstrated for exceptional detection and removal elemental mercury and Hg^{2+} [48][49][50][51]. In fact, detection of Hg^{2+} can be attained by assorted mechanisms, such as bands overlapping, ligand interaction, cation exchange, and framework collapse, etc. [20][33] On the contrary, removal of elemental mercury and Hg^{2+} ions are mostly achieved by tuning structural functionalities with organic ligands [52]. In addition, metal-organic coordination polymers and MOFs composited materials were demonstrated for mercury determination and removal [53][54]. So far, reviews on MOFs-based mercury detection and removal are deficient in valuable information, which encourages us to deliver a compact review to summarize the recent studies on this subject.

In this review, we described the sensory detection and removal utilities of simple and polymeric MOFs and composited MOFs towards elemental mercury and Hg^{2+} as noted in **Figure 1**. Moreover, mechanism, electron transport, and structural benefits for mercury quantification were outlined for reader′s clarifications. Finally, a brief note on the synthesis of MOFs involved in discrimination and removal of mercury and its analogous was provided in this paper.

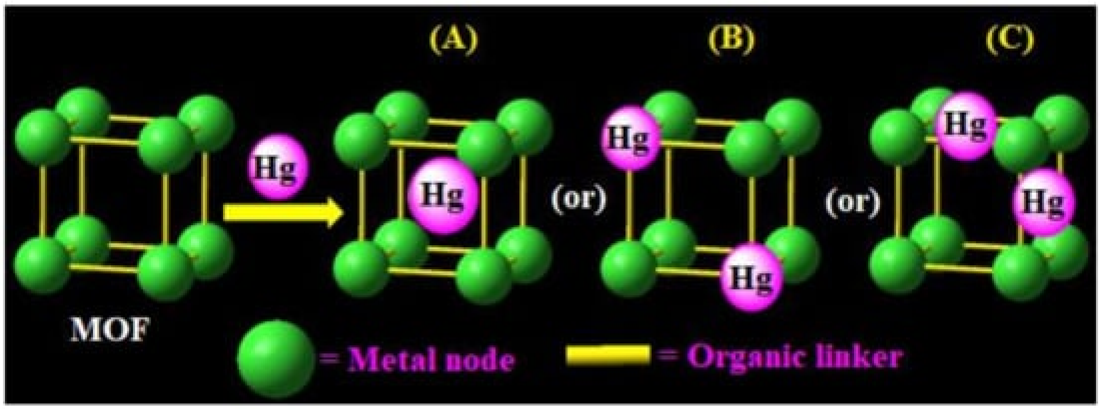

Figure 1. Schematic illustration of three possible MOFs-based mercury detection and removal mechanisms by (**A**) cavity trapping, (**B**) metal node displacement, and (**C**) interactive organic linkers.

2. Optimization Requirements for MOFs-Based Mercury Detection/Removal

To detect/remove mercury and it′s analogous by using MOFs, following optimization requirements must be taken into account.

A. Selection of suitable organic linkers that can form MOFs with designated metal nodes with greater surface area to interact with mercury analogous in the environment. Similarly, organic linkers with side chains, such as thiol (-SH; which shows the greater affinity to Hg^{2+}, Hg^0 and CH_3Hg^+), can be chosen for effective removal and detection mercury [55].

B. Selection of suitable metal nodes that can form MOFs with good stability in aqua/non-aqua solvents and afford large surface area for analyte (Hg^{2+}) adsorption or collision for improving signal detection or quantification [56].

C. Selection of appropriate synthetic tactics/conditions to afford high yield over impurities. Similarly, the selection of suitable solvent for sensory studies also needs attention [18].

D. Many MOFs are well known coordinating polymers with porous nano/micro-structures [27], the design for capturing mercury requires more attention with respect to linkers, nodes, adsorbing ability, and opto-electronic properties.

E. In the case of removal of mercury from environmental samples, design and development of MOFs with high adsorption efficiency and stability in aqua medium need more attention and optimization for improvement [57].

F. To avoid the interfering effect from competing species, a unique MOF design with selectivity only to the mercury analogous must require optimization either by modulation of organic linkers or metal nodes or by tuning the opto-electronic properties [58].

G. Post-modification of MOFs with certain materials to form composited structures towards mercury detection/removal also requires optimization for authorized applicability [59].

3. Synthetic Tactics Involved in MOFs Construction

By bridging the organic linkers with metal nodes, MOFs can be synthesized by many tactics as presented below [60].

(1) Diffusion method: This is a tactic that involves gradual conveyance of various species into interaction and can be sub-divided into (i) solvent liquid diffusion method, which takes place between precipitant solvent and product in the solvent and leads to crystallization at interface via gradual diffusion; (ii) gradual diffusion of reactants by adjusting the physical barriers, such as placing two reactant vials with different sizes to form MOFs [60][61].

(2) Hydro/solvothermal method: This technique involves self-assembly of products from soluble precursors. Wherein, precursors are introduced into the sealed tube under certain pressure and kept at 80–260 °C for days or weeks to produce the designated MOFs [60][62].

(3) Microwave method: In this tactic, solution containing small metal oxide particles is treated with microwave to raise temperature so that nano-sized metal crystals can be generated and leads to MOFs formation with controlled shape and size [63]. Contrary to other synthetic methods, microwave technology is a promising tactic with reduced reaction time and less processing energy consumption to have control over MOF properties. It is able to easily produce MOFs and MOF-hybrids in an isolated manner [64]. For example, Le et al. developed the mesoporous MOF-**MIL-100 (Fe)** via microwave-assisted continuous flow synthesis [by reacting iron(III) chloride hexahydrate ($FeCl_3{\cdot}6H_2O$), 1,3,5-benzenetricarboxylic acid (H_3BTC)] to support the construction of Cu(I) modified adsorbents towards CO/CO_2 separation [65].

(4) Electrochemical method: This tactic is generally used in the industry to produce MOFs in bulk. Contrary to solvothermal synthesis, this method has the advantage of quick synthesis at low temperature and also avoids usage of anionic metal salts, such as metallic nitrates [66]. However, fine tuning in applied voltage is required to attain better results towards designed MOFs.

(5) Mechanochemical method: Contrast to traditional way of synthesis (dissolving, heating, and stirring chemicals in a solution), this method is environmentally friendly for synthesizing MOFs via mechanical forces, such as grinding and ball milling at ambient temperature without any solvent consumption. Moreover, certain number of MOFs can be obtained in a short time (10–20 min). This method is also noted as a technique at the interface of mechanical engineering and chemistry [67].

(6) Sonochemistry method: This is a quick synthesis tactic reported for producing MOFs in an environmentally friendly manner via treating the reaction mixture with high energy ultrasound force (10–20 MHz with upper limit of

human hearing). During this process, dissolution of the starting materials can be enhanced, thereby becoming a special research topic for scientists for producing MOFs in bulk [68].

(7) Post-synthetic modifications: Apart from the aforementioned tactics, the designated MOFs can be synthesized via post-synthetic modifications, such as ligand exchange, metal exchange, opening of the coordinating sites, etc [69].

4. MOFs in Optical Detection of Hg^{2+}

Similar to nanomaterials-based sensors [70], MOFs in the form of micro/nano-structures can be used in effective detection of Hg^{2+}. In this light, the zirconium (Zr) metal-incorporated MOFs were reported for luminescent and colorimetric quantification of Hg^{2+} ions [71][72][73][74][75][76][77]. Yang and co-workers developed a porous phorpyrinic luminescent metal–organic framework (LMOF; **PCN-224**) with meso-tetra(4-carboxyphenyl) porphyrin (TCPP) ligands and Zr metal nodes via modified solvothermal method and applied in Hg^{2+} sensors [71]. During detection of Hg^{2+}, the probe displayed a bright red to dark red fluorescent quenching and a purple to light green colorimetric response within 2 min. The sensor response of **PCN-224** was not affected by the presence of any competing ions and was reversible in the presence of KI solution (up to seven cycles) as depicted in **Figure 2**. The **PCN-224** revealed a linear response to Hg^{2+} from 0.1 to 10 micromole (µM) with a detection limit (LOD) of 6 nanomole (nM). Moreover, probe **PCN-224** was also more effective towards the detection of Hg^{2+} in real samples, such as tab and river water.

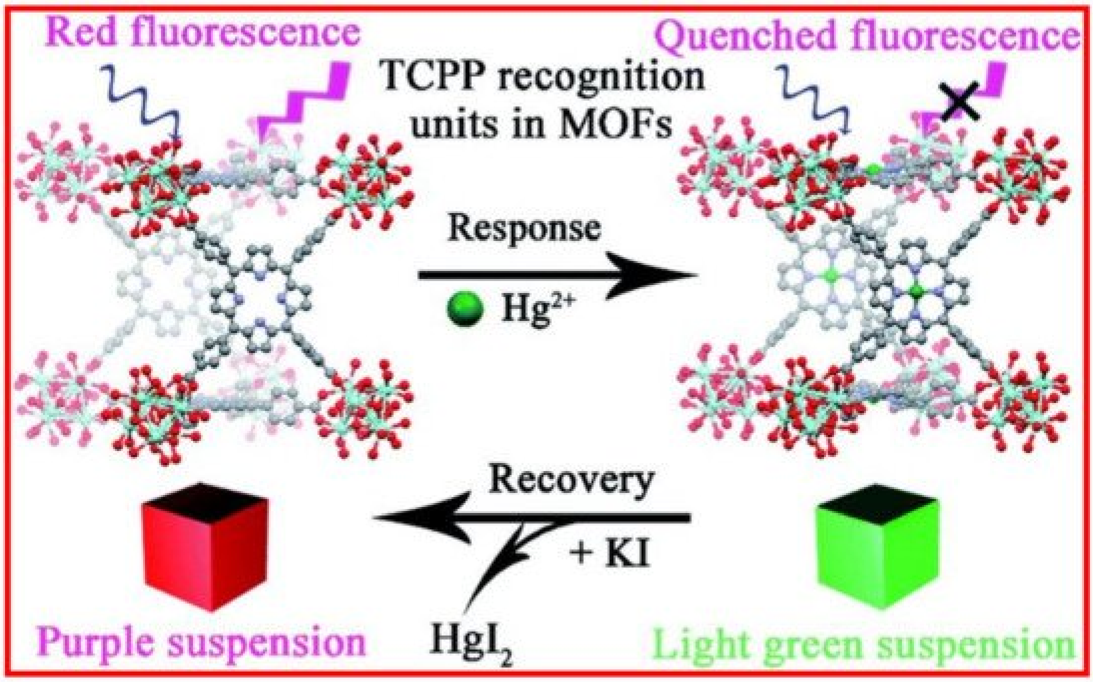

Figure 2. Illustration of the sensor construction protocol. The inherent TCPP linker was designed as the recognition site as well as the signal reporter for Hg^{2+} sensing at the same time. Upon the addition of solution into the **PCN-**

224-Hg^{2+} system, analytes were disassociated and fluorescence of **PCN-224** was recovered while the visual colour also turned from light green to purple (Reproduced with the permission from Ref [71]).

The **UIO-66** (archetypal metal–organic framework (MOF) was reported for effective detection of Hg^{2+}. It contains the metal nodes that comprise a zirconium oxide complex bridged by terepthalic acid (1,4-benzenedicarboxylic acid) ligands). Hg^{2+} detection in aqueous media can be further improved by tuning the structural features of **UIO-66** via modifying the terephthalic acid bridging unit or by post-doping process (PSM) [72][73][74]. Zhang et al. developed the fluorescent MOF (**UIO-66-PSM**) via coupling **UIO-66-N$_3$** with phenylacetylene to use in sensing of Hg^{2+} in aqueous media [72]. Terephthalic acid with azide group was used to synthesize the **UIO-66-N$_3$**, which showed reactivity to phenylacetylene. The Brunauer–Emmett–Teller (BET) surface area of **UIO-66-PSM** was estimated as 606 m^2 g^{-1} to N_2 gas at 77K. In this work, **UIO-66-PSM** displayed great selectivity to Hg^{2+} via fluorescence quenching with a linear behavior from 0 to 78.1 µM and an estimated LOD of 5.88 µM. Moreover, Hg^{2+} detection by the **UIO-66-PSM** was demonstrated in tap and lake water interrogations. However, the adsorption capability of **UIO-66-PSM** to Hg^{2+} in the presence of other ions still needs to be clarified. In a similar fashion, Samanta and co-workers described synthesis of the **UIO-66@Butyne** by reacting $ZrCl_4$ with 2,5-bis(but-3-yn-1-yloxy) terephthalic acid and applied it in quantifying Hg^{2+} in aqueous medium [73]. The **UIO-66@Butyne** displayed a fluorescence quenching response to Hg^{2+} via the reaction-based chemodosimeter mechanism. In which, the triple bonded acetylene unit present over the surface reacted with Hg^{2+} and led to green fluorescence quenching with a LOD of 10.9 nM. It also showed higher selectivity to Hg^{2+} than that of other ions. The BET surface area of **UIO-66@Butyne** was found to be 74 m^2 g^{-1} for Hg^{2+} at 77K. Regarding to structural modification, Xiaoxiong et al. proposed post doping of Eu^{3+} over the surface of **UIO-66** type MOF (**Eu^{3+}@UIO-66 (DPA)**) (synthesized by reacting $ZrCl_4$ and isophthalic acid with 2,6-pyridinedicarboxylic acid (DPA)) to apply in sensor studies [74]. Due to the doping of Eu^{3+}, the MOF displayed strong red fluorescence via coordination of Eu^{3+} with pyridine “nitrogen” and acid group. Upon the addition of metal ions to the above MOF system, only Fe^{3+} and Hg^{2+} ions showed fluorescence quenching at 615 nm (in water) via Eu^{3+} atom displacement. However, adding hydrogen peroxide (H_2O_2; acted as a masking agent for Fe^{3+}) eliminated the interfering effect of Fe^{3+} over Hg^{2+} selectivity and delivered a linear response between 10 nM to 2.5 µM with a LOD of 8.26 nM (lower than the allowed limit). In terms of the strategy and LOD, this work is an impressive one, but demonstrations in real time applications are missing in this report.

Wang and co-workers constructed a novel Zr-based MOF (**RuUIO-67**) integrated with ruthenium (Ru) complex for colorimetric sensing of Hg^{2+}, which was reversible with KI solution [75]. The **UIO-67** is comprised of $Zr_6O_4(OH)_4$ nodes strutted by linear 4,4′-biphenyldicarboxylic acid (H_2bpdc) bridging ligands. It is further doped with ruthenium complex $Ru(H_2bpydc)(bpy)(NCS)_2$ (achieved by reacting $[RuCl_2(p\text{-cymene})]_2$, 2,2′-bipyridine (bpy), 2,2′-bipyridine-5,5′-dicarboxy (H_2bpydc) with ammonium thiocyanate (NH_4NCS)) to yield the **RuUIO-67** MOF. Upon the addition of Hg^{2+} (in HEPES buffer, pH 7.4) to **RuUIO-67** in methanol-water (8:2), the initial absorption band at 540 nm gradually disappeared and a new band at 435 nm was visualized due to the strong binding of sulphur “S” atom present in the NCS group. The MOF showed a linear response between 0–13 µM with a LOD of 0.5 µM (0.1 ppm) and a naked eye LOD of 7.2 µM. Moreover, reversibility up to six cycles was achieved when I^- (KI solution) was added to the sensory system. However, it still needs to focus on competing interrogations. Li et al. described the modified **UIO-68** ($Zr_6O_4(OH)_4$ clusters linked with 4,4′-terphenyldicarboxylate (TPDC)) MOFs **UIO-68-NCS**, **UIO-68-R6G**, and **UIO-68-R6G′** via post-synthetic modification strategy towards colorimetric and fluorescent detection of Hg^{2+} [76]. Reaction of the **UIO-68-NH$_2$** with thio-phosgene and triethylamine led to formation of the **UIO-68-NCS**, which was further reacted with N-(rhodamine-6G) lactam-ethylenediamine (R6G-EDA) and $Hg(NO_3)_2$ hydrate to yield the **UIO-68-R6G** and **UIO-68-R6G′**, respectively. In the presence of Hg^{2+}, **UIO-68-R6G** displayed in red and enhanced "turn-on" red emission with corresponding changes in particle sizes as seen in **Figure 3**.

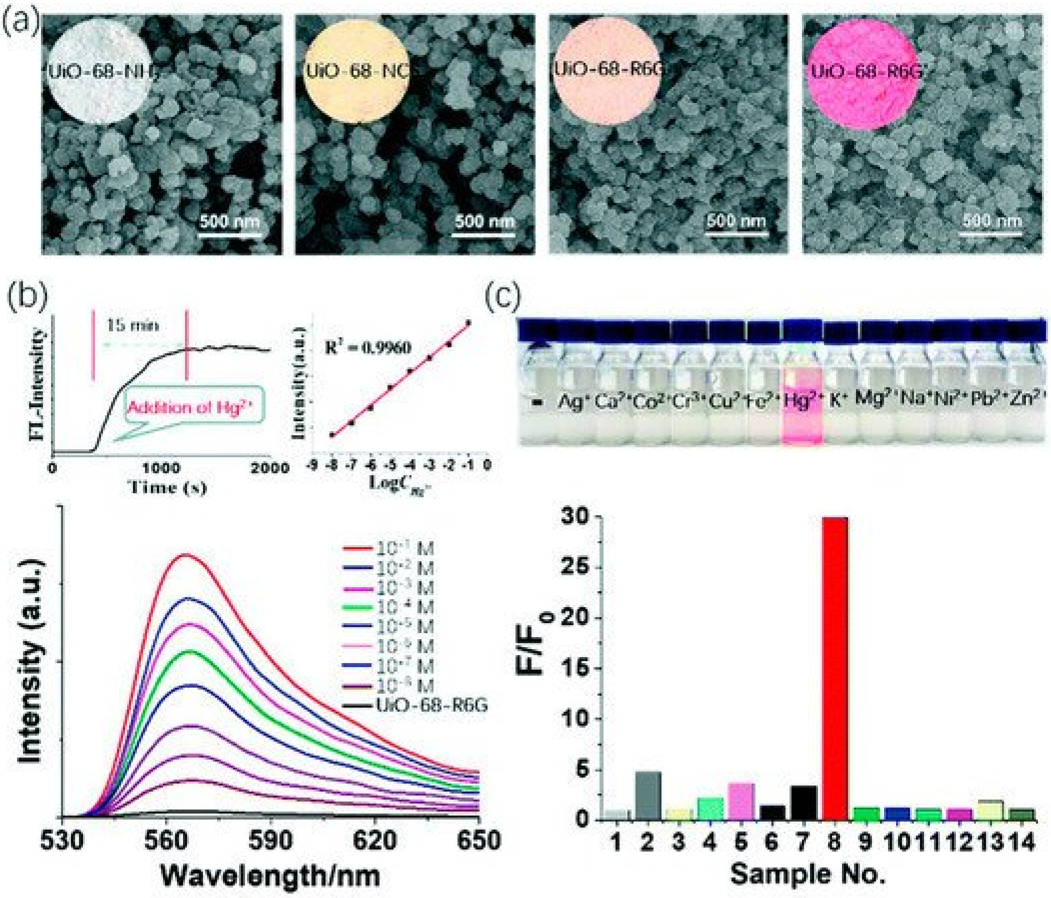

Figure 3. (**a**) SEM images of **UIO-68-NH$_2$**, **UIO-68-NCS**, **UIO-68-R6G**, and **UIO-68-R6G**′ and their as-synthesized samples. (**b**) Emission spectra of **UIO-68-R6G** (0.1 mg mL^{-1}) upon the addition of Hg^{2+} at different concentrations in the Tris-HCl buffer solution. $K_{sv} = 4.1 \times 10^9$ L mol^{-1}. The emission maximum was observed at 566 nm (λ_{ex} = 488 nm). Linearity relationship between Hg^{2+} with different concentrations and relative emission intensities, and the time-dependent emission of **UIO-68-R6G** with the sequential addition of Hg^{2+} are shown in the insets. (**c**) Emission response of **UIO-68-R6G** toward various metal ions (10^{-4} M) in an aqueous solution (0.9 mL) of **UIO-68-R6G** (0.1 mg mL^{-1}): (1) blank, (2) Ag^+, (3) Ca^{2+}, (4) Co^{2+}, (5) Cr^{3+}, (6) Cu^{2+}, (7) Fe^{2+}, (8) Hg^{2+}, (9) K^+, (10) Mg^{2+}, (11) Na^+, (12) Ni^{2+}, (13) Pb^{2+}, and (14) Zn^{2+}. The corresponding sample photographs are inserted (Reproduced with the permission from Ref [76]).

Based on the N_2 uptake at 77K, the BET surface area of **UIO-68-NH$_2$**, **UIO-68-NCS**, **UIO-68-R6G**, and **UIO-68-R6G′** were established as 674 cm^3 g^{-1}, 620 cm_3 g^{-1}, 405 cm^3 g^{-1}, and 326.83 cm^3 g^{-1}, correspondingly. The decrease in BET surface area was attributed to the incorporation of larger rhodamine-thiocarbamide unit, which reduced the porosity. The UIO-68-R6G in Tris-HCl buffer solution displayed a linear response to Hg^{2+} from 10^{-8} to 10^{-1} M with a LOD of 0.1 nM and was demonstrated with applicability in in-vitro/in- vivo bio-imaging studies. Thereafter, Kim and co-workers presented the MOF-**SALI-MAA**-3eq via incorporation of three equivalents of mercaptoacetic acid into **NU-1000** (comprised of $Zr_6(\mu_3\text{-}O)_4(\mu_3\text{-}OH)_4(H_2O)_4(OH)_4$ nodes and tetratopic 1,3,6,8-(*p*-benzoate)pyrene linkers) towards the determination of Hg^{2+} [77]. Based on the N_2 adsorption-desorption isotherms at 77K, the BET surface area of **NU-1000** and **SALI-MAA**-3eq were found as 2253 m^2 g^{-1} and 1906 m^2 g^{-1}, correspondingly. The decrease in surface area was related to the incorporation of mercaptoacetic acid. The **SALI-MAA**-3eq in water showed a linear response from 0.1 to 10 mM, however, the LOD was not provided. This work requires further investigations in competing and applicability studies.

Subsequently, by coordinating the 5-boronobezene-1, 3-dicarboxylic acid with Eu^{3+} ions, the boric acid (BA)-functionalized lanthanide metal-organic framework (**BA-Eu-MOF**) was reported in detection of Hg^{2+} and CH_3Hg^+ species in aqueous medium [78]. The **BA-Eu-MOF** was in the form of meso-porous nanoparticles with a uniform size distribution of ~400 nm. It also showed characteristics of red emission, good dispersive ability, and water solubility. Initially, the “antenna” effect was passivated by boric acid (BA) and the **BA-Eu-MOF** showed weak red emission. During detection of Hg^{2+} and CH_3Hg^+ species via chemodosimeter reaction between BA and the analytes, the “antenna” effect was recovered and led to strong red fluorescence under UV-lamp (λ_{ex} = 365 nm). The BET surface area of **BA-Eu-MOF** was established as 39.7 m^2 g^{-1} to N_2 gas at 77K. Upon the addition of the Hg^{2+} and CH_3Hg^+, photoluminescence (PL) response at 620 nm was linearly enhanced between 1–60 µM and 1–80 µM with a LODs of 220 nM and 440 nM. Moreover, **BA-Eu-MOF** showed higher selectivity over other competing mono- and di-valent cations in real time river water applications.

MOFs composed of other lanthanide metal nodes have also been engaged in the Hg^{2+} discrimination. By reacting the organic ligand “4,4′,4″-s-triazine-1,3,5-triyltri-p-amino-benzoic acid (H_3TATAB)” with lanthanide metals (Ln = Eu, Tb, Sm, Dy and Gd), the **Ln(TATAB)·(DMF)$_4$(H$_2$O)(MeOH)$_{0.5}$** MOFs were produced in quantitative yields and were interrogated towards metal ions detection [79]. Wherein, only the **TbTATAB** in water showed selective sensitivity to Hg^{2+} but not the other lanthanide ions (Eu, Sm, Dy and Gd) containing MOFs. During Hg^{2+} detection, luminescence of **TbTATAB** at 494, 544, 587, and 622 nm (quantum yield = 77.48%) was quenched linearly from 0 to 50 µM with a LOD of 4.4 nM. This work also demonstrated Hg^{2+} detection in real water samples (river water, drinking water, and tap water), but information on the nanostructure and BET surface area were missing. Recently, Li et al. developed two MOFs, namely **$\{[Tb_2(bpda)_3(H_2O)_3]\cdot H_2O\}_n$** and **$\{[Dy_2(bpda)_3(H_2O)_3]\cdot H_2O\}_n$**, by reacting 2,2′-bipyridine-4,4′-dicarboxylic acid (H_2bpda) with $LnCl_3.6H_2O$ (Ln = Tb and Dy) and engaged them in sensory investigations [80]. The **$\{[Dy_2(bpda)_3(H_2O)_3]\cdot H_2O$** showed fluorescent quenching with Hg^{2+} at 489, 543, 582, and 620 nm (λ_{ex} = 310 nm) with a K_{SV} value of 20,406 M^{-1} and a LOD of 7.2 nM. This work requires additional investigations on the BET surface area and interference studies.

Researches in Hg^{2+} sensing using zinc containing MOFs were also described as follows. Morsali′s research group proposed a double solvent sensing method (DSSM) to detect Hg^{2+} with great accuracy by using a zinc-based MOF $[Zn(OBA)\text{-}(DPT)_{0.5}]\cdot DMF$, namely **TMU-34(-2H)**, where OBA, DPT, and DMF represent 4,4′-oxybis(benzoic acid), 3,6-di(pyridin-4-yl)-1,2,4,5-tetrazine, and N, N-dimethylformamide, respectively [81]. The BET specific surface area of **TMU-34(-2H)** to N_2 gas at 77K was 667 $m^2\ g^{-1}$ and was able to adsorb 201 $cm^3\ g^{-1}$ of N_2 gas. In the presence of Hg^{2+}, the **TMU-34(-2H)** displayed 1D-transduction signals of 243% PL enhancement in water at 648 nm (λ_{ex} = 504 nm) and 90% PL quenching in acetonitrile at 618 nm (λ_{ex} = 458 nm) with estimated LODs as 1.8 µM and 6.9 µM, correspondingly, within 15 seconds. However, both solvents suffered interfering effects from other ions. Therefore, DSSM tactic was proposed to improve the sensitivity to Hg^{2+} by combining water and acetonitrile. Wherein, the sensing factor of Hg^{2+} was found as 41 by plotting 2D sensing curve, which was higher than that of all other metal ions with sensing factors between 0–2. Thus, the interfering effects was eliminated. However, its applicability is still in question due to the lack of mechanistic aspects. Thereafter an anionic MOF, namely **Zn-TPTC** (TPTC represents [2,2′:6′,2″-Terpyridine]-4,4′,4″-tricarboxylic acid), was presented for luminescent detection of Hg^{2+} [82]. Upon addition of Hg^{2+}, the **Zn-TPTC** displayed linear PL quenching at 492 nm in a concentration range of 1 to 100 µM and an estimated LOD of 3.7 nM. The ‘N′ atoms of the MOF may interact with Hg^{2+} because of the greater affinity. There is no information regarding the BET surface area as well as the competing and application studies.

Subsequently, Pankajakshan et al. described Hg^{2+} sensing ability of **$\{[Zn(4,4'\text{-}AP)\ (5\text{-}AIA)].\ (DMF)_{0.5}\}_n$**, (where 4,4′ AP = 4,4′-azopyridine, 5-AIA and DMF represent deprotonated 5-amino isophthalic acid and N,N′-dimethylformamide), via PL quenching at 405 nm in aqueous solution [83]. The MOF probe possessed a QY value of 11% and BET surface area of 173 $m^2\ g^{-1}$. It was stable in pH range 4 to 11 and exhibited a linear PL quenching response to Hg^{2+} in a concentration range of 9.99 µM to 20 mM. Moreover, the MOF displayed a high selectivity to Hg^{2+} over a wide range of competing mono-, di-, and tri-valent cationic species with a LOD down to 10^{-11} M and an estimated K_{SV} value of $1.011 \times 10^9\ M^{-1}\ s^{-1}$. In fact, the sensitivity was attributed to a specific interaction between Hg^{2+} and the free standing -N=N- of 4,4′-azopyridine. This work undoubtedly can be considered exceptional because of its performance in the real time Hg^{2+} detection (in seawater, river water, tap water, drinking water, and single crystals of MOF on an aluminum foil). Thereafter Khatun and co-workers developed the luminescent pillared paddle wheel MOF-**$Zn_2(NDC)_2(DPTTZ)$** with naphthalene dicarboxylate (NDC) antenna and N,N′-di(4-pyridyl)thiazolo-[5,4-d]thiazole (DPTTZ) pillars, which detected Hg^{2+} via red-shifts in PL emission [84]. In addition, MOF-**$Zn_2(1,4\text{-}BDC)_2(DPTTZ)_2$** was also synthesized for comparison, where the 1,4-BDC represents 1,4-benzenedicarboxylic acid. The BET surface area and pore volumes of MOFs-**$Zn_2(NDC)_2(DPTTZ)$** and **$Zn_2(1,4\text{-}BDC)_2(DPTTZ)_2$** to CO_2 were estimated as 106.8 $m^2\ g^{-1}$, 113.4 $m^2\ g^{-1}$ and $6.6 \times 10^{-2}\ cm^3\ g^{-1}$, $7.8 \times 10^{-2}\ cm^3\ g^{-1}$, respectively. The **$Zn_2(NDC)_2(DPTTZ)$** in DMF showed an exceptional selectivity only to Hg^{2+} among all ions via bathochromic PL shift from 410 nm to 450 nm. Although lacking experimental evidences, it was speculated that the PL change could be attributed to the interaction between Hg^{2+} and DPTTZ group. This work requires further attention regarding the LOD, competing studies, and real time applications. Recently, Zn-based MOF-**ZnAPA** with 5-aminoisophthalic acid (H_2APA) organic linkers was demonstrated for Hg^{2+} detection by means of fluorescence quenching in water [85]. Wherein, PL emission of MOF at 405 nm was linearly quenched during exposure to Hg^{2+} in a concentration range of 0–100 µM with a LOD of 0.12 µM. This might be due to the binding affinity of Hg^{2+} to 'N′ atom of amino group. This work showed a great selectivity over many other competing mono- and di-valent cationic species; however, it still needs to put more focus on the BET surface area and real applications.

The Cd-based MOFs were also engaged in discrimination of Hg^{2+}, in parallel to Zn-based MOFs. For example, Wu and co-workers constructed a Cd comprising 3D MOF-$\{[Cd_{1.5}(C_{18}H_{10}O_{10})]\cdot(H_3O)(H_2O)_3\}_n$-**Cd-EDDA** with dual emission and utilized it in ratiometric detection of Hg^{2+} in pure water [86]. By hydrothermally reacting 5,5′-[ethane-1,2-diylbis(oxy)]diisophthalic acid (H_4EDDA) with $Cd(ClO_4)_2\cdot 6H_2O$, the **Cd-EDDA** was produced with 80% yield. Upon addition of Hg^{2+} to the **Cd-EDDA**, intensity of PL emission at 350 nm decreased significantly (K_{SV} = 4.3 $\times 10^3$ M^{-1}) accompanied with a new PL peak at 410 nm with a linear response (within 15s) between 4–25 µM and a calculated LOD of 2 nM, which was lower than the permitted level. Be noted that the **Cd-EDDA** displayed great selectivity over a wide range of metal ions by means of crystallinity destruction and was not reversible with Na_2S. Thereby the probe behaves like a chemodosimeter. Information regarding the BET surface area and real time applicability requires further investigations. Subsequently, a MOF, namely **$[(Me_2NH_2)Cd_3(OH)(H_2O)_3(TATAB)_2](DMA)_6$**, was formed as yellow crystals through solvothermally reacting $Cd(NO_3)_2\cdot 6H_2O$ and 4,4′,4″-s-triazin-1,3,5-triyltri-p-aminobenzoic acid (H_3TATAB) in DMA (N,N-dimethylacetamide), methanol, and HCl at 95 °C for 3 days and was consumed towards luminescent Hg^{2+} detection in water [87]. Due to the binding between 'N′ atoms of amino and triazine groups, PL emission at 365 nm was quenched in the presence of Hg^{2+}. However, the selectivity was significantly affected by Fe^{3+}. Moreover, there was no details regarding the BET surface area and applicability. Recently, interaction of $Cd(ClO_4)_2.6H_2O$ with 2-aminoterephthalic acid (NH_2-H_2BDC) by microwave synthetic was used as a tactic to derive the Cd^{2+}-comprising MOF-**NH_2-Cd-BDC**, which was applied in sensing of Hg^{2+} via PL quenching at 427 nm [88]. The -NH_2 group of **NH_2-Cd-BDC** reacted with Hg^{2+} and led to linearly quenched emission in a concentration range from 1 to 20 µM and a K_{SV} value of 28.0 $\times 10^3$ M^{-1} and a LOD of 0.58 µM. Though the work seems to be comparatively good with respect to earlier reports, it still lacks information on the BET surface area, real time applicability, and competing studies.

The ferrous (Fe^{2+}) comprising MOF nanoparticles, namely **Fe(II)-MOF-NPs**, were developed via solvothermal reaction of $FeSO_4.7H_2O$ with nano linkers (synthesized via refluxing 1, 2-phenylenediamine and 5-aminoisophthalic acid) and were engaged in colorimetric and PL detection of Hg^{2+} [89]. The nanoparticles have a size in the range between 100 to 250 nm and possess magnetic properties as well. During addition of Hg^{2+}, PL emission at 416 nm displayed a 'turn-on′ response and was red-shifted to 422 nm. The absorption peak at 427 nm was also enhanced and red-shifted to 456 nm accompanied with changes in colour from yellow to colorless. Both absorption and PL showed a linear response in a concentration range from 1 nM to 1 µM and LODs of 1.17 and 1.14 nM and limit of quantifications (LOQs) of 1.59 and 1.48 nM, respectively. Moreover, the **Fe(II)-MOF-NPs** in DMSO were also effective in discrimination of Hg^{2+} in competing and real environment (tap, mineral, river, sea, and waste water). Based on above results, the **Fe(II)-MOF-NPs** can be an excellent candidate for the discrimination of Hg^{2+}, but mechanistic investigations and BET adsorption studies must be conducted to move towards Hg^{2+} removal studies. Towards sensing of Hg^{2+}, Li and co-workers presented the hydrostable bromine-functionalized Mn-based MOF-**$\{[Mn_2(Bript)_2(4,4'\text{-}bpy).5(DMF)]\cdot(H_2O)\}_n$**, where H_2Bript, 4,4′-bpy, and DMF represent 4-Bromoisophthalic acid, 4,4′-bipyridine, and dimethylformamide, respectively [90]. The BET surface area of the MOF was established as 210

m^2 g^{-1} and was further reduced to 33 m^2 g^{-1} upon loading of Hg^{2+}. Due to the binding affinity between Br atom and Hg^{2+}, PL emission at 468 nm was linearly quenched (K_{SV} = 1390.5 M^{-1}) from 0 to 0.03 M with an estimated LOD of 48 µM. The MOF showed high selectivity toward Hg^{2+} (in water) among variety of competing species. However, studies on the real time applicability and LODs need more focus before proceeding further. To this track, Song et al. reported highly selective sensing of Hg^{2+} using Ag coordinated MOF [91]. Wherein, they developed three Ag^+/Cu^{2+} comprising MOFs, namely **[Ag(2,4′-Hpdc)(4,4′-bpy)]$_n$**, **[Ag(2,2′-Hpdc)(4,4′-bpy)0.5]$_n$**, and **[Cu(2,2′-Hpdc)$_2$(1,4-bib)]$_n$**, via hydrothermal method, where 2,4′-Hpdc, 2,2′-Hpdc, 4,4′-bpy, and 1,4-bib represent 2,4′-biphenyldicarboxylic acid, 2,2′-biphenyldicarboxylic acid, 4,4′-bipyridine, and 1,4-bis(1-imidazolyl) benzene, respectively. Among them, only the **[Ag(2,4′-Hpdc)(4,4′-bpy)]$_n$** in water showed selectivity to Hg^{2+} via ‘turn-on′ response with PL emission at 401 nm. Note that the Fe^{3+} showed PL quenching in the selectivity studies as seen in **Figure 4**. Due to the binding affinity between 2,4′-Hpdc to Hg^{2+}, PL emission of the MOF (in water) was enhanced linearly between Hg^{2+} concentrations from 0 to 100 µM with a LOD of 9.63 nM. However, it still requires optimization for BET surface area, competing analysis, and real sample applications.

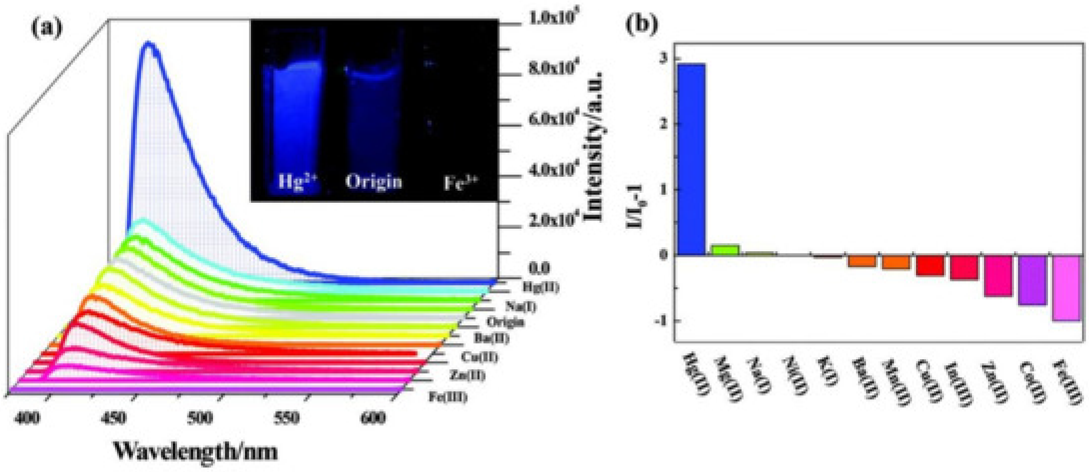

Figure 4. (**a**) Suspension-state PL spectra (inset: the images under UV-light irradiation at 365 nm) and (**b**) the relative intensities of **[Ag(2,4′-Hpdc)(4,4′-bpy)]$_n$** at 401 nm dispersed in aqueous solutions containing different metal ions (50 µM) when excited at 300 nm (reproduced with the permission from Ref [91]).

Many MOFs were also involved in detection of multiple analytes other than Hg^{2+} as detailed in the following. For example, 4,4′-(benzothiadiazole-4,7-diyl)dibenzoic acid ligand comprising MOFs, such as **[$Mn_4(C_{20}H_{10}N_2O_4S)_2$-$(HCOO)_4(DEF)_2$]** and **[$Pb(C_{20}H_{10}N_2O_4S)(DMF)$]** (where DEF and DMF represent N,N′-diethylformamide and N,N′-dimethylformamide; solvothermally synthesized), were described for the sensing of $Hg^{2+}$and Tl^{3+} metal cations and chromate, dichromate, and permanganate anions [92]. Detection of the metal ions was attributed to the interaction of ‘S′ atom with metal cations. Moreover, PL emission at 500 nm was quenched rapidly with LODs down to parts per billion/parts per million (ppb/ppm) in the presence of these analytes. Be noted that both MOFs can be used to detect Hg^{2+} in samples free of Tl^{3+}. Thus, these MOFs can be accounted as Hg^{2+} sensors. However, they are non-selective. Thereafter a ratiometric Hg^{2+} sensor was proposed by using MOF-**[Zn(tpbpc)$_2$]·solvent** prepared via solvothermal tactic, where Htpbpc (4′-[4,2′;6′,4″]-terpyridin-4′-yl-biphenyl-4-carboxylic acid and DMF solvent were used as an organic linker with Zn metal nodes [93]. This Zn-MOF was also demonstrated for detection of

CrO_4^{2-} and $Cr_2O_7^{2-}$ species in water via PL quenching at 414 nm. Above sensory results may arise from interactions between pyridine ‘N” atoms and Hg^{2+} or by inhibition of energy transfer processes by CrO_4^{2-} and $Cr_2O_7^{2-}$ ions. During addition of Hg^{2+} ions from 0 to 1200 µM, PL emission peak at 414 nm was quenched linearly with a LOD of 0.32 µM, accompanied with appearance of a new peak at 500 nm (green emission under UV lamp λ_{ex} = 365 nm). However, during competing studies, the selectivity may be affected in the presence of Cr(VI) ions (CrO_4^{2-} and $Cr_2O_7^{2}$). Thus, more interrogations are required due to lack of information on the selectivity, BET surface area and practical applications.

Ma′s research group developed the stable dye-incorporated MOF-**$[(CH_3)_2NH_2][In(TNB)_{4/3}].(2DMF)(3H_2O)$** via a solvothermal method, where H_3TNB (4,4′,4″-nitrilotribenzoicacid) was used as an organic linker and then incorporated with a dye 4-[p-(dimethylamino)styryl]-1-ethylpyridinium (DSM) to provide the **MOF-DSM** system [94]. The **MOF-DSM** system displayed sensing ability towards Hg^{2+}, $Cr_2O_7^{2-}$, and a wide variety of nitro-compounds. The BET surface area of MOF and **MOF-DSM** systems were estimated as 491 m^2 g^{-1} and 236 m^2 g^{-1}, respectively. During discrimination of Hg^{2+}, PL emission peaks of **MOF-DSM** (in water) at 478 and 630 nm were linearly quenched between 1–10 µM with an estimated LOD of 1.75 ppb and a K_{SV} value of 1.48 × 10^5 M^{-1}. The energy transfer efficiency of the π-π^* transitions diminished due to the binding affinity between Hg^{2+} and ‘N′ atoms of DSM. The MOF-DSM was found to be more effective in aqueous detection of $Cr_2O_7^{2-}$ and vapour/aqueous detection of nitro-compounds. Subsequently, Li et al. derived the Co-based MOF-**[Co (NPDC)(bpee)]·DMF·$2H_2O$** (where NPDC and bpee represent 2-nitro phenylenedicarboxylate and 1,2-bis(4-bipyridyl) ethylene) by means of the solvothermal tactic and established sensing ability towards Hg^{2+} and MnO_4^- [95]. This MOF in water displayed PL quenching in the presence of MnO_4^- and PL enhancement at 471 nm for Hg^{2+} ions. The linear response for Hg^{2+} ions by this MOF was found to be 1–120 µM with a LOD of 4.1 µM. However, this work still contains mechanistic flaws with non-optimal LODs and lacks information in applicability as well. To this track, Yang and co-workers synthesized two Cd-based MOFs, namely **$Cd(L)(atpa)]_n$** and **$[Cd(L)(tbta)(H_2O)]_n$** (where H_2atpa, H_2tbta, and L represent 2-aminoterephthalic acid, tetrabromoterephthalic acid, and 1,4-bis(benz-imidazol-1-yl)-2-butene, respectively) via a hydrothermal method and utilized them as dual luminescent sensors (Cu^{2+} and $Cr_2O_7^{2-}$ by **$[Cd(L)(atpa)]_n$**, and Hg^{2+} and $Cr_2O_7^{2-}$ by **$[Cd(L)(tbta)(H_2O)]_n$** in water [96]. PL intensity of **$[Cd(L)(tbta)(H_2O)]_n$** at 294 nm was linearly quenched during addition of Hg^{2+} from 0 to 0.25 mM with a LOD of 0.043 µM and a K_{SV} value of 1.72 × 10^5 M^{-1}. Moreover, fluorescence of **$[Cd(L)(tbta)(H_2O)]_n$** in water at 294 nm was also quenched in the presence of $Cr_2O_7^{2-}$. This work did not provide any details on the BET surface area, discriminative information between Hg^{2+} and $Cr_2O_7^{2-}$ (Cr^{6+}), and practicality.

Subsequently, 2,6-naphthalenedicarboxylic acid (NP) and 1,5 dihydroxy-2,6-naphthalenedicarboxylic (DNP) were conjugated with lanthanide cations (La^{3+} and Ce^{3+}) to produce luminescent MOFs, namely **AUBM-2 (Ce)** and **AUBM-2(La)** with NP ligand and **AUBM-3(Ce)** and **AUBM-3(La)** with DNP ligand. They were engaged in sensory studies [97]. Wherein, upon excitation at 300 and 370 nm, the **AUBM-2 (Ce)** and **AUBM-3(Ce)** displayed sensory responses to Hg^{2+}, Cr^{3+}, Pb^{2+}, Cd^{2+}, and As^{3+} by means of fluorescent enhancement or quenching responses. This study requires further optimization for Hg^{2+} analyte detection. Next, Ren et al. proposed utilization of MOF nanosheet **amino-MIL-53(Al)** (hydrothermally synthesized by reacting $AlCl_3.6H_2O$ with 2-amino-terephthalic acid) towards luminescent detection of Hg^{2+} and glutathione (GSH) [98]. Emission of **amino-MIL-**

53(Al) nanosheets at 435 nm (in water) was linearly quenched by Hg^{2+} with concentrations between 1.96 nM to 38.27 µM and a detection limit of 0.23 nM. Furthermore, luminescent quenching was partially restored by addition of GSH (linear range: 210 nM to 15.25 µM and LOD = 8.11 nM). However, this work still lacks of information about the BET surface area. Solvothermally synthesized Cd-based MOFs **$[(Cd(II)BPDC)_{0.5}(L1)(NO_3)]\cdot 3.4DMF$** (where BPDC, L1, and DMF represent 4,4′-biphenyldicarboxylic acid, 1-(3,5-di(1H-imidazol-1-yl)phenyl)-1H-imidazole), and Dimethylformamide, respectively) and **$[(Cd_2(4\text{-}tp\text{-}3\text{-}lad)(1,4\text{- }BDC)_2\}\cdot 2MeCN)_n$** (where 4-tp-3-lad, 4-BDC, and MeCN represent 2,3,5,6-tetra(pyridin-4-yl)-bicyclo [2.2.0]hexane, 1, deprotonated 1,4-benzenedicarboxylic acid, and acetonitrile, respectively) were also proposed towards the detection of Hg^{2+} and nitro-explosives via fluorescence quenching [99][100]. However, due to insufficient information regarding the BET surface area, competing studies, and practicality, these reports are not impressive. Later, Su et al. reported sensing ability of Co-based MOF-**$\{[Co_2(L)(hfpd)(H_2O)]\cdot 1.75H_2O\}_n$** (where H_4hfpd and L represent 4,4′-(hexa-fluoroisopropylidene)diphthalic acid and 4,4′-bis(imidazol-1-yl)-biphenyl) to Hg^{2+} and acetylacetone via luminescent quenching responses [101]. This hydrothermally synthesized MOF showed luminescence quenching in the presence of 0–200 µM Hg^{2+} with a K_{SV} of 6497 M^{-1} and a LOD of 4 µM. However, this work requires further interrogations on the BET surface area, nano/micro-structure, competing studies, and practicality.

5. Metal Coordinated Polymers as Luminescent Hg^{2+} Sensors

In addition to MOFs, metal containing coordination polymers were proposed towards luminescent sensing of Hg^{2+} [100]. For instance, Sun′s research group developed Zn- and Cd-based coordination polymers-**$[Zn(TPDC\text{-}2CH_3)(H_2O)_2].H_2O$** and **$[Cd(TPDC\text{-}2CH_3)(H_2O)_4].H_2O$** via solvothermally reacting 2′,5′-dimethyl-[1,1′:4′,1″-terphenyl]-4,4″-dicarboxylic acid (H_2TPDC-$2CH_3$) with Zn^{2+} and Cd^{2+} ions, separately, and engaged them in sensory interrogations towards metal ions [102]. Emission of the **$[Zn(TPDC\text{-}2CH_3)(H_2O)_2].H_2O$** metal polymer at 380 nm (in water) was linearly quenched between 1–10 femtomole (fM) with a LOD of 3.6 fM. The solid chelation-enhanced fluorescence quenching (CHEQ) effect can be attributed to coordination between carboxyl group and Hg^{2+}. However, this report did not provide any information regarding the BET surface area and practicality. Next, the **Eu/IPA CPNPs** (by solvothermal tactic) were prepared by reacting Eu^{3+} comprising coordination polymer nanoparticles (CPNPs) with isophthalic acid (IPA) bridging ligands and were employed in Hg^{2+} detection [103]. Initially, absorbance band of **Eu/IPA CPNPs** in Tris–HCl buffer (25 mM, pH 7.0) was overlapped with imidazole-4,5-dicarboxylic acid (Im), thus emission intensity at 615 nm was quenched due to the inner filter effect (IFE). During addition of Hg^{2+}, the IFE was supressed and recovery of emission at 615 nm was observed. The linear correlation of Hg^{2+} ranged between 2 nM to 2µM with a LOD of 2 nM. Effectiveness of the probe was further demonstrated with applicability in biological fluid samples. Nevertheless, information regarding BET surface area must be evaluated for its exceptional applicability.

Towards the development of metal coordination polymers for Hg^{2+} sensors, Li et al. described the solvothermally synthesized Zn-based 3D coordination polymer-**$\{[Zn_2(1,4\text{-}bpyvna)(1,3,5\text{-}BTC)(OH)]\cdot H_2O\}_n$** (where 1,4-bpyvna and 1,3,5-H_3BTC represent 1,4-bis(2-(pyridin-4-yl)vinyl)naphthalene and 1,3,5-benzene-tricarboxylic acid, respectively) as a Hg^{2+} sensor [104]. Due to the interactive effect of 1,4-bpyvna with Hg^{2+}, the **{[Zn$_2$(1,4-bpyvna)(1,3,5-BTC)(OH)]·H$_2$O}$_n$** in DMF displayed fluorescence quenching at 444 and 472 nm as seen in **Figure 5**.

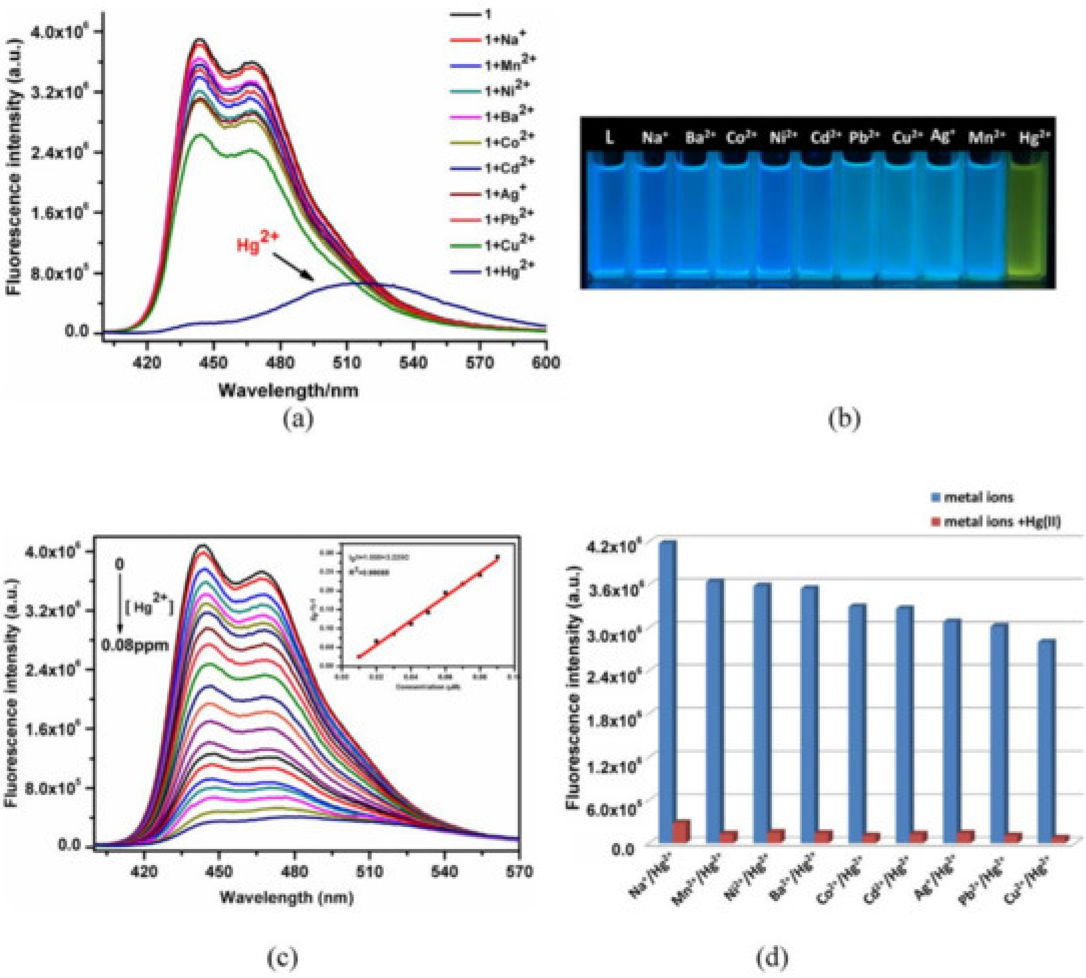

(a) (b)

(c) (d)

Figure 5. (**a**) Emission spectra of **{[Zn2(1,4-bpyvna)(1,3,5-BTC)(OH)]·H2O}$_n$** in DMF in the absence/presence of Mn+ ions. (**b**) The colours of the suspensions of **{[Zn2(1,4-bpyvna)(1,3,5-BTC)(OH)]·H2O}$_n$** with different metal ions under UV light. (**c**) Emission spectra of **{[Zn2(1,4-bpyvna)(1,3,5-BTC)(OH)]·H2O}$_n$** in the presence of increasing Hg^{2+} concentrations (0–0.08 ppm) in DMF. Inset: linear relation between the quenching efficiency and the concentration of Hg^{2+} in the range of 0–0.018 ppm. (**d**) Fluorescence intensities of **{[Zn2(1,4-bpyvna)(1,3,5-BTC)(OH)]·H2O}$_n$** immersed in the DMF solution of metal ion (blue colour) or mixed Hg2+ and metal ions (red colour) under an excitation of 389 nm (Reproduced with the permission from Ref [104]).

A linear response of the polymer was found from 0 to 0.018 ppm with a LOD of 0.057 ppm. A fluorescent colour change from blue to yellow was also observed. However, further interrogations for the BET surface area and real time applications are still required. Subsequently, Zhang and co-workers presented Hg^{2+} sensing ability of hydrothermally synthesized fluorescent coordination polymer, namely **[Zn(H$_3$TTA)(H$_2$O)$_2$]·2H$_2$O** (where H$_3$TTA represents [2,2′:6′,2″-terpyridine]-4,4′,4″-tricarboxylic acid)), in aqueous solution [105]. Emission band at 500 nm was quenched in the presence of Hg^{2+} with a K$_{SV}$ value of 4695 M^{-1}. This work is incomplete due to lack of information in the BET surface area, LODs, and practicality. Utilization of Zn- and Cd-based luminescent coordination polymers towards the quantitation of Hg^{2+} and $Cr_2O_7^{2-}$ has been reported by many research groups [106][107][108]. Since $Cr_2O_7^{2-}$ is a well-known source of Cr^{6+} ions, discrimination between them are not available in those reports. Therefore, those works cannot be considered as exceptional Hg^{2+} sensor studies. Similarly, Lin et al. demonstrated Pb^{2+} and Hg^{2+} sensing ability of Eu^{3+} containing coordination polymer, namely **$\{[Ln_2(PBA)_3(H_2O)_3]\cdot DMF\cdot 3H_2O\}_n$**, in DMF and aqueous media, where PBA, DMF, and H_2O represent deprotonated 5-(4-pyridin-3-yl-benzoylamino)-isophthalic acid, Dimethylformamide, and water molecules, respectively [109]. Wherein, the polymer can be used to detect Hg^{2+} in samples free of Pb^{2+}. Thus, these MOFs can be accounted as Hg^{2+} sensors. However, they are non-selective.

In addition to metal coordination polymer-based Hg^{2+} sensor, Rachuri and co-workers reported a luminescent coordination polymer, namely **$[Zn(\mu_2\text{-1H-ade})(\mu_2\text{-}SO_4)]$** (by solvothermal reaction of adinine (HAde) and $Zn(SO_4)\cdot 7H_2O$), as discussed in the following [110]. In the report, fluorescence intensity of the **$[Zn(\mu_2\text{-1H-ade})(\mu_2\text{-}SO_4)]$** at 395 nm (in water) was linearly quenched between 0–1 mM of Hg^{2+} with a LOD of 70 nM and a K_{SV} value of 7.7×10^3 M^{-1}. Moreover, this polymer also has an additional advantage that it showed selective sensing of the 2,4,6-trinitrophenol (TNP) in aqueous medium. The underlying mechanism of detection of Hg^{2+} was attributed to the interaction with basic sites (N atoms) of the adenine and TNP through the resonance energy transfer (RET). It should be noted that this work also described the Hg^{2+} detection in paper strips, therefore, it can be extended for effective Hg^{2+} removal in real samples with directed BET surface area analysis. Thereafter, Zhu et al. demonstrated Hg^{2+} sensing utility of two luminescent coordination polymers, namely **$[Cd(L)(NTA)]_n$** and **$[Ni(L)(NPTA)\cdot H_2O]_n$** (obtained by solvothermal method, where L, H_2NTA, and H_2NPTA represent 1,6-bis(benzimidazol-1-yl)hexane, 2-nitroterephthalic acid, and 3-nitrophthalic acid, respectively) [111]. Emission peaks at 292 nm and 295 nm of the polymers **$[Cd(L)(NTA)]_n$** and **$[Ni(L)(NPTA)\cdot H_2O]_n$** (in water), respectively, were linearly quenched by Hg^{2+} in a concentration range between 1–200 μM with corresponding LODs of 3.05 μM and 2.29 μM and K_{Sv} values of 3565 M^{-1} for 1 and 7432 M^{-1}. In addition, both polymers displayed selectivity only to acetylacetone among all solvents. However, this work requires information on the BET surface area, competing studies, mechanistic investigations, and practicality.

6. MOFs Holding Composites for Optical Recognition of Hg^{2+}

To enhance sensing ability of MOFs to Hg^{2+}, researchers also proposed to synthesize MOFs comprising composites as detailed in the following. A metal−polydopamine framework (**MPDA**—a dopamine loaded Co-based MOF developed by sonochemical reaction of $Co(NO_3)_2$ and 2-methylimidazole to afford **ZIF-67** primarily) was reported as a fluorescent quencher towards the detection of Hg^{2+} and Ag^+ via exonuclease III signal amplification activity with pico-molar level LODs (1.3 pM and 34 pM, respectively) [112]. Upon addition of Hg^{2+} to **MPDA**-T-rich ssDNA (T-rich ssDNA represents thymine rich single stranded Deoxyribonucleic acid) system, ‘turn-on′ PL emission enhancement at 520 nm was observed with a linear response from 0 to 2 nM and a LOD of 1.3 pM. The quenched luminescence of **MPDA** conjugated with T-rich ssDNA was recovered through T-Hg^{2+}-T complexation during addition of Hg^{2+}. This work was also well demonstrated in tap and river water applications. To this way, Huang and co-workers reported Cu-based MOFs as a hybrid sensory system with C-rich or T-rich DNA probes to detect the

Ag^+, Hg^{2+}, and thiol comprising species at nanomolar-level via T-Hg^{2+}-T complexation [113][114]. Wherein, Huang et al. developed a MOF, namely **$[Cu_4(Dcbb)_4(Dps)_2(H_2O)_2]_n$** (by reacting $H_2DcbbBr$ = 1-(3,5-dicarboxybenzyl)-4,4′-bipyridinium bromide and Dps (4,4′-dipyridyl sulfide) with $Cu(NO_3)_2{\cdot}3H_2O$), to detect Ag^+, Hg^{2+}, and biothiols with nM LODs [113]. Similarly, the MOF, namely **$[Cu(Cdcbp)(H_2O)_2{\cdot}2H_2O]_n$** (synthesized by reacting $H_3CdcbpBr$ (3-carboxyl-(3,5-dicarboxybenzyl)-pyridinium bromide) with $CuSO_4{\cdot}5H_2O$) was engaged in detection of Hg^{2+} and biothiols with nM LODs [114]. In both cases, the MOF tended to form a hybrid system initially with fluorescent dye loaded thymine rich (T-rich) DNA (labelled as P-DNA) which led to fluorescent quenching. It was then recovered upon addition of metal ions, Hg^{2+} in particular, via T-Hg^{2+}-T complexation. The above hybrid MOFs-DNA system-based detection of Hg^{2+} and biothiols and the corresponding mechanism are illustrated in **Figure 6**. Following the same strategy, Zr- and Ce-based MOFs (**UIO-66-NH_2** and **Ce/TBC**) were also demonstrated to discriminate Hg^{2+} with nanomolar LODs [115][116]. Wherein the **Ce/TBC** (also noted as mixed-valence state cerium-based metal-organic framework (**MVC-MOF**) combined with thymine-rich ssDNA was engaged in colorimetric peroxidase like sensors to detect Hg^{2+} using oxidase substrate 3,3′,5,5′-tetramethylbenzidine [116]. Results of Hg^{2+} detection showed a linear response in a concentration range of 0.05 to 6 μM with a LOD of 10.5 nM and were further supported by environmental water analysis. In fact, many MOF-DNA hybrid systems were reported for detection of metal ions, aminoacids, and nucleic acids [117][118], which make the strategy as precise one.

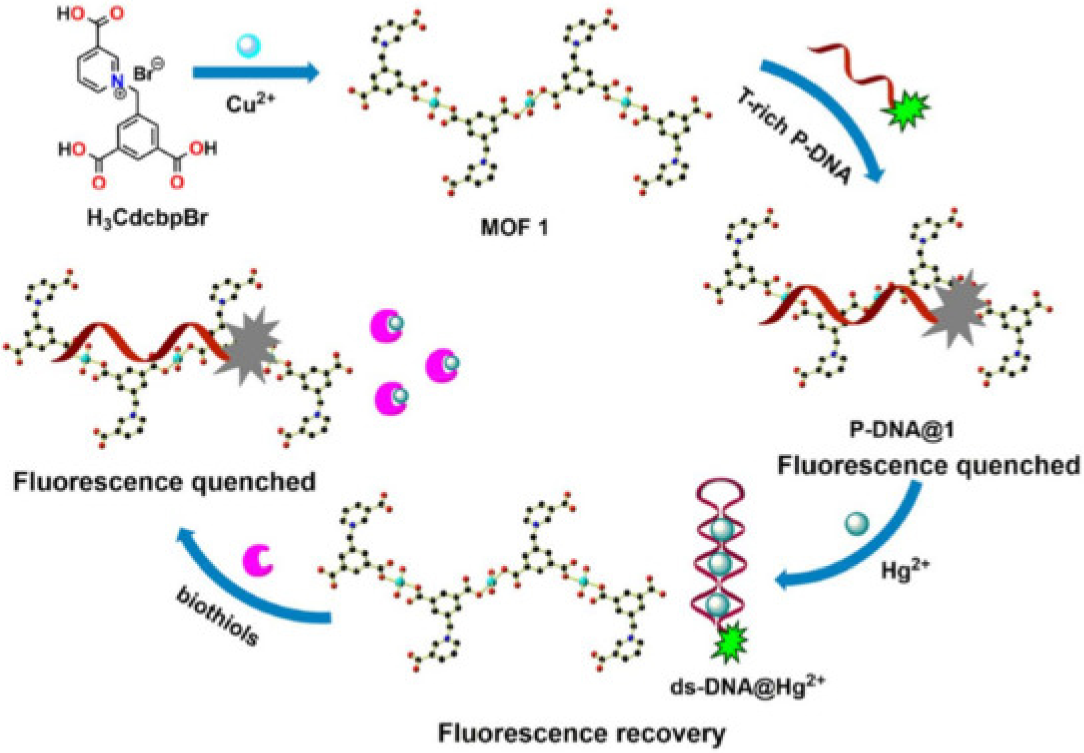

Figure 6. The proposed Hg^{2+} and biothiols detection mechanism based on the P-DNA@1 hybrid (Reproduced with the permission from Ref [114]).

Recently, gold nanoclusters composited MOFs, namely **AuNCs/MIL-68(In)-NH_2/Cys** and **AuNCs@UIO-66**, were demonstrated in discrimination of Hg^{2+} [119][120]. To develop the **AuNCs/MIL-68(In)-NH_2/Cys**, **MIL-68(In)-NH_2** was first solvothermally synthesized by reacting $In(NO_3)_3{\cdot}xH_2O$ with 2-Aminoterephthalic acid (H_2ATA) followed by evenly dispersing the AuNCs on its surface. The AuNCs exhibited emission bands at 438 nm and 668 nm (λ_{ex} = 370 nm). By adding cysteine into above mixture, the **AuNCs/MIL-68(In)-NH_2/Cys** was produced with enhanced emission [119]. Upon addition of Hg^{2+} to the **AuNCs/MIL-68(In)-NH_2/Cys** at pH 7.4 (phosphate buffer), emission at 638 nm was quenched without affecting the peak at 438 nm. Due to the binding affinity of Hg^{2+} with thiol (-SH) of cysteine, PL quenching exhibited two linear responses (with a concentration range from 20 pM to 0.2 μM and from 0.2 μM to 60 μM) with a LOD of 6.7 pM, which was further supported by real water analysis and microfluidic paper device. Subsequently, the **UIO-66** was obtained by solvothermally reacting zirconium chloride with 1,4-benzenedicarboxylic acid (H_2BDC). The synthesized **UIO-66** was then conjugated with AuNCs to afford **AuNCs@UIO-66** with 11% quantum yield [120]. PL emission of the **AuNCs@UIO-66** at pH 7.2 was observed at 650 nm and was quenched linearly by Hg^{2+} with concentrations from 800 nM to 10 μM and a LOD of 77 pM. The emission quenching was attributed to the Au-Hg amalgamation via interactive amino groups of bovine serum albumin (BSA) present over AuNCs surface. The applicability of the sensory study was also successfully demonstrated in tap and river water which can be accounted as a good candidate for Hg^{2+} discrimination.

To this track, Marieeswaran and co-workers presented Hg^{2+} sensing ability of the MOF containing composite consisted of magnetic nanoscale metal–organic framework (**MNMOF**) conjugated with fluorescein amidite (FAM)-labeled ssDNA [121]. The **MNMOF** was developed by one-pot reaction between Fe_3O_4 nano-spheres (synthesized hydrothermally), $FeCl_3.6H_2O$, and 2-aminoterephthalic acid. Emission intensity at 495 nm (in Tris-HCl buffer) was quenched up to 62% with adsorption of FAM-labeled ssDNA on the **MNMOF**. Addition of Hg^{2+} further lowered the emission quenching at 495 nm down to 52% via T-Hg^{2+}-T complexation. The linear regression of Hg^{2+} detection was between 2–20 nM with a LOD of 8 nM. This work was also demonstrated in environmental water samples. However, the BET surface area information and competing studies still need to be updated. In addition to the **MOF-DNA** hybrid system, Hu and co-workers revealed the utilization of the **$\{[Cu(Dcbb)(Bpe)]\cdot Cl\}_n$** (where $H_2DcbbBr$ and Bpe represent 1-(3,5-dicarboxybenzyl)-4,4′-bipyridinium bromide and trans-1,2-bis(4-pyridyl)ethylene, respectively) towards sequential quantitation of Hg^{2+} and I^- via the T−Hg^{2+}−T motif and “off-on-off” fluorescence response [122]. Detection of Hg^{2+} and I^- was verified by circular dichroism (CD) and the underlying mechanism was clarified by fluorescence anisotropy, binding constant, and simulation studies. LODs for Hg^{2+} and I^- sensors were estimated as 3.2 and 3.3 nM, respectively. Though the sensor showed high selectivity, it can be considered a supplementary work due to the similar T−Hg^{2+}−T motif approach.

The **AuNP@MOF** composite nanoparticles were used in colorimetric Hg^{2+} assay via gold amalgam-triggered reductase mimetic activity in aqueous medium [123]. The **AuNP@MOF** composite was developed by immobilizing Au NPs over the porous surface of iron-5,10,15,20-tetrakis (4-carboxyl)-21H,23H-porphyrin-based MOF- (**Fe-TCPP-MOF**) and was utilized in colorimetric sensing of Hg^{2+}. Wherein, Hg^{2+} triggered the Au-mediated catalytic reduction of methylene blue and turned the blue colour to colourless, which was accompanied with quenching in absorbance peak of methylene blue at 665 nm as shown in **Figure 7**. Moreover, the absorbance at 665 nm was linearly quenched within 2s by Hg^{2+} with concentrations from 200–400 pM and a LOD of 103 pM. Apart from lack of the BET surface area information, the competing studies, tap and river water investigations attested the utility of the **AuNP@MOF** in Hg^{2+} detection.

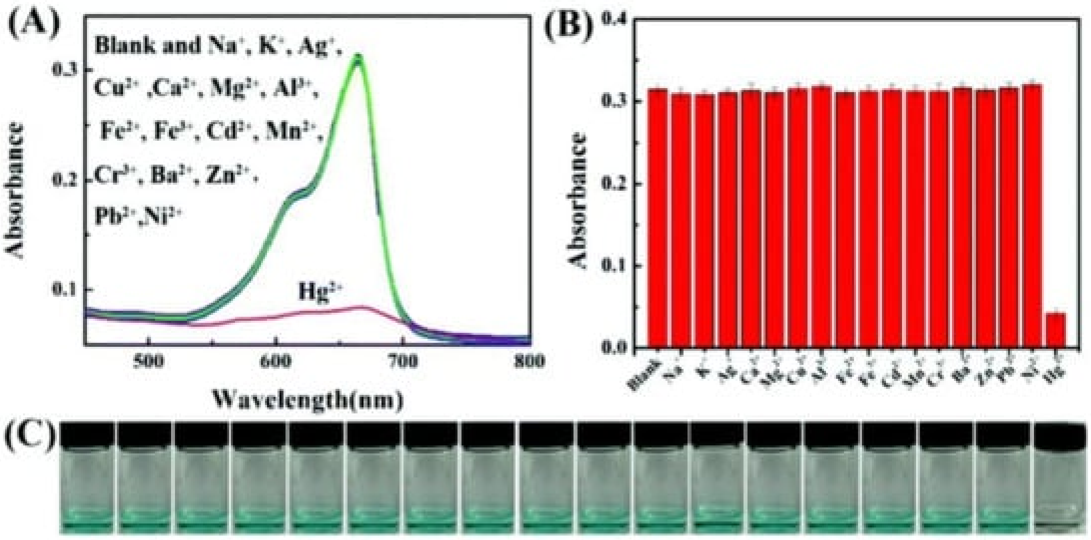

Figure 7. Selectivity of the sensing method by **AuNP@MOF** to other metal ions. Concentrations of Hg^{2+} and other metal ions (Na^+, K^+, Ag^+, Ca^{2+}, Mg^{2+}, Cu^{2+}, Al^{3+}, Fe^{3+}, Fe^{2+}, Cd^{2+}, Mn^{2+}, Cr^{3+}, Ba^{2+}, Zn^{2+}, Pb^{2+} and Ni^{2+}) were 1 nM and 10 nM, respectively. (**A**) The UV spectra of the sensing system in response to various metal ions; (**B**) The UV absorbance of the sensing system at 665 nm towards various metal ions; (**C**) photographs of the sensing system responding to various metal ions (Reproduced with the permission from Ref [123]).

In this light, Zhang et al. deposited Au nanoparticles on titanium-based MOF **(NH_2-MIL-125(Ti))** by solvothermal reaction between 2-aminoterephthalate and tetrabutyl titanate) to afford **Au@NH_2-MIL-125(Ti)** for colorimetric detection of H_2O_2, cysteine, and Hg^{2+} via peroxidase-like activity using 3,3′,5,5′-tetramethylbenzidine (TMB-catalyst) [124]. The **Au@NH_2-MIL-125(Ti)** and TMB showed a blue colour and a “turn-on” absorbance response at 652 nm in the presence of H_2O_2 via peroxidase like mimic. Upon addition of cysteine to above sensory system, absorbance at 652 nm was quenched accompanied with disappearance of the blue colour. However, the blue colour and absorbance peak were recovered by adding Hg^{2+}. The Hg^{2+} detection showed a linear response in concentrations from 1 to 5 µM with a LOD of 100 nM and was authenticated by real sample analysis. A masking tactic with EDTA was proposed in this report to avoid the interference effect from other metal ions, however, this work required more complicated detection procedures.

A “**CDs/AuNCs@ZIF-8**” composite consisted of zeolitic imidazolate framework-8 (**ZIF-8**) encapsulated with carbon dots (CDs) and gold nanoclusters was produced and utilized in detection of Hg^{2+} [125]. The **CDs/AuNCs@ZIF-8** in aqueous medium displayed emission bands at 440 and 640 nm (λ_{ex} = 360 nm) due to the encapsulated CDs and AuNCs. In the presence of Hg^{2+}, PL peak at 640 nm was quenched but emission band at 440 nm was not affected. Therefore, it was noted as a ratiometric sensor. Due to the Au-Hg amalgamation, the probe showed linear ratiometric response (I_{640}/I_{440}) between 3–30 nM with a LOD of 1 nM accompanied with visualization of red blue emission colour changes under UV-irradiation. This work was also demonstrated in tap and river water samples. Following the ratiometric sensing approach, Yang et al. constructed a ratiometric sensor **MOF/CdTe QDs** via physically mixing **CdTe QDs** (λ_{em} = 605 nm) with MOF (**Fe-MIL-88NH_2**, λ_{em} = 425 nm) towards Hg^{2+} and Cu^{2+} discrimination [126]. During detection of metal analytes, ratiometric responses at I_{425}/I_{605} due to the strong binding interaction between CdTe QDs and metal ions were evaluated by monitoring the colour changes (from pink to blue). Although this work was well supported by paper-based analysis, lake water, fruit juice, and red wine samples, but it lacks information in competing studies.

7. MOFs in Electrochemical Recognition of Hg^{2+}

Similar to many inorganic electrochemical sensors [127], MOFs were also engaged in electrochemical-based detection of Hg^{2+} as described subsequently. For example, Zhang et al. demonstrated electrochemical sensing of Hg^{2+} in the presence of glucose by using the Cu^{2+} anchored MOFs as enzyme free catalyst [128]. MOFs were firstly synthesized By solvothermally reacting amino terephthalic acid (NH_2-BDC) with $Cu(NO_3)_2$. The as-synthesized MOFs were then combined with Au NPs and sDNA to obtain the **sDNA/MOF-Au** probe. The **cDNA/GO@Au/GCE** electrode was immersed in the mixed solution of **sDNA/MOF-Au** and Hg^{2+} at certain concentration for Hg^{2+} sensing. The **sDNA/MOF-Au** probe detected Hg^{2+} via T-Hg^{2+}-T coordination and induced a oxidase-like catalytic response. This work showed a linear response to Hg^{2+} in concentrations from 0.10 aM to 100 nM (aM = attomole = 10^{-18} M) with a LOD of 0.001 aM. Moreover, this work was also demonstrated in dairy product samples, which was impressive. However, careful optimization is required to attain the reproducible results. Recently, the **ZIF-8** was synthesized via hydrothermal reaction of $Zn(NO_3)_2·4H_2O$ and 2-methylimidazole and employed in electrochemical discrimination of Hg^{2+} by coupling with Ag and Au nanoparticles [129]. This work also involved the electrochemical aptasensor based on the Au electrode (AE). Signals were obtained from the "**APT/Ag@Au/ZIF-8/AE**" aptasensor by means of differential pulse voltammetry (DPV) and electro-chemical impedance spectroscopy (EIS). Due to the T-Hg-T complexation from T rich aptamer, Hg^{2+} detection became feasible. Linear responses were observed from detection of Hg^{2+} in concentrations from 1.0×10^{-16} to 1.0×10^{-12} M and from 5.0×10^{-15} to 1.0×10^{-12} M with LODs of $1.8 \pm 0.04 \times 10^{-17}$ M and $1.3 \pm 0.01 \times 10^{-16}$ M by DPV and EIS, respectively. This work was well supported by real water samples, thereby can be considered a report in T-Hg^{2+}-T motif featured electrochemical sensors.

Similar results were reported from many MOFs-based electrochemical sensors with fM LODs [130][131][132]. Wherein, the Cu-based MOFs (**Cu-MOFs**), thioether side groups attached Zr-based MOFs (**S-Zr-MOFs**), and 2D-Co-based MOFs (**PPF-3** nanosheets) were engaged in the fabrication of **Cu-MOFs**/Au, **S-Zr-MOF**/SPE (SPE represents screen printed electrode), and anchor−Au NPs@**PPF-3** attached DNB/depAu/GCE (Au NPs, anchor, anchor, DNB, and depAu/GCE represent gold nanoparticles, dibenzocyclooctyne (DBCO), 3D DNA "nanosafe-box", and gold nanoparticle-coated glassy carbon electrode, represtively) electrodes towards the specific detection of Hg^{2+} ions. The GCE/AuNPs/DNA_2 sensor was incubated in a mixture of **Cu-MOFs**/DNA_1 probes (T-rich DNA used in study) and Hg^{2+}. It demonstrated a linear DPV response from 10 fM to 100 nM with a LOD of 4.8 fM and also real time applications [130]. Similarly, the **S-Zr-MOF**/SPE showed a linear differential pulse anodic stripping voltammetry (DPASV) response for Hg^{2+} between 0.03 nM to 3 µM with a LOD of 7.3 fM via multiple Hg-S interaction (by thio-ether side chains) and T-Hg^{2+}-T formation [131]. By dropping the anchor−AuNPs@**PPF-3** [the **PPF-3** was synthesized by solvothermally reacting $Co(NO_3)_2·6H_2O$, 5,10,15,20-tetrakis(4-carboxyl-phenyl)-porphyrin (TCPP), and 4′-bipyridine (BPY)] over the surface of DNB/depAu/GCE, the proposed electrode fabrication was completed.

The electrode was subjected to Hg^{2+} detection to reveal a linear DPV response between 0.1 pM to 10 nM with a LOD of 33 fM [132]. Next, the **Cu-MOF**-mediated Hg^{2+} detection by means of differential pulse voltammetry (DPV) and cyclic voltammetry (CV) tactics in 0.1 M phosphate buffer (PB) at pH 9 was reported by Singh and co-workers [133]. In the report, $CuNO_3{\cdot}3H_2O$ and 2-aminoterephthalic acid were solvothermally reacted to afford porous **Cu-MOF** nanoparticles, which could absorb large amount of Hg^{2+}. Through coupling with the GCE, the Cu-MOF detected Hg^{2+} linearly in concentrations from 0.1 to 50 nM with a LOD of 0.0633 nM. Reliability of this work was well demonstrated by the real tuna-fish and tap water samples investigations.

Thereafter Kokkinos and co-workers proposed utilization of the **Ca-MOF** modified working electrodes towards 3D-printed lab-in-a-syringe voltammetric cell mediated electrochemical detection of Hg^{2+} [134]. The **Ca-MOF**, namely **$[Ca(H_4L)(DMA)_2]{\cdot}2DMA$**, where H_6L and DMA represent N,N′-bis(2,4-dicarboxyphenyl)-oxalamide and N,N-dimethylacetamide), showed exceptional selectivity to Hg^{2+}. Moreover, the voltammetric lab-in-a-syringe device consisted of a vessel assimilating two thermoplastic conductive electrodes (act as counter and pseudo-reference electrodes) was fabricated by a single-step process. A small detachable 3D-printed syringe loaded with a graphite paste/**Ca-MOF** mixture was used as a working electrode. The Ca-MOF participated in the ion exchange to form "**Hg@CaMOF**". The device showed a linear response to Hg^{2+} with concentrations between 2–40 μg L^{-1} and a LOD of 0.6 μg L^{-1}. Practicality of this work was also demonstrated in the fish oil and bottle water samples.

In contrast to direct electrochemical sensors, Zhang et al. proposed the MOF-involved light driven electrochemical (photoelectrochemical; PEC) sensor for Hg^{2+} discrimination as described next [135]. Firstly, $Co(NO_3)_2{\cdot}6H_2O$ and 2-methylimidazole were solvothermally reacted to afford the ZIF-67. The **ZIF-67** was then reacted with $Cd(NO_3)_2{\cdot}4H_2O$ and thioacetamide (TAA) to yield the **CoSx@CdS** nanocomposites (CdS nanoparticles were grown over the surface of cobalt sulfide (CoSx) by using ZIF-67 polyhedrons as the sacrificial templates and cobalt precursors). The synthesized composite was drop casted on the ITO electrodes to engage in the photoelectrochemical sensing of Hg^{2+} as illustrated in **Figure 8**.

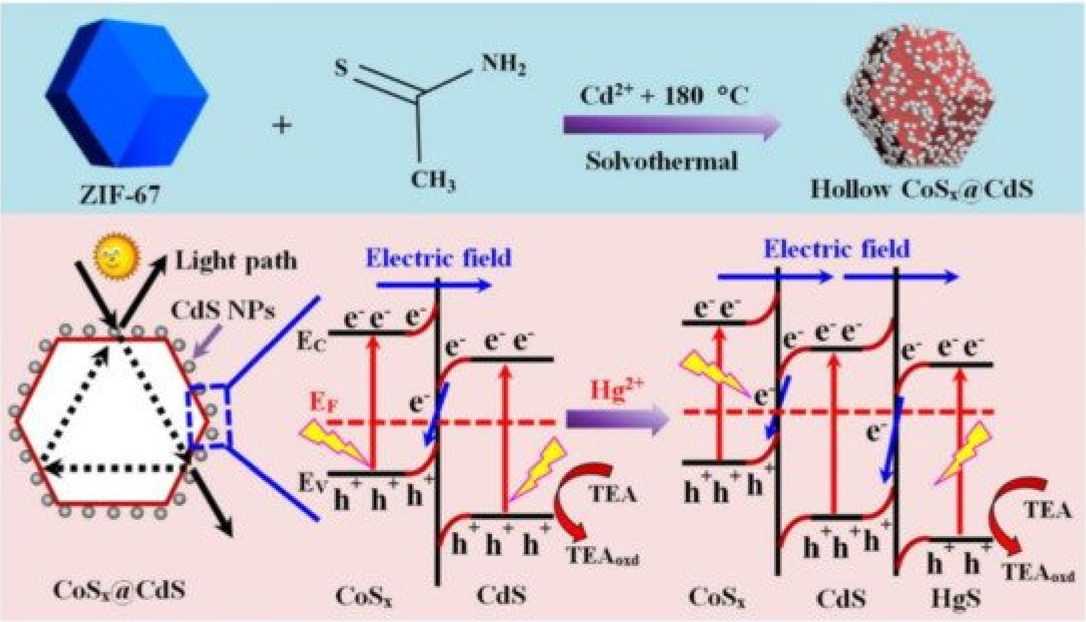

Figure 8. Synthetic process of hollow **CoS_x** polyhedrons and **CoS_x@CdS** composites and the mechanism of photocurrent responses of **CoS_x@CdS** composites, showing the band structures of **CoS_x@CdS/HgS** composites and charge separation under the visible-light illumination (Reproduced with the permission from Ref [135]).

In the presence of Hg^{2+} ions in PBS (pH 7.4) containing 0.15 M triethanolamine (TEA) (see **Figure 8**), carrier transport and photocurrent of the device were improved and enhanced under illumination due to the combined CoS_x and CdS components. In fact, the ion-exchange reaction took place to trigger in-situ generation of **CoS_x@CdS/HgS** (new Z-scheme heterojunction photocatalyst) during the detection process. This sensor showed a linear response to Hg^{2+} with concentrations between 0.010–1000 nM and a LOD of 2 pM. It was also validated by tap and lake water analysis.

8. MOFs in Removal of Hg^{2+}

Other than optical and electrochemical recognition of metal analytes, MOFs were also engaged in the selective removal heavy metal ions [136]. In this section, removal/extraction of Hg^{2+} in particular was described in detail. Many Zr-based MOFs displayed great adsorption capacity to Hg^{2+} due to their porous nature. For example, Kahkha and co-workers described the consumption of mesoporous porphyrinic containing Zr-MOF-**PCN-222/MOF-545** for effective pipette-tip solid-phase extraction of Hg^{2+} [137]. The MOF was solvothermally synthesized by reacting meso-tetrakis(4-carboxyphenyl)porphyrin (H_2TCPP) and $ZrOCl_2·8H_2O$. The as-synthesized MOF was then inserted into a Bio Plas pipette-tip attached to a 2000-μL micro pipette for Hg^{2+} adsorption. It was shown that 2 mg of MOF- sorbent was enough to accomplish extraction and desorption of Hg^{2+} up to 15 cycles at pH 5 by using 10% HCl as eluting solvent (fixed at 15 μL volume). A LOD of this method was estimated as 20 ng L^{-1} with an adsorption capacity (contrast to other ions), enrichment factor, and total extraction time of 35.5 mg g^{-1}, 120-fold, and 7 min, respectively. This work was demonstrated for Hg^{2+} determination in the fish samples, however, information regarding the BET surface area and Langmuir/Freundlich isotherms requires further interrogations. Hasankola et al. engaged the MOF-**PCN-221** (synthesized by solvothermal reaction), which comprised of 5,10,15,20-tetrakis(4-carboxyphenyl) porphyrin (H_2TCPP) organic linker and ‘Zr’ metal node, towards selective removal of Hg^{2+} [138]. Wherein the time required for Hg^{2+} adsorption was 30 min at an optimal pH of 7.1 and an adsorption capacity of **PCN-221** was established as 233 mg g^{-1}. Be noted that the adsorption process of Hg^{2+} by **PCN-221** can be properly interpreted with the pseudo-second-order kinetic model (with $R^2 = 0.99$) and followed the Langmuir model adsorption isotherms for Hg^{2+}. Investigations on the Hg^{2+} adsorption mechanism indicated that Hg^{2+} could not be replace with Zr ions. For the desorption process, 0.01 M HNO_3 was used. This work requires more investigations for the BET surface area, practicality, and structural features.

Li et al. described the utilization of porous and highly defective Zr-based MOF-UIO-66-$Zr_6(OH)_4O_4(BDC)_6$ (where BDC represents benzene-1,4-dicarboxylate), namely **UIO-66-50Benz** (Benz represents benzene-1,4-dicarboxylate), for Hg^{2+} removal [139]. By means of topotactic transformations of MOFs and ligand extraction process, **ZrOx** (obtained by immersion of **UIO-66-50Benz** in 10 mol L^{-1} NaOH), **ZrOxyPhos** (obtained by immersion of **UIO-66-50Benz** in 210 mM Na_3PO_4), and **ZrSulf** (obtained by immersion of **UIO-66-50Benz** in 250 mg of Na_2S solution in 10 mL) were developed and engaged in Hg^{2+} removal as seen in **Figure 9**.

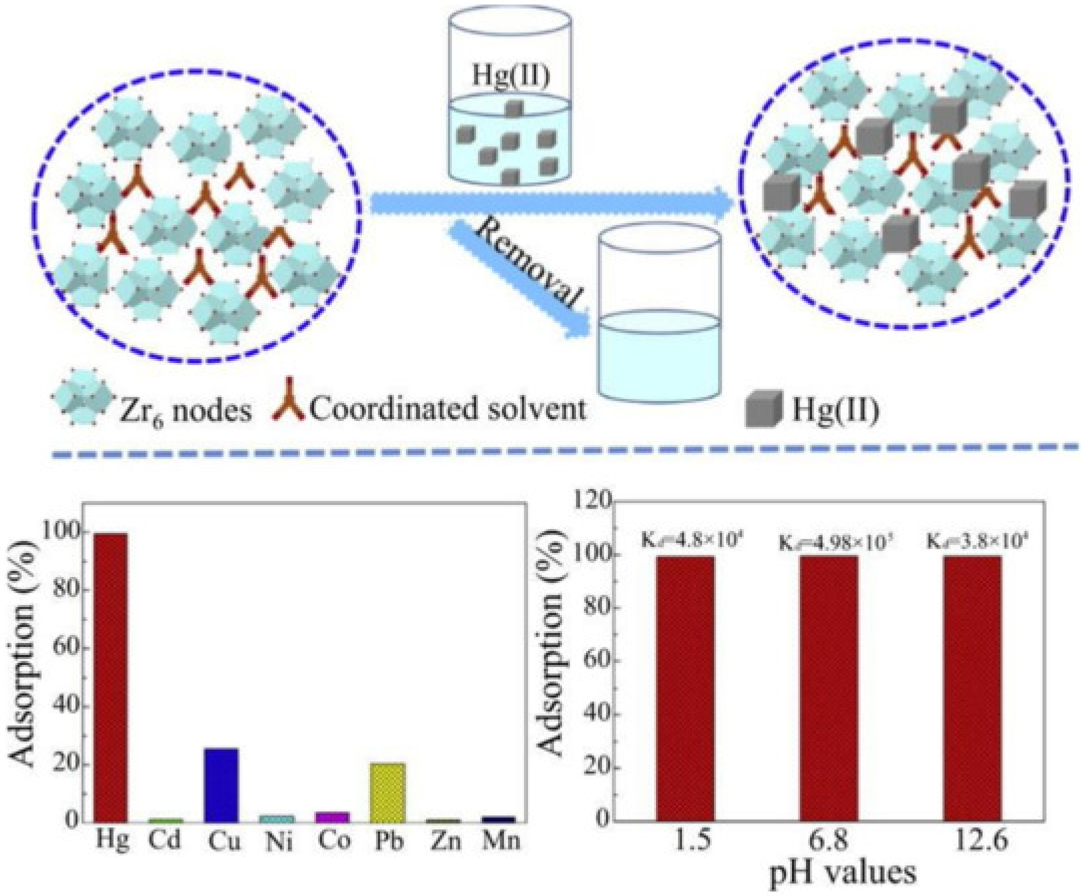

Figure 9. Schematic of the utilization of highly defective Zr-based porous MOFs- **ZrOx**, **ZrOxyPhos**, and **ZrSulf** towards Hg^{2+} removal and excellent Hg^{2+} removal performance by **ZrSulf** compared to other metal ions and at different pH ranges; coordinated solvents NaOH, Na_3PO_4, and Na_2S were used to afford **ZrOx**, **ZrOxyPhos**, and **ZrSulf**, respectively. (Reproduced with the permission from Ref [139]).

The BET surface area of **ZrOx**, **ZrOxyPhos**, and **ZrSulf** were estimated as 430, 290, and 560 m^2 g^{-1}, correspondingly, which also confirmed the high effectiveness of **ZrSulf**. Among these materials, **ZrSulf** possessed the fastest adsorption kinetics (1.1×10^{-2} g (mg min)$^{-1}$ and the highest adsorption capacity of 824 mg g^{-1}. The distribution coefficient (K_d) of **ZrSulf** to Hg^{2+} was estimated as 4.98×10^5 mL g^{-1} at pH 6.8 Moreover, it was reusable for more than five cycles after washing with HCl and thio-urea. The high selectivity of Hg^{2+} was attributed to the covalent bond formation with sulfur-based functionality. From kinetic studies, it was established that the adsorption followed the pseudo-second order model and, at the same time, controlled by the film diffusion and pore diffusion. This material can be considered as a good candidate for Hg^{2+} removal in terms of its adsorption capacity and practicality.

Subsequently, Leus and co-workers solvothermally synthesized the thiolated Zr-based MOF-**UIO-66-(SH)$_2$** (by reacting $ZrOCl_2.8H_2O$ and 2,5-dimercaptoterephthalic acid-(H_2BDC-2,5SH)) and applied it for selective removal of Hg species [140]. The Langmuir surface area of **UIO-66-(SH)$_2$** was estimated as 499 m^2 g^{-1}. The **UIO-66-(SH)$_2$** showed a maximum Hg^{2+} adsorption capacity of 236.4 mg g^{-1} between pH 3.0–5.0. Due to the presence of -SH group, adsorption of Hg^{2+} showed the best fit with Langmuir isotherm and followed the pseudo-second order kinetics. Moreover, adsorption and desorption of Hg^{2+} can be extended up to three cycles by using 1 M HCl and 0.66 M thiourea. This work was also applied in waste water-based Hg^{2+} removal. The use of thiolated **UIO-66-SH** (an archetypal thiolated Zr-based MOF- $Zr_6(OH)_4O_4(BDC)_6$, where BDC represents benzene-1,4-dicarboxylate) towards Hg species removal applications was also demonstrated by Li and co-workers [141]. However, the presence of Zn^{2+} and Pb^{2+} may reduce the adsorption of Hg^{2+} by **UIO-66-SH**.

Next, Fu et al. employed the post-functionalized **UIO-66-NH$_2$** (Zr-based MOF) with 2,5-Dimercapto-1,3,4-thiadiazole to produce the **UIO-66-DMTD** for effective removal of Hg^{2+} in water [142]. Due to the Hg^{2+} adsorption over the MOF surface, the calculated BET surface area of **UIO-66-DMTD**-Hg decreased from 651 $m^2\ g^{-1}$ to 42 $m^2\ g^{-1}$, thereby confirming the adsorbing ability of the proposed MOFs. The maximum adsorption of Hg^{2+} was 670.5 mg g^{-1} at pH 3. The adsorption kinetic followed the pseudo-second-order and was linearly fitted with Langmuir isotherm. Moreover, selectivity to Hg^{2+} by the **UIO-66-DMTD** and its analogous (**UIO-66-NH$_2$** and **UIO-66-SO$_3$H**) was higher than that of other species as seen in **Figure 10**.

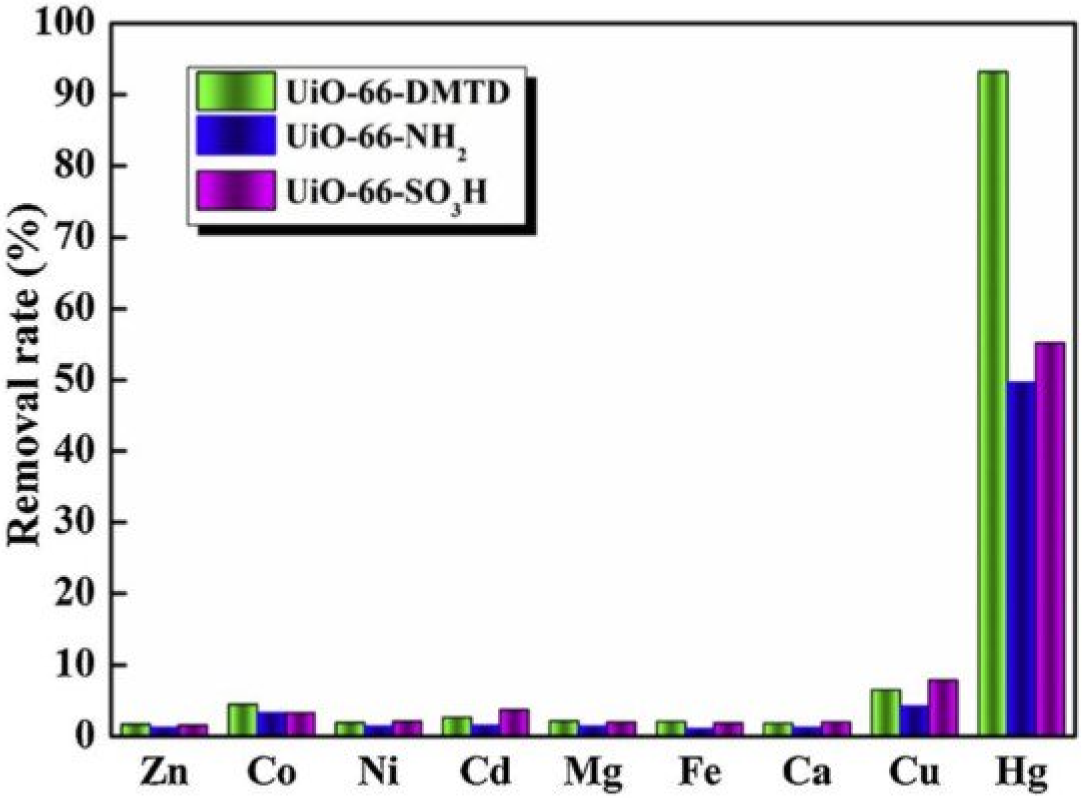

Figure 10. Selective removal of Hg^{2+} by **UIO-66-NH$_2$**, **UIO-66-SO$_3$H** and **UIO-66-DMTD** (Reproduced with the permission from Ref [142]).

At a fixed Hg^{2+} removal time of 120 min, recyclable usage of the **UIO-66-DMTD** was found to be effective up to 10 times. The Hg^{2+} removal is highly fascinated and can be effective in the lab wastewater-based extraction due to the high affinity of thiol (-SH) group to Hg^{2+}.

Similar to the MOF-**UIO-66-(SH)$_2$** [140], Ding and co-workers proposed the Zr-based MOF-**Zr-DMBD** (synthesized by reacting 2,5-Dimercapto-1,4-benzenedicarboxylic acid (H_2DMBD) and $ZrCl_4$) for Hg^{2+} removal [143]. However, due to a high degree of similarity to the **UIO-66-(SH)$_2$**-based research, this work will not be further discussed. Regarding the effectiveness of thiol functionalized or thiol comprising MOFs towards removal of Hg^{2+} species, Li et al. described the utilization of dense thiol arrays containing Zr-based MOF, namely **ZrOMTP** (via reacting 4,4′,4″,4‴-(pyrene-1,3,6,8-tetrayl)tetrakis(2,6-dimercaptobenzoic acid)(H_4OMTP) with $ZrCl_4$), in Ref. [144]. The BET surface area of **ZrOMTP** to N_2 gas was estimated as 1290 m^2 g^{-1} and the distribution coefficient (K_d) for Hg^{2+} was calculated as 1.60×10^8 mL g^{-1}, which is far better than that of other thiol containing MOFs. This could be attributed to the dense thiol arrays present in **ZrOMTP** framework. Adsorption of Hg^{2+} followed the first order kinetic model and was best fitted with Langmuir isotherms. Moreover, this MOFs lowered Hg-based contaminants from ppm to below the allowed drinkable limit of 2 ppb.

Highly dense alkyl thiol comprising MOF-**Zr-MSA** was developed by hydrothermally reacting $ZrCl_4$ and mercaptosuccinic acid (HOOC-CHSH-CH_2-COOH, **MSA**) in aqueous phase and was engaged in Hg^{2+} removal [145]. The **Zr-MSA** showed an adsorption efficiency of 99.99% to Hg^{2+} in a pH range of 0–7 pH within 5 min and was reusable (with 6 M HCl) for up to five cycles. Moreover, the **Zr-MSA** showed a maximum adsorption capacity of 734 mg g^{-1} and a K_d value of 1.82×10^8 mL g^{-1}, which was best correlated with Langmuir isotherm. Due to the higher affinity of -SH to Hg^{2+}, this work reduced the Hg content from 10,000 ppb to 0.11 ppb, which was far below the drinking water limit. In addition to thiol containing MOFs, the **Zr-MOFs** (**Zr-MOFs-SH(O)**) was synthesized by one-pot reaction of $ZrCl_4$, meso-tetra(4-carboxyphenyl)porphine (H_2TCPP), and modulators—mercaptoacetic acid (MAA) or alpha lipoic acid (ALA)—and was employed in Hg^{2+} adsorption [146]. For comparison, the **Zr-MOFs-SH(P)** was synthesized via post-synthetic modification of the **Zr-MOFs-SH(O)** and was engaged in adsorption studies. Due to the higher -SH content in the **Zr-MOFs-SH(O)**, it showed a higher adsorption capacity (for Hg^{2+}) of 843.6 mg g^{-1} than that of the **Zr-MOFs-SH(P)** (138.5 mg g^{-1}). Hg^{2+} adsorption of the **Zr-MOFs-SH(O)** followed the pseudo-second-order kinetic model and was best fitted with Langmuir isotherm. In addition, this study showed good selectivity, recyclability, and chemical stability. By functionalizing the **NH$_2$-UIO-66** with L-cysteine, the **Cys-UIO-66** was obtained and was used for Hg^{2+} removal from solution [147]. The **Cys-UIO-66** showed a maximum adsorption capacity of 350.14 mg g^{-1} (after 180 min) at pH 5.0 of Hg^{2+} adsorption which followed the pseudo-second-order model and was fitted with Langmuir isotherm. Due to the -SH (from cysteine) affinity to Hg^{2+}, reusability of Hg^{2+} adsorption/desorption was up to five cycles (with 0.1 M HNO_3 and 1% thiourea solution). In terms of the capacity and time consumption, this study could need more improvements. By following the similar approach, Liu and co-workers presented the cysteamine functionalized **MOFs-MIL-101-SH (Cr)** and **UIO-66-SH (Zr)** for Hg^{2+} removal [148]. The MOFs showed adsorption capacities of 10 and 250 mg g^{-1} at pH of 5, respectively, with certain reusability.

By utilizing four different types of organic ligands with bulky sulphur side chains, four Zr-based MOFs, namely **Zr-L1**, **Zr-L2**, **Zr-L3**, and **Zr-L4** (Zr(IV)-carboxylate frameworks; where **L1-L4** represents the deprotonated four thioether-equipped carboxylic acid linker molecules), were constructed for selective removal of Hg^{2+} ions [149]. The K_ds values of **Zr-L1**, **Zr-L2**, **Zr-L3**, and **Zr-L4** were estimated as 1.95×10^3 mL g^{-1}, 1.47×10^4 mL g^{-1}, 4.47×10^3 mL g^{-1}, and 2.40×10^4 mL g^{-1}, respectively. Moreover, Hg adsorption of **Zr-L1**, **Zr-L2**, **Zr-L3**, and **Zr-**

L4 followed the Langmuir isotherm with capacities of 193 mg g^{-1}, 275 mg g^{-1}, 245 mg g^{-1}, and 322 mg g^{-1} at pH 6.8, correspondingly. However, this work needs further investigations on interference studies and real time applications. The Zr-based MOF-**DUT-67 (Zr)** synthesized by solvothermal reaction of zirconium chloride with 2, 5-thiophene-dicarboxylic acid showed removal efficiencies for Hg^{2+} and CH_3Hg^+ from 69% to 90% and from 30% to 77%, respectively [150]. At pH 6, the **DUT-67 (Zr)** showed a great efficiency to Hg^{2+} and CH_3Hg^+ with adsorption capacities of 0.0451 mg g^{-1} and 0.0374 mg g^{-1}, respectively. The adsorption followed the pseudo-second-order kinetic model. This work was also demonstrated in river and lake water samples, but mechanism and interference studies require further investigations. The ZrO_2-based **(MOF)-808** synthesized by a sol-gel method was grafted with amidoxime (AO) via wet-chemistry process to afford **MOF-808/AO**, which was used in Hg^{2+} removal and displayed high efficiencies [151]. In particular, the **MOF-808/AO** showed a higher adsorption efficiency in all pHs. The BET surface area of **MOF-808** and **MOF-808/AO** were established as 2152 and 1899 m^2 g^{-1}, respectively. Moreover, adsorption capacities of **MOF-808** and **MOF-808/AO** towards Hg^{2+} were estimated as 383.8 mg g^{-1} and 343.6 mg g^{-1} (at 70 min), correspondingly. The Hg^{2+} adsorption in both MOFs followed the pseudo-second-order kinetic model and was fitted with Langmuir isotherms. This work requires more efforts to obtain additional information on the mechanism, interference effect, and real time analysis.

The Zr-based MOFs and Zn-metal nodes comprising MOFs were also engaged in Hg^{2+} removal as detailed next. The $Zn_2(DHBDC)(DMF)_2{\cdot}(H_2O)_2$, namely **MOF-74-Zn**, was synthesized by solvothermally reacting $ZnNO_3$ and 2,5-dihydroxy-1,4-benzenedicarboxylic acid (DHBDC) and was applied in Hg^{2+} removal [152]. The **MOF-74-Zn** showed a maximum adsorption capacity of 63 mg g^{-1} (for Hg^{2+} at pH 6 in 90 min). The Hg^{2+} adsorption followed the pseudo-second-order kinetic model but was best fitted with the Langmuir isotherm rather than the Freundlich isotherm. The -OH group was directly involved in adsorption of Hg^{2+}. However, this work showed a minimum adsorption capacity and lacked information on the interference effect. Wang and co-workers presented the Zn-based MOF, namely **NTOU-4** (hydro(solvo)thermally synthesized by reacting $ZnNO_3$ with 1H-1,2,4-triazole-3,5-diamine and 1,4-benzenedicarboxylate organic linkers) for Hg^{2+} removal applications [153]. The **NTOU-4** showed an adsorption capacity of 163 mg g^{-1} at 30 min and was operable between pH 3–11. However, the underlying mechanism, kinetic model, and isotherm studies require further clarification. Next, Esrafili et al. described the utilization of dual functionalized Zn-based MOF, namely **TMU-32S** (synthesized by incorporation of different percentile of N1,N3-di(pyridine-4-yl) malonamide in **TMU-32** (a Zn containing MOF with urea linkers)), towards Hg^{2+} adsorption and removal [154]. Due to the strong binding forces produced by urea and malonamide functional units, the **TMU-32S** showed a high adsorption capacity of 1428 mg g^{-1} (in just 17 min) and became more efficient at pH 4.4. The system followed the linear pseudo-second-order model and was linearly fitted with the Langmuir isotherm. Moreover, the material showed adsorption and desorption (with 0.2 M of EDTA) up to three cycles with 65% efficiency. This work requires more studies regarding the interference effect with several metal analytes.

Subsequently, the Cu-based MOFs were authorized as efficient adsorbents for Hg^{2+} removal as described next. Wu et al. developed the copper and 3,30,5,50-azobenzenetetracarboxylic acid containing porous MOF, namely **JUC-62**, for Hg^{2+} removal in tea and mushroom samples [155]. The adsorption capacity of the **JUC-62** to Hg^{2+} was established as 836.7 mg g^{-1} at pH 4.6 in 15 min in aqueous media. This work followed the pseudo-second-order model and was fitted with Langmuir adsorption isotherm. Moreover, it was reusable with EDTA up to four cycles. However, further interrogations are required on the interference studies. Mon and co-workers described utilization of a Cu-based MOF, namely **$\{Cu_4^{II}[(S,S)\text{-methox}]_2\}.5H_2O$** (where methox represents bis[(S)-methionine]oxalyl diamide), for $HgCl_2$ removal studies [156]. This microporous MOF was decorated with thioalkyl chains, thereby was able to adsorb $HgCl_2$ efficiently to afford the $HgCl_2S_2$ adduct. This MOF adsorbed 99.95% of $HgCl_2$ within 15 min and reduced the Hg^{2+} concentration from 10 ppm to below 2 ppb in drinking water. However, this work lacked information on the reusability, kinetic studies, and real applications. Next, the polysulfides functionalized benzene-1,3,5-tricarboxylic acid and Cu containing **S_x-MOF** (where MOF represents Cu-BTC (by solvothermal tactic) and S_x^{2-}, X = 3, 4, 6) were described for efficient adsorption of Hg^{2+} [157]. Among these materials, the **S_4-MOF** displayed great selectivity to Hg^{2+} with a LOD of 0.13 μg L^{-1} and a linear response from 30–200 μg L^{-1} at pH 6 in 30 min. The **S_4-MOF** showed different adsorbing capacities to different metal ions in the following orders: Hg(II) > > Pb(II) > Zn(II) > Ni(II) > Co(II). By means of Hg^{2+}-S bonding, adsorption was efficient and applicable in sea, tap, and wastewater. However, information regarding kinetic studies is still missing. A copper metallacycle complex, namely **$Cu_2(PDMA)_2(DMF)$** (comprised of 3,3′-((1E,1′E)-(pyrimidine-4,6-diylbis(2-methylhydrazin-2-yl-1-ylidene)) bis (methanylylidene)dibenzoic acid (H_2PDMA)), was demonstrated for Hg^{2+} removal [158]. Due to the multi ‘N′ binding sites, the MOF showed an adsorption efficiency of 61.4% for Hg^{2+} (among Hg^{2+}, Mn^{2+}, Cd^{2+}, Pb^{2+} ions) with an adsorption capacity of 300 mg g^{-1}. Moreover, this MOF was reusable with EDTA. The Hg^{2+} adsorption followed the pseudo-second-order kinetic model. Xu and co-workers proposed utilization of the **SH@Cu-MOF** towards adsorption of Hg^{2+} and $Hg^{(0)}$ species by grafting dithioglycol from the post-synthetic modified **Cu-MOF** (Cu with 5-aminoisophthalic) [159]. Though the material seems to be impressive compared to others reports, however, its adsorption capacity (173 mg g^{-1} in 6 h) was not up to standard. However, this work does point to a new direction for future development of the Cu-based MOFs.

Liang and co-workers described utilization of the sulfur-functionalized Co-based MOF, namely **FJI-H12** (composed of NCS^-, Co(II) and 2,4,6-tri(1-imidazolyl)-1,3,5-triazine (Timt)), for Hg^{2+} removal in water [160]. The **FJI-H12** showed a K_d value of 1.85 × 10^6 mL g^{-1} with an adsorption capacity of 439.8 mg g^{-1} at pH 7. The adsorption was efficient because of the Hg^{2+} to S (of SCN^-) affinity and it could be applied for continuous removal purpose. Moreover, this work followed the pseudo-second-order kinetic model and was also reusable, thereby is attested a nice work. Jiang et al. designed a stable sulfur containing Co-based MOF $\{[Co_3(\mu_3\text{-}OH)(DMTDC)_3(INT)_3]\text{-}[Co_2(OH)(H_2O)_2](NO_3)_{19}\text{-}(H_2O)_7(DMA)_{11}\}_n$, namely **NENU-401** (where DMTDC, INT, DMF, and DMA represent 3,4-dimethylthieno[2,3-b]thiophene-2,5-dicarboxylic acid, isonicotinate, N,N-dimethylformamide, and N,N-dimethylacetamide), via introducing an INT group in **NENU-400**-$\{[Co_3(\mu_3\text{-}OH)(H_2O)_3(DMTDC)_3](NO_3)_{10}\text{-}(H_2O)_6(DMF)_6\}$ and utilized it successfully in Hg^{2+} removal [161]. Unlike the **NENU-400**, which collapsed easily during Hg^{2+} adsorption, the **NENU-401** preserved its structural features, thereby was highly applicable for Hg^{2+} extraction. The K_d value of NENU-401 at 25 °C was estimated as 8.3 × 10^6 mL g^{-1} with an adsorption capacity of 596.57 mg g^{-1} in 10 min. The **NENU-401** performed far better than many thiol containing MOFs. Moreover, Hg^{2+} extraction by the **NENU-401** was recovered up to 90% of its original by thioglycol solution and was reusable for more than four cycles because of the effective coordination between Hg^{2+} and ‘-S′ atom. Note that the **NENU-401**-based Hg^{2+} extraction followed the pseudo-second-order kinetic model and was linearly fitted with Langmuir isotherm. This work demonstrated an impressive approach to improve the structural stability of MOFs.

Moreover, it also displayed certain selectivity to Pb^{2+} (nearly 70%) but still required further optimization. Recently, Sun′s research group proposed employment of the sulfur-rich two-dimensional (2D) Co-based MOF nanosheets, namely **2D-NCS** ($\{[Co(NCS)_2(pyz)_2]\}_n$; where pyz represents pyrazine), for exceptional removal of $HgCl_2$ [162]. The BET surface area of **2D-NCS** to N_2 gas at 77K was established as 365 $m^2\ g^{-1}$ with a maximum adsorption capacity of 1698 mg g^{-1} in 15 min and a K_d value of 2.26×10^6 mL g^{-1}. The MOF nanosheets reduced Hg^{2+} concentrations from 10 ppm to 1 ppb within 15 min and were also effective in environmental samples between pH 4–9. This work followed the pseudo-second-order model and was fitted with Langmuir isotherm. Due to the strong Hg–S interactions, extraction was efficient up to five cycles (by thioglycol solution) and could be further tuned towards development of 3D materials for future environmental remediation. Similar to the **FJI-H12** [152], another Co-based MOF- $[Co_3(SCN)_6(TPMA)_4]n$, namely **FJI-H30** (synthesized by solvothermally refluxing TPMA (tris(pyridin-4-ylmethyl)amine) and $Co(SCN)_2$), was engaged in Hg^{2+} adsorption [163]. Due to the exceptional interaction between SCN^- groups to Hg^{2+}, its maximum adsorption capacity reached 705 mg g^{-1} with negligible interference. The BET surface area of **FJI-H30** to CO_2 gas at 195K was determined as 221 $m^2\ g^{-1}$. This material showed a K_d value of 1.84×10^5 mL g^{-1} and operated efficiently between pH 4–9 with regeneration (by KSCN solution) of >90% up to three cycles. This work followed the pseudo-second-order model and was fitted with Langmuir isotherm. It can be applied in industrial waste water, thereby is considered a nice work.

Halder et al. engaged the thiocyanato ligand (SCN^-) comprising Ni-based 3D MOF, namely **$[Ni(3\text{-}bpd)_2(NCS)_2]_n$** (where 3bpd represents 1,4-bis(3-pyridyl)-2,3-diaza-1,3-butadiene), for effective removal of Hg^{2+} in aqueous solution [164]. Because the uncoordinated S atom of SCN^- was strongly bonded with Hg^{2+} and formed the mercuric thiocyanate adduct, therefore, a great adsorption capacity of 713 mg g^{-1} was achieved. Nevertheless, this work still requires further optimization for the interference effect, adsorption kinetics, and practicality. A post-synthetic modified tactic was proposed to develop the thiol (-SH) functionalized In-based MOF, namely **SH-MIL-68(In)** (primarily **NH_2-MIL-68(In)** obtained by solvothermally reacting 2-amino-benzene-1, 4-dicarboxylic acid (NH_2-H_2BDC) with In $(NO_3)_3$ followed by post-synthetic modification), towards Hg^{2+} extraction [165]. The **SH-MIL-68(In)** showed a highest Hg^{2+} adsorption capacity of 450 mg g^{-1} and a large adsorption rate (rate constant k_2 = 1.25 g $mg^{-1}\ min^{-1}$). As seen in **Figure 11**, the adsorption process took place within 2 min at pH 4 due to the presence of free -SH group.

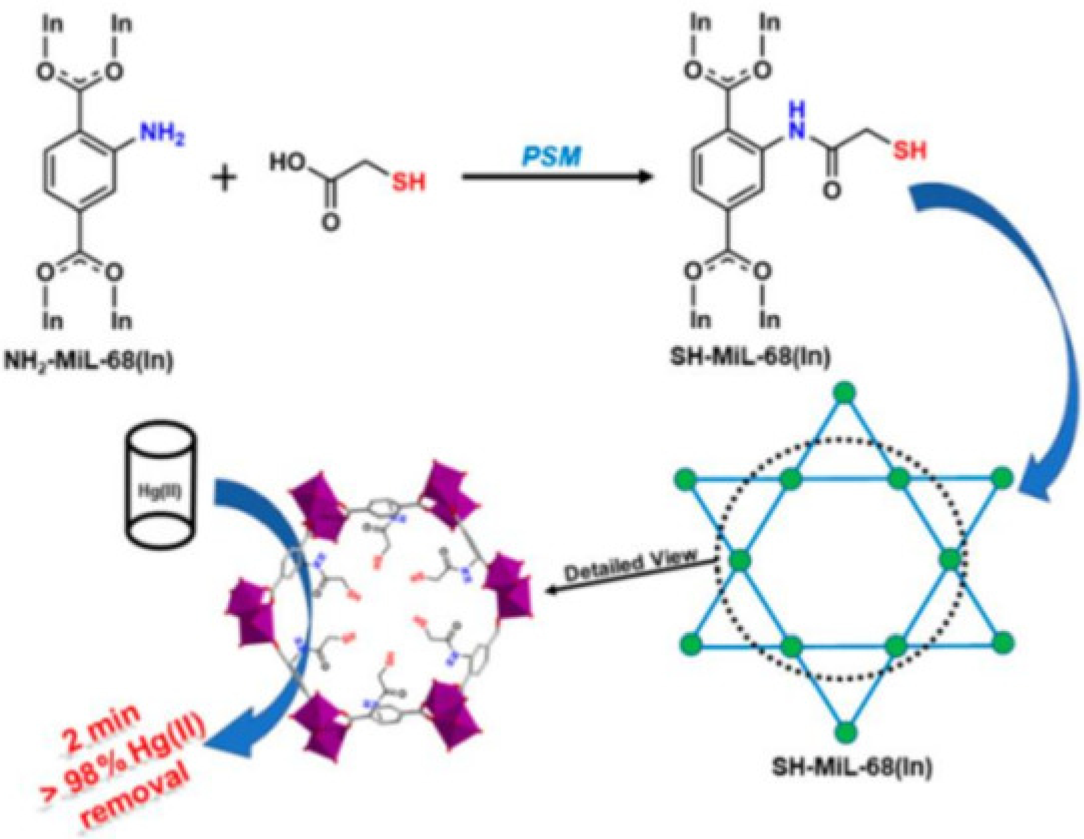

Figure 11. Schematic of post-synthetic modification of **NH_2-MIL-68(In)** to afford **SH-MIL-68(In)** and its utilization in Hg^{2+} extraction (Reproduced with the permission from Ref [165]).

The material was reusable (in the presence of 0.01 M HCl, 0.1% thiourea) up to five cycles. This work followed the pseudo-second-order model and was linearly fitted with Langmuir isotherm. It is an impressive work considering its short process time and negligible interferences. However, real time applicability still needs to be demonstrated. By means of diffusion and solvothermal strategies, Li et al. developed three thioether-based MOFs, namely **$[(ZnCl_2)_3(L_1)_2\cdot{}_\chi(solvent)]_n$-(1), $[(Cu_2I_3O_2)_4(CH_4N_{0.5})_4(L_1)_4(DMA)_4\cdot 3(H_2O)\cdot{}_\chi(solvent)]_n$-(2), and $[(CuBr_2)_2(L_2)_2\ CH_3CN\cdot{}_\chi(solvent)]_n$-(3)** (where L_1 and L_2 represent 1,3,5-tris((pyridin-4-ylthio)methyl)benzene and 2,4,6-trimethoxy-1,3,5-tris((pyridin-4-ylthio) methyl)benzene; DMA = Dimethylacetamide) to utilize them for effective removal of Hg^{2+} in water [166]. These MOFs removed 90% of Hg^{2+} within 5 min at optimum pHs 4 and 5. The maximum adsorption capacities of MOFs **(1)**, **(2)**, and **(3)** were estimated to be 362.3 mg g^{-1}, 227.4 mg g^{-1}, and 341.7 mg g^{-1}, respectively. The observed higher efficiencies to Hg^{2+} was attributed to the strong binding between Hg-S. They were reusable up to five cycles (with Na_2S). This work followed the pseudo-second-order model and was linearly correlated with the Langmuir isotherm. This work is considered a good one because of the negligible interference effect, but further optimization is required to improve the adsorption capacity.

The bi-metallic MOFs were also employed in Hg^{2+} removal/extraction as described next. Han and co-workers constructed the heterometallic metal−organic framework (HMOF): $\{[(CH_3)_2NH_2]InCu_4L_4\cdot{}_xS\}_n$, namely **BUT-52** (where L represents 6,6′-dithiodinicotinic acid), to engage in Hg^{2+} removal, in which $In(COO)_4$ and Cu_6S_6 clusters were rationally embedded [167]. The BET surface area of **BUT-52** to N_2 gas at 77K was 126.2

cm^3 g^{-1}. It showed 92% of mercury removal efficiency in ethanol. This work requires further optimization in anti-interference, pH, time, and real time application studies. Mon et al. described utilization of the Ca and Cu-based porous bimetallic MOF, namely **$\{Ca^{II}Cu^{II}_6[(S,S)\text{-methox}]_3(OH)_2(H_2O)\}\cdot 16H_2O$** (where methox represents bis[(S)-methionine]oxalyl diamide), for Hg^{2+} and CH_3Hg^+ removal in aqueous media [168]. This BioMOF reduced Hg^{2+} and CH_3Hg^+ contents from 10 ppm to 5 and 27 ppb, respectively, with corresponding adsorbing ability of 99.95% and 99.0% (via Hg–S interactions) for dissolved $HgCl_2$ and CH_3HgCl salts. However, optimization is required to study the adsorption kinetics and real applications. In parallel with MOFs-based extraction/removal of Hg^{2+}, a few MOFs were also reported in multiple heavy metal ions, including Hg^{2+} [169][170][171][172][173]. Though those reports demonstrated effective removal of Hg^{2+}, but they were also affected by interfering effects from other ions. To avoid the interfering effects, complicated masking procedure is required. Therefore, those reports will not be discussed in this review.

9. MOFs Comprised Composites for Hg^{2+} Removal

Compared to MOFs, composites comprised of MOFs also become effective in Hg^{2+} removal [174]. For example, the Pt NPs encapsulated **UIO-66-NH_2**-(denoted as Pt NP@**UIO-66-NH_2**) was engaged in facile colorimetric detection and removal of Hg^{2+} in water [175]. The **Pt NP@UIO-66-NH** displayed a linear colorimetric response from 0 to 10 nM with a LOD 0.35 nM due to the peroxidase like activity which took place in the presence of 3,3′,5,5′-tetramethylbenzidine and H_2O_2. Moreover, the **Pt NP@UIO-66-NH_2** was used as an adsorbent for Hg^{2+} with a maximum adsorption capacity of 206.25 mg g^{-1}. This material showed Hg^{2+} removal of 99% and reduced Hg^{2+} concentrations from 5 ppm to 2.39 ppb. Reusability of this composite was established up to four cycles by Na_2S. This work followed the pseudo-second-order model and was linearly fitted with the Langmuir isotherm. With respect to multiple applications, this work is considered a nice one. The mercapto-functionalized Zr-MOF/melamine sponge composite (**Zr-MOF-SH/MF**) was proposed for removal of Hg^{2+} from water [176]. Firstly, zirconium chloride ($ZrCl_4$) was reacted with meso-tetra(4-carboxyphenyl)porphine (H_2TCPP). The product was then interacted with mercaptoacetic acid to afford **PCN-224-MAA**, which formed the composite structure with melamine sponge. In particular, the **PCN-224-MAA/MF** (where MAA and MF represent mercaptoacetic acid and melamine formaldehyde) showed great ability for Hg^{2+} removal (among other heavy metal ions) with a maximum adsorption capacity of 412.5 mg g^{-1} at pH 3 as seen in **Figure 12**. Due to the Hg–S interactions, the removal process was found to be efficient and effective. The presence of melamine sponge extended the Hg^{2+} adsorption cycle up to five times. This work showed more effectiveness in Hg^{2+} removal from water-oil mixture, but the underlying kinetics require further studies.

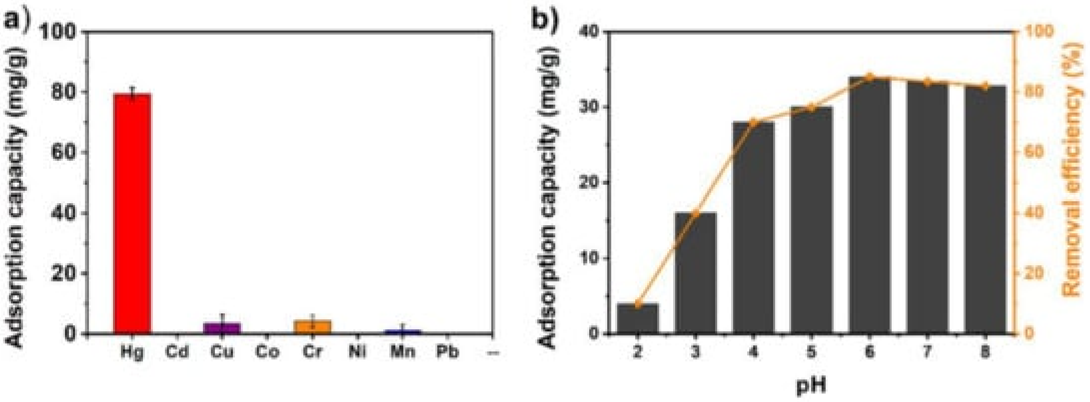

Figure 12. (**a**) Adsorption of mixed heavy metal ions (concentration of each ion was 100 mg L^{-1} on the **PCN-224-MAA/MF** composite at pH 3. (**b**) Effect of pH on the removal of Hg^{2+} ions with an initial concentration of 20 mg L^{-1} on a **PCN-224-MAA/MF** (Reproduced with the permission from Ref [176]).

Novel **ZnS-ZIF-8** monolith was explored in Hg^{2+} capture in wastewater [177]. The **ZIF-8** filter paper was first developed by reacting Zn $(NO_3)_2{\cdot}6H_2O$ with 2-methylimidazole followed by sulfurization to obtain the **ZnS-ZIF-8** monolith, which possessed a hierarchical porous crystalline structure. At an optimum value of pH 5, the monolith showed a maximum adsorption capacity of 925.9 mg g^{-1} with recyclability with Na_2S. The efficiency was found to be high because of the effective Hg–S interaction. This work followed the pseudo-second-order kinetic and was correlated with Langmuir isotherm. This work is considered a nice one in terms of its selectivity and applicability. Nosike and co-workers proposed utilization of the **Fe_3O_4@ZIF-90-Cysteine** composite towards Hg^{2+} adsorption as detailed below [178]. Wherein, the Fe_3O_4 was first embedded into the **ZIF-90** (a Zn-based zeoliticimidazolate framework) as a core. Cysteine was then covalently attached to the **Fe_3O_4@ZIF-90** via Schiff base reaction and post-synthetic modification strategy to obtain the **Fe_3O_4@ZIF-90-Cysteine**. Poly-acrylic acid (PAA) was capped on the above composite to avoid agglomeration of nanoparticles. Because of the pore size and free thiol (-SH) group of cysteine, this composite showed good adsorbing ability to Hg^{2+} with a maximum capacity of 900 mg g^{-1} at optimal pH 4. The adsorption followed the pseudo-second-order model. Desorption and regeneration were accomplished with HCl (0.1 M) up to four cycles. However, the synthetic complications may affect its applicability. Huang et al. described the magnetic MOF composite, namely **bi-I-functionalized Fe_3O_4@SiO_2@HKUST-1** (where HKUST-1 represents Cu-based MOF), with core–shell nanostructures for enhanced removal of Hg^{2+} in water [179]. The bismuthiol I (1,3,4-thiadiazole-2,5-dithiol, Bi-I) was functionalized over the **Fe_3O_4@SiO_2@HKUST-1** via post-synthetic modification. As shown in **Figure 13**, the **bi-I-functionalized Fe_3O_4@SiO_2@HKUST-1** displayed high adsorption ability to Hg^{2+} with a maximum capacity of 264 mg g^{-1} between pHs 2–9. This work followed the pseudo second order model and was linearly fitted with the Langmuir isotherm. In both composites, the Fe_3O_4 was used to afford the magnetic property and played a vital role to improve the adsorption capacity. Performance of the **bi-I-functionalized Fe_3O_4@SiO_2@HKUST-1** was effective in the presence of other competing species. However, the main drawback of this study is that it cannot be reused with any eluent because of the strong Hg–S bond and the hydrolysis of Bi-I. Thereby this material can only be consumed for one-time removal of Hg^{2+} ions in water.

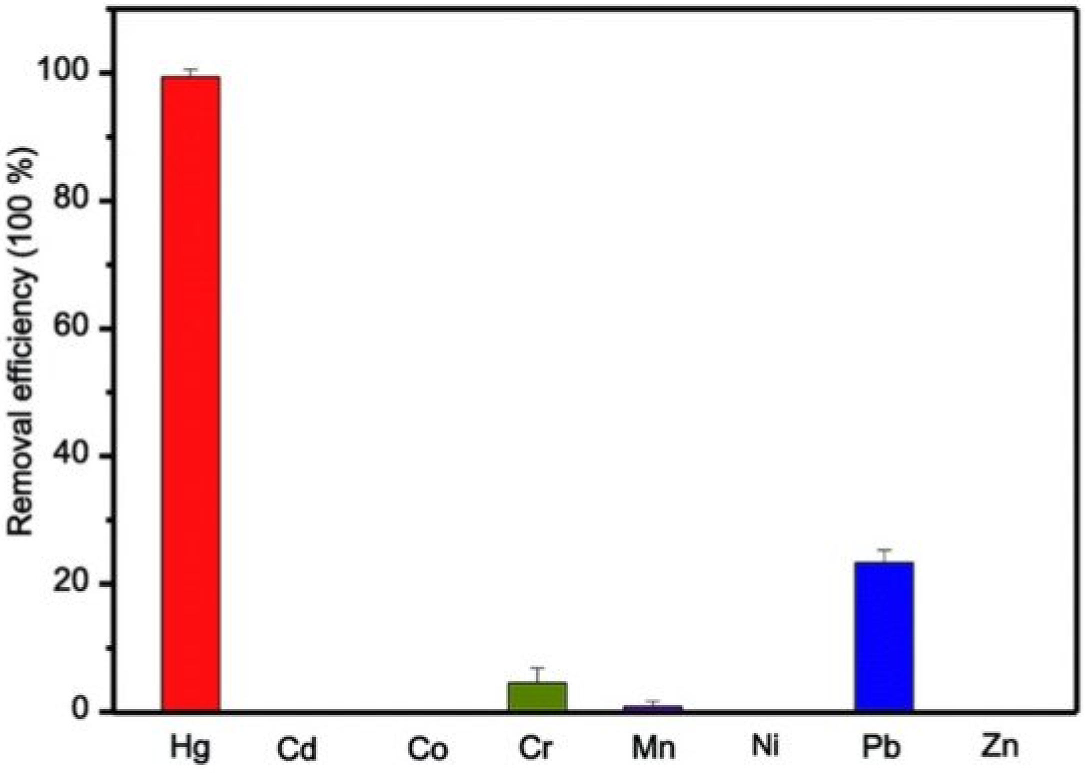

Figure 13. Selectivity of **bi-I-functionalized Fe_3O_4@SiO_2@HKUST-1** for Hg^{2+} conditions: each ion of 10 mg L^{-1} and pH 3 (reproduced with the permission from Ref [179]).

Liang and co-workers reported incorporation of In_2S_3 nanoparticles into the **MIL-101** (a Cr-based MOF) to afford the **In_2S_3@MIL-101** for effective removal of Hg^{2+} with an efficiency of 99.95% within a minute [180]. The BET surface area of the **In_2S_3@MIL-101** to N_2 gas at 77K was 1476 m^2 g^{-1} with a maximum adsorption capacity of 518.2 mg g^{-1} for Hg^{2+}. This work followed the pseudo second order kinetic model and was linearly correlated with the Langmuir isotherm. The strong affinity between Hg^{2+} to S was the main reason for high efficiency of the **In_2S_3@MIL-101**, which was able to reduce Hg^{2+} concentrations from 10 ppm to 1.75 ppb. Moreover, the composite operated between pHs 3 to 8 and was effective in the presence of competing species. By using 0.1 M KCl solution, the materials can be recycled up to three times, thereby is noted a remarkable work. In fact, incorporation of In_2S_3 nanoparticles improves the adsorption ability of MIL-101 to Hg^{2+} ions. Similar to selective removal of Hg species, the MOF containing composites were also engaged in adsorption and capture of Pb^{2+} [181][182][183]. However, those reports will not be discussed in this review due to the possible interference effects.

10. MOFs and Its Analogous in Elemental Mercury (Hg^0) Adsorption

Due to the high toxic effect of elemental mercury (Hg^0) from flue gas, its adsorption and separation is in high demand. Moreover, feasible utilization of MOFs and its analogous have been predicted theoretically [184][185]. For example, Zhao et al. reported Hg^0 removal from flue gas of iron and steel by using the **MIL-101(Cr)**. Performance of the **MIL-101(Cr)** was compared to the **Cu-BTC** (BTC represents benzene-1,3,5-tricarboxylate), **UIO-66**, and activated carbon [186]. Wherein, Hg^0 was primarily adsorbed over the surface of **MIL-101(Cr)** and was oxidized by the open metal site Cr^{3+}. Be noted that the **MIL-101(Cr)** captured 88% of Hg^0 at 250 °C and also showed good thermal and chemical stability. Exceptional adsorption ability of the **MIl-101(Cr)** was further demonstrated by Dong and co-workers through Hg^0 removal from the coal-fired boiler flue gas experiment [187]. Simulation studies also agreed with the experimental results, in which Hg^0 adsorption over the **MIL-101(Cr)** surface followed the pseudo-second-order model as shown in **Figure 14**. Moreover, the **MIl-101(Cr)** showed the Langmuir-type rate expression with an estimated equilibrium adsorption capacity for the MOF-sorbent of 25.656 μg g^{-1} at 200 °C. Thus, the **MIL-101(Cr)** is considered a potential candidate for Hg^0 removal.

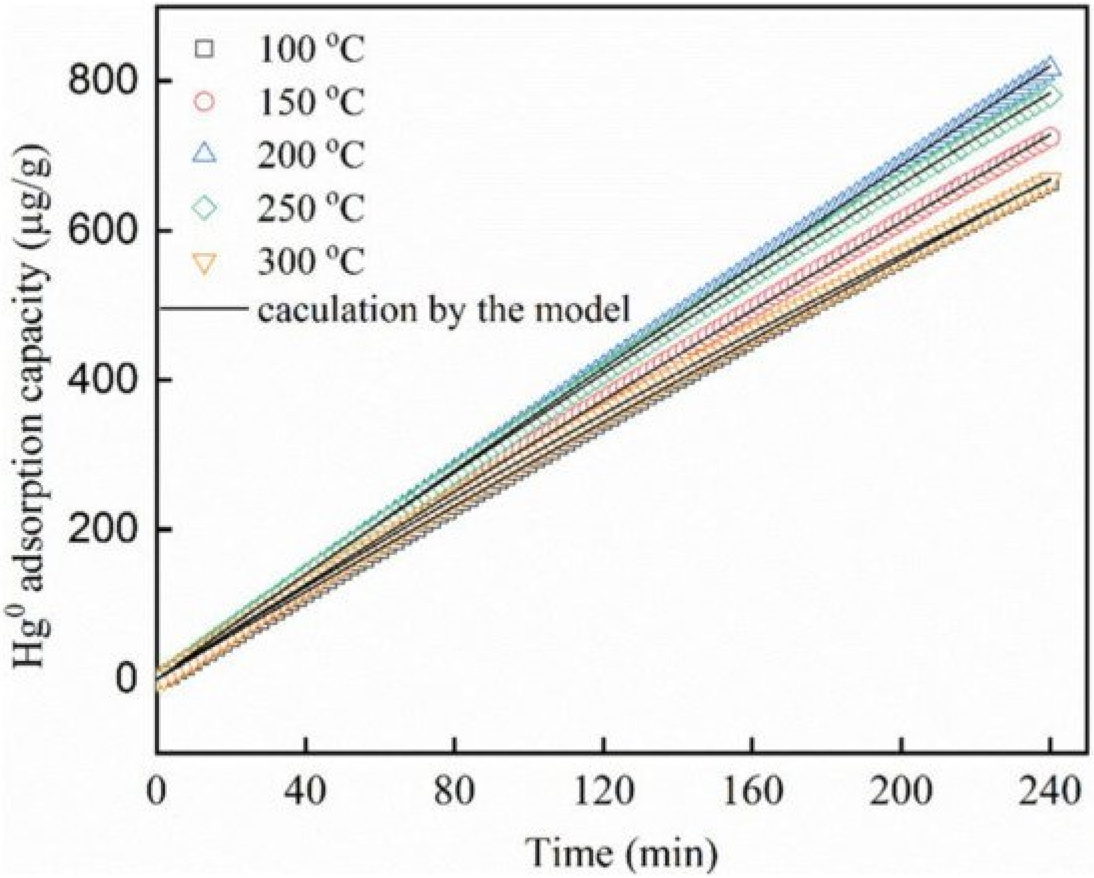

Figure 14. Simulation of Hg^0 adsorption on **MIL-101(Cr)** by the pseudo-second-order model. Reaction conditions: N_2 + 5% O_2, inlet concentration of Hg^0 = 203 μg m^{-3}, gas hourly space velocity (GHSV) = 8 × 10^5 h^{-1}, 200 °C (reproduced with the permission from Ref [187]).

Utilization of the **Cu-BTC** (BTC represents benzene-1,3,5-tricarboxylate) for Hg^0 removal from sintering gas was discussed by Chen and co-workers [188]. The **Cu-BTC** showed great efficiency in the presence of 15 ppm HCl with the combination of O_2. The chemisorbed O_2 (over Cu^{2+} surface) oxidized the Hg^0 to Hg^{2+}, which was then converted to $HgCl_2$ in the presence of HCl. Moreover, the inhibition effect of SO_2 was overcome by HCl, thereby the **Cu-BTC** is noted a material with good performance for Hg^0 adsorption. The MnO_x loaded on the **MIL-100(Fe)** (77.4% efficiency at 250 °C; GHSV = 18,000 h^{-1}) and α-MnO_2 anchored **MIL-96(Al)** were reported for Hg^0 removal from flue gas [189][190]. Because the presence of both MnO_x and α-MnO_2 can enhance adsorption of

Hg^0 and oxidation process, therefore, such composited MOFs can be engaged for environmental remediation. Subsequently, Yang et al. reported the nanosized CuSe functionalized Zn-comprising zeolitic imidazolate framework-8 (**CuSe/ZIF-8**) for Hg^0 adsorption and removal studies [191]. The as-prepared **CuSe/ZIF-8** with the 80% mass ratio of CuSe to ZIF-8 (to afford 0.8NC-ZIF) displayed an equilibrium Hg^0 adsorption capacity with an average rate of 309.8 mg g^{-1} and 105.3 μg g^{-1} min^{-1}, correspondingly, which were far better than that of the reported metal sulfide and activated carbon sorbents. The HgSe, which is more stable than HgS, can be easily formed because of the strong affinity between Hg and Se^{2-} (from CuSe). The composite can be used for continuous removal of Hg^0, thereby is considered an exceptional material. Following the similar approach, the Se functionalized MIL-101-Cr (**Se/MIL-101-Cr**) was proposed for Hg^0 removal [192]. By means of stable and water-insoluble HgSe formation, the **Se/MIL-101-Cr** showed a maximum Hg adsorption capacity of 48.19 mg g^{-1}, which was far better than commercially activated carbon. Moreover, the adsorption rate reached a value of 44.8 μg g^{-1} min^{-1} and became more-effective in flue gas atmosphere containing SO_2, NO, and H_2O. Thus, it is noted as a nice candidate for Hg^0 sorption.

Zhao and co-workers reported Hg^0 removal by combining Ag NPs with the Zr-based MOF-**UIO-66** [193]. The adsorption capacity reached a value of 3.7 mg g^{-1} at 50°C because of the significant synergistic effect of Ag NPs over the **UIO-66**. Removal of Hg^0 was attributed to the Ag amalgam formation and channel adsorption at low temperature. At high temperature, removal of Hg^0 was driven by the Ag-activated oxygen oxidation and channel capture. Zhang et al. proposed the consumption of the Mn–Ce loaded MOF (**MnCe@MOF**) for removal of Hg^{2+} and NO from flue gas at low temperature [194]. However, this study reported a possible interfering effect of NO over Hg^0 adsorption.

11. MOFs for Simultaneous Detection and Removal of Hg^{2+}

As suggested by earlier studies [153][175], MOFs were also engaged in simultaneous detection and removal studies as discussed in this section. For instance, Rudd et al. demonstrated heavy metal ions sensing and removal using solvothermally synthesized Zn-based luminescent MOFs, namely $Zn_2(ofdc)_2(tppe)$-**LMOFs-261**, $Zn_2(hfdc)_2(tppe)$-**LMOFs-262**, and $Zn_2(dbtdcO_2)_2(tppe)$-**LMOFs-263**), where H_2ofdc, $H_2dbtdcO_2$, and tppe represent [9-oxo-9H-fluorene-2,7-dicarboxylic acid], [dibenzo[b,d]thiophene-3,7-dicarboxylic acid-5,5-dioxide], and 1,1,2,2-tetrakis(4-(pyridine-4-yl)phenyl)ethane, respectively [195]. Among these MOFs, the **LMOFs-263** displayed the highest luminescent selectivity to Hg^{2+} and Pb^{2+} with LODs of 3.3 and 19.7 ppb, respectively. Moreover, it showed a maximum adsorption capacity of 380 mg g^{-1} (for $Hg^{2=}$ within 30 min) and the adsorption followed pseudo-second-order kinetics. A K_d value of 6.45 × 10^5 mL g^{-1} was determined for the **LMOFs-263**. The effective adsorption was attributed to the strong interaction between Hg^{2+} and SO_2^{2-} (of $H_2dbtdcO_2$) and the pore size. The BET surface area of **LMOFs-263** was estimated as 1004 m^2 g^{-1} to N_2 gas at 77K, however, further investigations are required to overcome the Pb^{2+} interference. Al-based imidazolate framework, namely **NH2-MIL-53(Al)**, for selective detection and removal of Hg^{2+} was reported by Zhang and co-workers [196]. Because of the coordination of amino ($-NH_2$) group and ligand-to-metal charge transfer (LMCT) effect with Hg^{2+}, fluorescent intensity of the **NH2-MIL-53(Al)** at 427 nm (λ_{ex} = 330 nm) was linearly quenched between 1−17.3 μM with a LOD of 0.15 μM. In addition,

Hg^{2+} sensing ability of the **NH2-MIL-53(Al)** was good at pHs 4–10 without any interference. The MOF showed an adsorption capacity of 53.85 mg g^{-1} (for Hg^{2+}) and was reusable with 0.1 M HCl and 10% thiourea eluent. This work followed pseudo second order kinetic model and was linearly correlated with the Langmuir isotherm, thereby is a nice probe.

By loading the (bis(4-(dimethylamino)phenyl)methanethione) probe over the Al-based MOF (which was solvothermally synthesized by reacting $Al(NO_3)_3{\cdot}9H_2O$ and terephthalic acid), detection and removal of Hg^{2+} in water and skin-whitening cosmetics was delivered by Radwan and co-workers [197]. These thioketone Al-MOFs monitors (**TAM**) acted as microporous carriers towards Hg^{2+} via fluorescent quenching at 470 nm and enhancement at 610 nm with a linear range from 2 nM to 2.1 µM and a LOD of 4.4 nM. Moreover, the thioketone Al-MOF (**TAM**) nanorods were used in effective adsorption of Hg^{2+}, which showed a maximum adsorption capacity of 1110 mg g^{-1} with exceptional applicability in water and skin-whitening cosmetics. Shahat et al. engaged the modified amino-functionalized Al-MOF for optical recognition and removal of Hg^{2+} [198]. $AlCl_3{\cdot}6H_2O$ and 2-amino terephthalic acid was first solvothermally reacted to yield the **MOF-NH2-MIL-101(Al)** followed by modification with ninhydrin to obtain the final adduct **Nin-NH-MIL-101(Al)**. The **Nin-NH-MIL-101(Al)** showed a BET surface area of 896.6 m^2 g^{-1} for N_2 gas at 77K. It was used as a colorimetric sensory probe for Hg^{2+} with a LOD of 0.494 µg L^{-1} and was further applied in removal studies. The probe displayed a maximum adsorption capacity of 127.4 mg g^{-1} and was recyclable in the presence of 0.1 M thiourea as shown in **Figure 15**. This work followed the pseudo second order kinetic model and was linearly fitted Langmuir isotherm. Be noted that the **Nin-NH-MIL-101(Al)**-based optical detection and removal of Hg^{2+} was not affected by any interference.

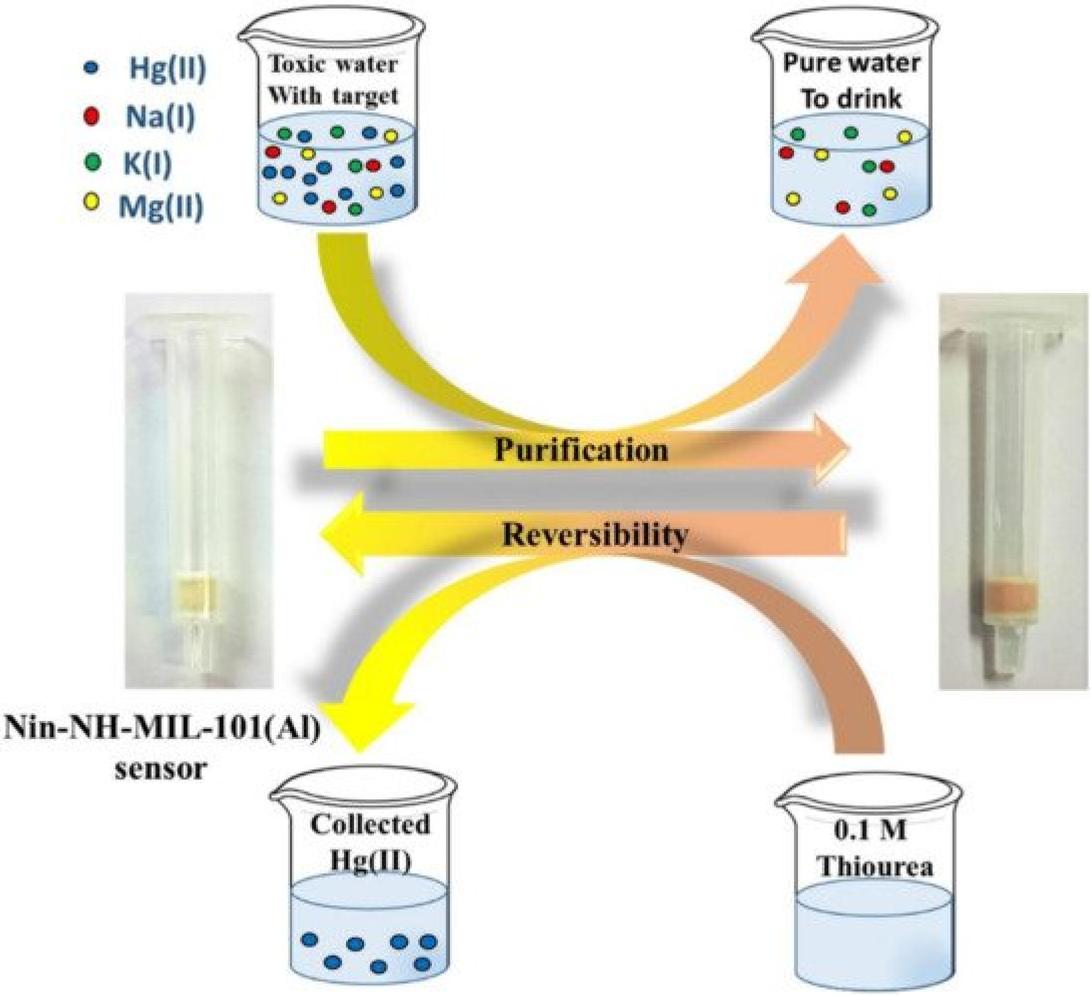

Figure 15. Representative design of the **Nin-NH-MIL-101(Al)** sensor applied to purification of water polluted with Hg(II) ions and the reversible process by using 0.1 M thiourea solution for several times (reproduced with the permission from Ref [198]).

By means of hydrothermal reactions, the Cu-based MOFs and amide-functionalized pillar ligands (–NH–CO–), namely **TMU-46**, **47**, and **48**, were synthesized and then decorated with suitable functional group malonamide (S) to produce the labelled dual functionalized materials-**TMU-46S**, **TMU-47S**, and **TMU-48S**, respectively. They were applied towards Hg^{2+} sensing and removal [199]. The BET surface areas of **TMU-46S**, **TMU-47S**, and **TMU-48S** were 510 m^2 g^{-1}, 520 m^2 g^{-1}, and 408 m^2 g^{-1}, respectively. Because of the strong coordination of Hg to S, the **TMU-48S** displayed the highest selectivity to Hg^{2+} via fluorescent quenching at 480 nm (λ_{ex} = 330 nm) with a K_{SV} value of 86,087 M^{-1}. Moreover, the **TMU-48S** showed a maximum adsorption capacity of 714 mg g^{-1}. However, it also showed some selectivity to Pb^{2+} and Ag^{+}. The CuS particles (**PCuS**) were synthesized via wet-treatment of Cu-based MOF- **HKUST-1** and were engaged in colorimetric detection of Hg^{2+} in the presence of 3,3′,5′,5-tetramethylbenzidine (TMB) and H_2O_2 (by peroxidase like activity) [200]. The BET surface area of **PCuS** was calculated to be 35 m^2 g^{-1} with a linear colorimetric response between 3–40 µM and an established LOD of 0.22 µM. Moreover, the **PCuS** showed a maximum adsorption capacity of 2105 mg g^{-1}. The system followed the pseudo second order kinetic and was linearly fitted with the Langmuir isotherm.

A porphyrinic Zr-based MOF, namely **PCN-221** (by solvothermal reaction between meso-tetra(4-carboxyphenyl) porphyrin (TCPP) and $ZrCl_4$), was proposed for fluorescent sensing and removal of Hg^{2+} in water [201]. The **PCN-221** showed linear quenching at 436 nm (λ_{ex} = 280 nm) in the presence of Hg^{2+} concentrations from 0 to 300 μM with a K_{SV} value of 4021.9 M^{-1} and a LOD of 0.01 μM. Moreover, sensing ability of DMF by **PCN-221** was also described in this report with extensive Hg^{2+} adsorption studies. The **PCN-221** displayed a maximum capacity of 233.65 mg g^{-1} towards Hg^{2+} adsorption and was highly effective at pH 7. Three adsorption-desorption cycles were achieved in the presence of 0.2 M Na_2EDTA without any interference effect. This study followed the pseudo second order model and was linearly correlated by the Langmuir isotherm. Recently, a 3D-microporous carbon/Zr-2,5-dimercaptoterephthalic acid MOFs (**Zr-DMBD MOFs/3D-KSC**) nanocomposite was delivered towards electrochemical detection and removal of Hg^{2+} [202]. Sensitivity of the nanocomposite to Hg^{2+} was established as 24.58 μA $μM^{-1}$ cm^{-2} with a linear range of 0.25–3.5 μM and a LOD of 0.05 μM. It was confirmed that specificity and effectiveness of the composite were similar to sensory and other utilities of nanomaterials [203][204][205][206]. This may be due to the presence of thiol (-SH) group of 2,5-dimercaptoterephthalic acid, which has great affinity to Hg^{2+}. The **Zr-DMBD MOFs/3D-KSC** showed a maximum adsorption capacity (for Hg^{2+}) of 19.3 ± 0.52 mg g^{-1} (within 60 min at pH 6) and was reusable up to five cycles with EDTA. This work was also applied in real water samples. However, information regarding adsorption kinetics still needs to be discussed. Apart from specific Hg^{2+} sensing/adsorption utilization of MOFs, the Hg-metalated MOF scaffold can be employed for detection of other species. For example, Hg-metalated **PCN-222** was reported as fluorescent and visual sensors for cysteine [207], which pointed out the possible future direction of MOFs-based Hg^{2+} sensors.

12. Advantages

Consumption of MOFs and their analogous for selective Hg^{2+} detection and removal possess many advantages and some restrictions as follows.

- The majority of MOFs and their derivatives detect or adsorb the Hg species in aqueous media, therefore, MOFs-based detection and removal experiments could sustain the eco-friendly process via decontaminating the toxic mercury from aquatic environment.

- Due to the porous nano/micro structural features, MOFs can be tuned towards encapsulation of specific Hg species, which could be further enhanced by post-synthetic modification or loading of specific groups, such as thiols (-SH).

- MOFs and their analogous have the advantage of recognition of multiple analytes, including Hg^{2+}, via variations of detection conditions, masking agents, and analyte concentrations.

- MOFs can act as probes towards recognition and removal of Hg species through many tactics, such as optical, electrochemical, photoelectrochemical, etc. Thus, they are noted as materials with exceptional advantages.

- By tuning the compositions to adjust the specific porous surface, many composites comprised of MOFs have unique advantages of capturing Hg species in the presence of other interfering analytes.

- MOFs mediated Hg detection/removal process can be further extended towards recognition of specific bio-analytes, such as glutathione, cysteine, and thiol containing species.

13. Limitations

- Synthesis of designated MOFs and their analogous is still considered a tough task due to certain limitations, such as possible co-adduct formation, suitable tactics, reaction conditions, solvent, etc.

- Though MOFs display high sensitivity via fluorescence quenching or enhancement, however, many of them are consisted of toxic metals, such as Al, Cr, Zr, Lanthanides, etc. Therefore, bioimaging or biological assays of Hg^{2+} by these MOFs are restricted.

- MOFs with free thiol (-SH) containing organic linkers also showed selectivity to Pb^{2+}, Cd^{2+}, and Ag^{+}, thereby limiting high selectivity towards Hg species via certain interfering effect.

- Majority of MOFs-based Hg^{2+} adsorption or removal studies were limited by many factors, such as MOFs concentration, structural stability, porosity, pH, time, operating temperature, suitable eluent, etc. Those factors require further attention.

- Design and development of certain MOFs comprised composites are also limited by the multiple complicated procedures, which not only increase the cost of the processes but also restrict the commercialization of materials.

- Complete characterizations of the Hg assay and removal processes also requires many costly instruments, such as scanning electron microscopy (SEM), powder-X-ray diffraction analyzer (PXRD), elemental analyzer, thermogravimetric analyzer (TGA), etc., which limits future research towards development of MOFs-based materials for mercury remediations.

- Finally, adsorption capacities of a few MOFs were found to be affected by the multiple interference effects and physical/chemical stability of MOFs during the Hg assays in real samples. Thus, much focus is anticipated to address this problem.

References

1. Huang, J.-H.; Shetaya, W.H.; Osterwalder, S. Determination of (Bio)-available mercury in soils: A review. Environ. Pollut. 2020, 263, 114323.

2. Botasini, S.; Heijo, G.; Méndez, E. Toward decentralized analysis of mercury (II) in real samples. A critical review on nanotechnology-based methodologies. Anal. Chim. Acta 2013, 800, 1–11.
3. Xie, Z.-J.; Bao, X.-Y.; Peng, C.-F. Highly Sensitive and Selective Colorimetric Detection of Methylmercury Based on DNA Functionalized Gold Nanoparticles. Sensors 2018, 18, 2679.
4. Shellaiah, M.; Simon, T.; Venkatesan, P.; Sun, K.W.; Ko, F.-H.; Wu, S.-P. Cysteamine-modified diamond nanoparticles applied in cellular imaging and Hg2+ ions detection. Appl. Surf. Sci. 2019, 465, 340–350.
5. Aderinto, S.O. Fluorescent, colourimetric, and ratiometric probes based on diverse fluorophore motifs for mercuric(II) ion (Hg2+) sensing: Highlights from 2011 to 2019. Chem. Pap. 2020, 74, 3195–3232.
6. Kobielska, P.A.; Howarth, A.J.; Farha, O.K.; Nayak, S. Metal–organic frameworks for heavy metal removal from water. Coord. Chem. Rev. 2018, 358, 92–107.
7. Selid, P.D.; Xu, H.; Collins, E.M.; Face-Collins, M.S.; Zhao, J.X. Sensing Mercury for Biomedical and Environmental Monitoring. Sensors 2009, 9, 5446–5459.
8. Bernhoft, R.A. Mercury Toxicity and Treatment: A Review of the Literature. J. Environ. Public Health 2011, 2012, 1–10.
9. Langford, N.J.; Ferner, R.E. Toxicity of mercury. J. Hum. Hypertens. 1999, 13, 651–656.
10. Rana, M.; Balcioglu, M.; Robertson, N.M.; Hizir, M.S.; Yumak, S.; Yigit, M.V. Low picomolar, instrument-free visual detection of mercury and silver ions using low-cost programmable nanoprobes. Chem. Sci. 2017, 8, 1200–1208.
11. Gauthama, B.; Narayana, B.; Sarojini, B.; Suresh, N.; Sangappa, Y.; Kudva, A.K.; Satyanarayana, G.; Raghu, S.V. Colorimetric “off–on” fluorescent probe for selective detection of toxic Hg2+ based on rhodamine and its application for in-vivo bioimaging. Microchem. J. 2021, 166, 106233.
12. Busairi, N.; Syahir, A. Recent Advances in Mercury Detection: Towards Enabling a Sensitive and Rapid Point-of-Check Measurement. J. Toxicol. Risk Assess 2018, 4, 010.
13. Nolan, E.M.; Lippard, S.J. Tools and Tactics for the Optical Detection of Mercuric Ion. Chem. Rev. 2008, 108, 3443–3480.
14. Shellaiah, M.; Sun, K.W. Luminescent Metal Nanoclusters for Potential Chemosensor Applications. Chemosensors 2017, 5, 36.
15. Shuai, H.; Xiang, C.; Qian, L.; Bin, F.; Xiaohui, L.; Jipeng, D.; Chang, Z.; Jiahui, L.; Wenbin, Z. Fluorescent sensors for detection of mercury: From small molecules to nanoprobes. Dyes Pigment. 2021, 187, 109125.

16. Dai, D.; Li, Z.; Yang, J.; Wang, C.; Wu, J.-R.; Wang, Y.; Zhang, D.; Yang, Y.-W. Supramolecular Assembly-Induced Emission Enhancement for Efficient Mercury(II) Detection and Removal. J. Am. Chem. Soc. 2019, 141, 4756–4763.
17. Zhao, L.; Zhang, Z.; Liu, Y.; Wei, J.; Liu, Q.; Ran, P.; Li, X. Fibrous strips decorated with cleavable aggregation-induced emission probes for visual detection of Hg2+. J. Hazard. Mater. 2020, 385, 121556.
18. Kumar, P.; Deep, A.; Kim, K.-H. Metal organic frameworks for sensing applications. TrAC Trends Anal. Chem. 2015, 73, 39–53.
19. Li, Y.; Hu, T.; Chen, R.; Xiang, R.; Wang, Q.; Zeng, Y.; He, C. Novel thiol-functionalized covalent organic framework as adsorbent for simultaneous removal of BTEX and mercury (II) from water. Chem. Eng. J. 2020, 398, 125566.
20. Chen, L.; Liu, D.; Peng, J.; Du, Q.; He, H. Ratiometric fluorescence sensing of metal-organic frameworks: Tactics and perspectives. Coord. Chem. Rev. 2020, 404, 213113.
21. Razavi, S.A.A.; Morsali, A. Metal ion detection using luminescent-MOFs: Principles, strategies and roadmap. Coord. Chem. Rev. 2020, 415, 213299.
22. Devaraj, M.; Sasikumar, Y.; Rajendran, S.; Ponce, L.C. Review—Metal Organic Framework Based Nanomaterials for Electrochemical Sensing of Toxic Heavy Metal Ions: Progress and Their Prospects. J. Electrochem. Soc. 2021, 168, 037513.
23. Vardali, S.C.; Manousi, N.; Barczak, M.; Giannakoudakis, D.A. Novel Approaches Utilizing Metal-Organic Framework Composites for the Extraction of Organic Compounds and Metal Traces from Fish and Seafood. Molecules 2020, 25, 513.
24. Li, X.; Ma, W.; Li, H.; Zhang, Q.; Liu, H. Sulfur-functionalized metal-organic frameworks: Synthesis and applications as advanced adsorbents. Coord. Chem. Rev. 2020, 408, 213191.
25. Chen, L.; Luque, R.; Li, Y. Controllable design of tunable nanostructures inside metal–organic frameworks. Chem. Soc. Rev. 2017, 46, 4614–4630.
26. Xia, W.; Mahmood, A.; Zou, R.; Xu, Q. Metal–organic frameworks and their derived nanostructures for electrochemical energy storage and conversion. Energy Environ. Sci. 2015, 8, 1837–1866.
27. Lee, K.J.; Lee, J.H.; Jeoung, S.; Moon, H.R. Transformation of Metal–Organic Frameworks/Coordination Polymers into Functional Nanostructured Materials: Experimental Approaches Based on Mechanistic Insights. Acc. Chem. Res. 2017, 50, 2684–2692.
28. Xie, Z.; Xu, W.; Cui, X.; Wang, Y. Recent Progress in Metal–Organic Frameworks and Their Derived Nanostructures for Energy and Environmental Applications. ChemSusChem 2017, 10, 1645–1663.

29. Song, Y.; Li, X.; Sun, L.; Wang, L. Metal/metal oxide nanostructures derived from metal–organic frameworks. RSC Adv. 2014, 5, 7267–7279.
30. Heo, D.Y.; Do, H.H.; Ahn, S.H.; Kim, S.Y. Metal-Organic Framework Materials for Perovskite Solar Cells. Polymers 2020, 12, 2061.
31. Kaur, H.; Sundriyal, S.; Pachauri, V.; Ingebrandt, S.; Kim, K.-H.; Sharma, A.L.; Deep, A. Luminescent metal-organic frameworks and their composites: Potential future materials for organic light emitting displays. Coord. Chem. Rev. 2019, 401, 213077.
32. Wu, G.; Huang, J.; Zang, Y.; He, J.; Xu, G. Porous Field-Effect Transistors Based on a Semiconductive Metal–Organic Framework. J. Am. Chem. Soc. 2017, 139, 1360–1363.
33. He, J.; Xu, J.; Yin, J.; Li, N.; Bu, X.-H. Recent advances in luminescent metal-organic frameworks for chemical sensors. Sci. China Mater. 2019, 62, 1655–1678.
34. Wu, S.; Min, H.; Shi, W.; Cheng, P. Multicenter Metal–Organic Framework-Based Ratiometric Fluorescent Sensors. Adv. Mater. 2020, 32, 1805871.
35. Samanta, P.; Let, S.; Mandal, W.; Dutta, S.; Ghosh, S.K. Luminescent metal–organic frameworks (LMOFs) as potential probes for the recognition of cationic water pollutants. Inorg. Chem. Front. 2020, 7, 1801–1821.
36. Huang, S.-Z.; Liu, S.-S.; Zhang, H.-j.; Han, Z.; Zhao, G.; Dong, X.-Y.; Zang, S.-Q. Dual-Functional Proton-Conducting and pH-Sensing Polymer Membrane Benefiting from a Eu-MOF. ACS Appl. Mater. Interfaces 2020, 12, 28720–28726.
37. Wang, Y.; Hu, Y.; He, Q.; Yan, J.; Xiong, H.; Wen, N.; Cai, S.; Peng, D.; Liu, Y.; Liu, Z. Metal-organic frameworks for virus detection. Biosens. Bioelectron. 2020, 169, 112604.
38. Gai, S.; Zhang, J.; Fan, R.; Xing, K.; Chen, W.; Zhu, K.; Zheng, X.; Wang, P.; Fang, X.; Yang, Y. Highly Stable Zinc-Based Metal-Organic Frameworks and Corresponding Flexible Composites for Removal and Detection of Antibiotics in Water. ACS Appl. Mater. Interfaces 2020, 12, 8650–8662.
39. Tang, J.; Feng, D.; Yang, J.; Ma, X.; Wang, X.-Q. A turn-on luminescent probe for Fe3+ and ascorbic acid with logic gate operation based on a zinc(ii)-based metal–organic framework. New J. Chem. 2020, 44, 8728–8735.
40. Wu, R.-Z.; Yang, X.; Zhang, L.-W.; Zhou, P.-P. Luminescent lanthanide metal–organic frameworks for chemical sensing and toxic anion detection. Dalton Trans. 2017, 46, 9859–9867.
41. Hu, Z.; Deibert, B.J.; Li, J. Luminescent metal–organic frameworks for chemical sensing and explosive detection. Chem. Soc. Rev. 2014, 43, 5815–5840.
42. Dalapati, R.; Nandi, S.; Biswas, S. Post-synthetic modification of a metal-organic framework with a chemodosimeter for the rapid detection of lethal cyanide via dual emission. Dalton Trans. 2020, 49, 8684–8692.

43. Koo, W.-T.; Jang, J.-S.; Kim, I.-D. Metal-Organic Frameworks for Chemiresistive Sensors. Chem 2019, 5, 1938–1963.
44. Lustig, W.P.; Mukherjee, S.; Rudd, N.D.; Desai, A.V.; Li, J.; Ghosh, S.K. Metal–organic frameworks: Functional luminescent and photonic materials for sensing applications. Chem. Soc. Rev. 2017, 46, 3242–3285.
45. Goswami, R.; Mandal, S.C.; Pathak, B.; Neogi, S. Guest-Induced Ultrasensitive Detection of Multiple Toxic Organics and Fe3+ Ions in a Strategically Designed and Regenerative Smart Fluorescent Metal-Organic Framework. ACS Appl. Mater. Interfaces 2019, 11, 9042–9053.
46. Tchalala, M.R.; Bhatt, P.M.; Chappanda, K.N.; Tavares, S.R.; Adil, K.; Belmabkhout, Y.; Shkurenko, A.; Cadiau, A.; Heymans, N.; De Weireld, G.; et al. Fluorinated MOF platform for selective removal and sensing of SO2 from flue gas and air. Nat. Commun. 2019, 10, 1–10.
47. Chen, G.; Guo, Z.; Zeng, G.; Tang, L. Fluorescent and colorimetric sensors for environmental mercury detection. Analyst 2015, 140, 5400–5443.
48. Rouhani, F.; Morsali, A. Goal-Directed Design of Metal-Organic Frameworks for HgII and PbII Adsorption from Aqueous Solutions. Chem. Eur. J. 2018, 24, 17170–17179.
49. Tan, H.; Liu, B.; Chen, Y. Lanthanide Coordination Polymer Nanoparticles for Sensing of Mercury(II) by Photoinduced Electron Transfer. ACS Nano 2012, 6, 10505–10511.
50. Sohrabi, M.R. Preconcentration of mercury(II) using a thiol-functionalized metal-organic framework nanocomposite as a sorbent. Microchim. Acta 2014, 181, 435–444.
51. Zhang, X.; Shen, B.; Zhu, S.; Xu, H.; Tian, L. UiO-66 and its Br-modified derivates for elemental mercury removal. J. Hazard. Mater. 2016, 320, 556–563.
52. Li, X.; Wang, B.; Cao, Y.; Zhao, S.; Wang, H.; Feng, X.; Zhou, J.; Ma, X. Water Contaminant Elimination Based on Metal–Organic Frameworks and Perspective on Their Industrial Applications. ACS Sustain. Chem. Eng. 2019, 7, 4548–4563.
53. Fang, X.; Zong, B.; Mao, S. Metal-Organic Framework-Based Sensors for Environmental Contaminant Sensing. Nano-Micro Lett. 2018, 10, 1–19.
54. Yao, C.-X.; Zhao, N.; Liu, J.-C.; Chen, L.-J.; Liu, J.-M.; Fang, G.-Z.; Wang, S. Recent Progress on Luminescent Metal-Organic Framework-Involved Hybrid Materials for Rapid Determination of Contaminants in Environment and Food. Polymers 2020, 12, 691.
55. Yee, K.-K.; Reimer, N.; Liu, J.; Cheng, S.-Y.; Yiu, S.-M.; Weber, J.; Stock, N.; Xu, Z. Effective Mercury Sorption by Thiol-Laced Metal–Organic Frameworks: In Strong Acid and the Vapor Phase. J. Am. Chem. Soc. 2013, 135, 7795–7798.
56. Wang, Q.; Astruc, D. State of the Art and Prospects in Metal-Organic Framework (MOF)-Based and MOF-Derived Nanoca-talysis. Chem. Rev. 2020, 120, 1438–1511.

57. Cui, J.; Ren, S.; Sun, B.; Jia, S. Optimization protocols and improved strategies for metal-organic frameworks for immobilizing enzymes: Current development and future challenges. Coord. Chem. Rev. 2018, 370, 22–41.
58. Hu, M.-L.; Razavi, S.A.A.; Piroozzadeh, M.; Morsali, A. Sensing organic analytes by metal–organic frameworks: A new way of considering the topic. Inorg. Chem. Front. 2020, 7, 1598–1632.
59. Dalapati, R.; Biswas, S. Post-synthetic modification of a metal-organic framework with fluorescent-tag for dual naked-eye sensing in aqueous medium. Sens. Actuators B Chem. 2017, 239, 759–767.
60. Safaei, M.; Foroughi, M.M.; Ebrahimpoor, N.; Jahani, S.; Omidi, A.; Khatami, M. A review on metal-organic frameworks: Synthesis and applications. TrAC Trends Anal. Chem. 2019, 118, 401–425.
61. Al-Ghoul, M.; Issa, R.; Hmadeh, M. Synthesis, size and structural evolution of metal–organic framework-199 via a reaction–diffusion process at room temperature. CrystEngComm 2016, 19, 608–612.
62. Al Amery, N.; Abid, H.; Al-Saadi, S.; Wang, S.; Liu, S. Facile directions for synthesis, modification and activation of MOFs. Mater. Today Chem. 2020, 17, 100343.
63. Klinowski, J.; Almeida Paz, F.A.; Silva, P.; Rocha, J. Microwave-Assisted Synthesis of Metal-Organic Frameworks. Dalton Trans. 2011, 40, 321–330.
64. Thomas-Hillman, I.; Laybourn, A.; Dodds, C.; Kingman, S.W. Realising the environmental benefits of metal-organic frameworks: Recent advances in microwave synthesis. J. Mater. Chem. A 2018, 6, 11564–11581.
65. Le, V.N.; Kwon, H.T.; Vo, T.K.; Kim, J.-H.; Kim, W.-S.; Kim, J. Microwave-assisted continuous flow synthesis of mesoporous metal-organic framework MIL-100 (Fe) and its application to Cu(I)-loaded adsorbent for CO/CO2 separation. Mater. Chem. Phys. 2020, 253, 123278.
66. Li, W.-J.; Tu, M.; Cao, R.; Fischer, R.A. Metal-organic framework thin films: Electrochemical fabrication techniques and corresponding applications & perspectives. J. Mater. Chem. A 2016, 4, 12356–12369.
67. Wang, Z.; Li, Z.; Ng, M.; Milner, P.J. Rapid mechanochemical synthesis of metal–organic frameworks using exogenous organic base. Dalton Trans. 2020, 49, 16238–16244.
68. Vaitsis, C.; Sourkouni, G.; Argirusis, C. Chapter 11—Sonochemical synthesis of MOFs. In Metal-Organic Frameworks for Bio-medical Applications; Mozafari, M., Ed.; Woodhead Publishing: Cambridge, UK, 2020; pp. 223–244.
69. Kalaj, M.; Cohen, S.M. Postsynthetic Modification: An Enabling Technology for the Advancement of Metal-Organic Frameworks. ACS Cent. Sci. 2020, 6, 1046–1057.

70. Shellaiah, M.; Sun, K.W. Review on Sensing Applications of Perovskite Nanomaterials. Chemosensors 2020, 8, 55.

71. Yang, J.; Wang, Z.; Li, Y.; Zhuang, Q.; Zhao, W.; Gu, J. Porphyrinic MOFs for reversible fluorescent and colorimetric sensing of mercury(II) ions in aqueous phase. RSC Adv. 2016, 6, 69807–69814.

72. Zhang, X.; Xia, T.; Jiang, K.; Cui, Y.; Yang, Y.; Qian, G. Highly sensitive and selective detection of mercury (II) based on a zirconium metal-organic framework in aqueous media. J. Solid State Chem. 2017, 253, 277–281.

73. Samanta, P.; Desai, A.V.; Sharma, S.; Chandra, P.; Ghosh, S.K. Selective Recognition of Hg2+ ion in Water by a Functionalized Metal–Organic Framework (MOF) Based Chemodosimeter. Inorg. Chem. 2018, 57, 2360–2364.

74. Xiaoxiong, Z.; Wenjun, Z.; Cuiliu, L.; Xiaohong, Q.; Chengyu, Z. Eu3+-Postdoped UIO-66-Type Metal-Organic Framework as a Luminescent Sensor for Hg2+ Detection in Aqueous Media. Inorg. Chem. 2019, 58, 3910–3915.

75. Wang, Z.; Yang, J.; Li, Y.; Zhuang, Q.; Gu, J. Zr-Based MOFs integrated with a chromophoric ruthenium complex for specific and reversible Hg2+sensing. Dalton Trans. 2018, 47, 5570–5574.

76. Li, W.-Y.; Yang, S.; Li, Y.-A.; Li, Q.-Y.; Guan, Q.; Dong, Y.-B. Synthesis of an MOF-based Hg2+-fluorescent probe via stepwise post-synthetic modification in a single-crystal-to-single-crystal fashion and its application in bioimaging. Dalton Trans. 2019, 48, 16502–16508.

77. Kim, J.; Oh, J.S.; Park, K.C.; Gupta, G.; Lee, C.Y. Colorimetric detection of heavy metal ions in water via metal-organic framework. Inorg. Chim. Acta 2019, 486, 69–73.

78. Wang, H.; Wang, X.; Liang, M.; Chen, G.; Kong, R.-M.; Xia, L.; Qu, F. A Boric Acid-Functionalized Lanthanide Metal-Organic Framework as a Fluorescence “Turn-on” Probe for Selective Monitoring of Hg2+ and CH3Hg+. Anal. Chem. 2020, 92, 3366–3372.

79. Xia, T.; Song, T.; Zhang, G.; Cui, Y.; Yang, Y.; Wang, Z.; Qian, G. A Terbium Metal-Organic Framework for Highly Selective and Sensitive Luminescence Sensing of Hg2+ Ions in Aqueous Solution. Chem. A Eur. J. 2016, 22, 18429–18434.

80. Liu, X.; Lin, H.; Xiao, Z.; Fan, W.; Huang, A.; Wang, R.; Zhang, L.; Sun, D. Multifunctional lanthanide–organic frameworks for fluorescent sensing, gas separation and catalysis. Dalton Trans. 2016, 45, 3743–3749.

81. Razavi, S.A.A.; Masoomi, M.Y.; Morsali, A. Double Solvent Sensing Method for Improving Sensitivity and Accuracy of Hg(II) Detection Based on Different Signal Transduction of a Tetrazine-Functionalized Pillared Metal-Organic Framework. Inorg. Chem. 2017, 56, 9646–9652.

82. Wan, Y.; Zou, D.; Cui, Y.; Yang, Y.; Qian, G. A Zn based anionic metal-organic framework for trace Hg2+ ion detection. J. Solid State Chem. 2018, 266, 70–73.
83. Pankajakshan, A.; Kuznetsov, D.; Mandal, S. Ultrasensitive Detection of Hg(II) Ions in Aqueous Medium Using Zinc-Based Metal-Organic Framework. Inorg. Chem. 2019, 58, 1377–1381.
84. Khatun, A.; Panda, D.K.; Sayresmith, N.; Walter, M.G.; Saha, S. Thiazolothiazole-Based Luminescent Metal-Organic Frameworks with Ligand-to-Ligand Energy Transfer and Hg2+-Sensing Capabilities. Inorg. Chem. 2019, 58, 12707–12715.
85. Jiang, J.; Lu, Y.; Liu, J.; Zhou, Y.; Zhao, D.; Li, C. An acid-base resistant Zn-based metal-organic framework as a luminescent sensor for mercury(II). J. Solid State Chem. 2020, 283, 121153.
86. Wu, P.; Liu, Y.; Liu, Y.; Wang, J.; Li, Y.; Liu, W.; Wang, J. Cadmium-Based Metal-Organic Framework as a Highly Selective and Sensitive Ratiometric Luminescent Sensor for Mercury(II). Inorg. Chem. 2015, 54, 11046–11048.
87. Liu, B.-H.; Liu, D.-X.; Yang, K.-Q.; Dong, S.-J.; Li, W.; Wang, Y.-J. A new cluster-based metal-organic framework with triazine backbones for selective luminescent detection of mercury(II) ion. Inorg. Chem. Commun. 2018, 90, 61–64.
88. El Taher, B.J.; Sabouni, R.; Ghommem, M. Luminescent metal organic framework for selective detection of mercury in aqueous media: Microwave-based synthesis and evaluation. Colloids Surf. A Physicochem. Eng. Asp. 2020, 607, 125477.
89. Basaleh, A.S.; Sheta, S.M. Novel advanced nanomaterial based on ferrous metal-organic framework and its application as chemosensors for mercury in environmental and biological samples. Anal. Bioanal. Chem. 2020, 412, 3153–3165.
90. Li, Y.; Ma, D.; Chen, C.; Chen, M.; Li, Z.; Wu, Y.; Zhu, S.; Peng, G. A hydrostable and bromine-functionalized manganese-organic framework with luminescence sensing of Hg2+ and antiferromagnetic properties. J. Solid State Chem. 2019, 269, 257–263.
91. Song, Y.; Fan, R.; Fan, J.; Xing, K.; Du, X.; Wang, P.; Yang, Y. Highly sensitive and selective fluorescent probes for Hg2+ in Ag(i)/Cu(ii) 3D supramolecular architectures based on noncovalent interactions. Dalton Trans. 2016, 45, 16422–16432.
92. Jana, A.K.; Natarajan, S. Fluorescent Metal-Organic Frameworks for Selective Sensing of Toxic Cations (Tl3+, Hg2+) and Highly Oxidizing Anions ((CrO4)2−, (Cr2O7)2−, (MnO4)−). ChemPlusChem 2017, 82, 1153–1163.
93. Xiao, J.; Liu, J.; Gao, X.; Ji, G.; Wang, D.; Liu, Z. A multi-chemosensor based on Zn-MOF: Ratio-dependent color transition detection of Hg (II) and highly sensitive sensor of Cr (VI). Sens. Actuators B Chem. 2018, 269, 164–172.

94. Fu, H.-R.; Zhao, Y.; Xie, T.; Han, M.-L.; Ma, L.-F.; Zang, S.-Q. Stable dye-encapsulated indium-organic framework as dual-emitting sensor for the detection of Hg2+/Cr2O72− and a wide range of nitro-compounds. J. Mater. Chem. C 2018, 6, 6440–6448.
95. Li, F.; Hong, Y.-S.; Zuo, K.-X.; Sun, Q.; Gao, E.-Q. Highly selective fluorescent probe for Hg2+ and MnO4− by the two-fold interpenetrating metal-organic framework with nitro functionalized linkers. J. Solid State Chem. 2019, 270, 509–515.
96. Yang, Y.-J.; Liu, D.; Li, Y.-H.; Dong, G.-Y. Two new luminescent ternary Cd(II)-MOFs by regulation of aromatic dicarboxylate ligands used as efficient dual-responsive sensors for toxic metal ions in water. Polyhedron 2019, 159, 32–42.
97. Mahmoud, M.E.; Moussa, Z.; Prakasam, T.; Li, L.; Abiad, M.G.; Patra, D.; Hmadeh, M. Lanthanides based metal organic frameworks for luminescence sensing of toxic metal ions. J. Solid State Chem. 2020, 281, 121031.
98. Ren, M.; Wang, H.; Liu, Y.; Ma, Q.; Jia, W.; Liu, M.; Wang, H.; Lu, Y. Fluorescent Determination of Mercury (II) and Glutathione Using Amino-MIL-53(Al) Nanosheets. Anal. Lett. 2020, 53, 2700–2714.
99. Yang, L.; Li, X.; Qin, C.; Shao, K.-Z.; Su, Z.-M. A fluorescent sensor for highly selective sensing of nitro explosives and Hg(ii) ions based on a 3D porous layer metal–organic framework. CrystEngComm 2016, 18, 4765–4771.
100. Gong, W.-J.; Ren, Z.-G.; Li, H.-X.; Zhang, J.-G.; Lang, J.-P. Cadmium(II) Coordination Polymers of 4-Pyr-poly-2-ene and Carboxylates: Construction, Structure, and Photochemical Double [2 + 2] Cycloaddition and Luminescent Sensing of Nitroaromatics and Mercury(II) Ions. Cryst. Growth Des. 2017, 17, 870–881.
101. Su, Y.-Q.; Qu, Y.-H.; Fu, L.; Cui, G.-H. An unprecedented binodal (4,6)-connected Co(II) MOF as dual-responsive luminescent sensor for detection of acetylacetone and Hg2+ ions. Inorg. Chem. Commun. 2020, 118, 108013.
102. Sun, X.; Yang, P.; Hou, G.; Wei, J.; Wang, X.; Yang, D.; Zhang, X.; Dong, H.; Zhang, F. Luminescent Functionalised Supramolecular Coordination Polymers Based on an Aromatic Carboxylic Acid Ligand for Sensing Hg2+ Ions Aust. J. Chem. 2017, 70, 786–791.
103. Li, Q.; Wang, C.; Tan, H.; Tang, G.; Gao, J.; Chen, C.-H. A turn on fluorescent sensor based on lanthanide coordination polymer nanoparticles for the detection of mercury(ii) in biological fluids. RSC Adv. 2016, 6, 17811–17817.
104. Li, W.-X.; Li, H.-X.; Li, H.-Y.; Chen, M.-M.; Shi, Y.-X.; Lang, J.-P. 1,4-Bis(2-(pyridin-4-yl)vinyl)naphthalene and Its Zinc(II) Coordination Polymers: Synthesis, Structural Characterization, and Selective Luminescent Sensing of Mercury(II) Ion. Cryst. Growth Des. 2017, 17, 3948–3959.

105. Zhang, S.-R.; Wang, W.; Xu, G.-J.; Yao, C.; Xu, Y.-H.; Su, Z.-M. A fluorescent sensor for selective, sensitive, and recyclable detection of mercury(II) in aqueous solution based on a zinc(II) coordination polymer. Inorg. Chem. Commun. 2018, 89, 73–77.

106. Gong, W.-J.; Yao, R.; Li, H.-X.; Ren, Z.-G.; Zhang, J.-G.; Lang, J.-P. Luminescent cadmium(ii) coordination polymers of 1,2,4,5-tetrakis(4-pyridylvinyl)benzene used as efficient multi-responsive sensors for toxic metal ions in water. Dalton Trans. 2017, 46, 16861–16871.

107. Wang, X.; Han, Y.; Han, X.X.; Hou, X.; Wang, J.-J.; Fu, F. Highly selective and sensitive detection of Hg2+, Cr2O72−, and nitrobenzene/2,4-dinitrophenol in water via two fluorescent Cd-CPs. New J. Chem. 2018, 42, 19844–19852.

108. Fang, Y.-M.; Ye, X.; Xia, L.; Dong, W.-W.; Zhao, J.; Li, D.-S. Four different dimensional Zn(II) coordination polymers as fluorescent sensor for detecting Hg2+, Cr2O72− in aqueous solution. J. Solid State Chem. 2018, 266, 181–188.

109. Lin, J.; Cheng, Q.; Zhou, J.; Lin, X.; Reddy, R.C.K.; Yang, T.; Zhang, G. Five 3D lanthanide-based coordination polymers with 3,3,6T13 topology: Structures and luminescent sensor for Hg2+ and Pb2+ ions. J. Solid State Chem. 2019, 270, 339–345.

110. Rachuri, Y.; Parmar, B.; Bisht, K.K.; Suresh, E. Multiresponsive Adenine-Based Luminescent Zn(II) Coordination Polymer for Detection of Hg2+ and Trinitrophenol in Aqueous Media. Cryst. Growth Des. 2017, 17, 1363–1372.

111. Zhu, H.; Han, C.; Li, Y.-H.; Cui, G.-H. Two new coordination polymers containing long flexible bis(benzimidazole) ligand as luminescent chemosensors for acetylacetone and Hg(II) ions detection. J. Solid State Chem. 2020, 282, 121132.

112. Ravikumar, A.; Panneerselvam, P.; Morad, N. Metal-Polydopamine Framework as an Effective Fluorescent Quencher for Highly Sensitive Detection of Hg(II) and Ag(I) Ions through Exonuclease III Activity. ACS Appl. Mater. Interfaces 2018, 10, 20550–20558.

113. Huang, N.-H.; Liu, Y.; Li, R.-T.; Chen, J.; Hu, P.-P.; Young, D.J.; Chen, J.-X.; Zhang, W.-H. Sequential Ag+/biothiol and synchronous Ag+/Hg2+ biosensing with zwitterionic Cu2+-based metal–organic frameworks. Analyst 2020, 145, 2779–2788.

114. Huang, N.-H.; Li, R.-T.; Fan, C.; Wu, K.-Y.; Zhang, Z.; Chen, J.-X. Rapid sequential detection of Hg2+ and biothiols by a probe DNA-MOF hybrid sensory system. J. Inorg. Biochem. 2019, 197, 110690.

115. Wu, L.-L.; Wang, Z.; Zhao, S.-N.; Meng, X.; Song, X.-Z.; Feng, J.; Song, S.-Y.; Zhang, H.-J. A Metal-Organic Framework/DNA Hybrid System as a Novel Fluorescent Biosensor for Mercury(II) Ion Detection. Chem. A Eur. J. 2015, 22, 477–480.

116. Wang, C.; Tang, G.; Tan, H. Colorimetric determination of mercury(II) via the inhibition by ssDNA of the oxidase-like activity of a mixed valence state cerium-based metal-organic framework.

Microchim. Acta 2018, 185, 475.

117. Wu, F.; Ye, J.; Cao, Y.; Wang, Z.; Miao, T.; Shi, Q. Recent advances in fluorescence sensors based on DNA-MOF hybrids. Luminescence 2020, 35, 440–446.
118. Chen, H.-L.; Li, R.-T.; Wu, K.-Y.; Hu, P.-P.; Zhang, Z.; Huang, N.-H.; Zhang, W.-H.; Chen, J.-X. Experimental and theoretical validations of a one-pot sequential sensing of Hg2+ and biothiols by a 3D Cu-based zwitterionic metal−organic framework. Talanta 2020, 210, 120596.
119. Wu, X.-J.; Kong, F.; Zhao, C.-Q.; Ding, S.-N. Ratiometric fluorescent nanosensors for ultra-sensitive detection of mercury ions based on AuNCs/MOFs. Analyst 2019, 144, 2523–2530.
120. Govindaraju, S.; Puthiaraj, P.; Lee, M.-H.; Yun, K. Photoluminescent for Ultrasensitive Detection of Mercury in Water Samples. ACS Omega 2018, 3, 12052–12059.
121. Marieeswaran, M.; Panneerselvam, P. A magnetic nanoscale metal-organic framework (MNMOF) as a viable fluorescence quencher material for ssDNA and for the detection of mercury ions via a novel quenching-quenching mechanism. RSC Adv. 2020, 10, 3705–3714.
122. Hu, P.-P.; Liu, N.; Wu, K.-Y.; Zhai, L.-Y.; Xie, B.-P.; Sun, B.; Duan, W.-J.; Zhang, W.-H.; Chen, J.-X. Successive and Specific Detection of Hg2+ and I– by a Biosensor: Experimental and Simulation Studies. Inorg. Chem. 2018, 57, 8382–8389.
123. Wang, X.; Wang, H.; Guo, L.; Chen, G.; Kong, R.; Qu, F.; Xia, L. Colorimetric detection of Hg(ii) based on the gold amalgam-triggered reductase mimetic activity in aqueous solution by employing nanoparticles. Analyst 2020, 145, 1362–1367.
124. Zhang, Y.; Song, J.; Pan, Q.; Zhang, X.; Shao, W.; Quan, C.; Li, J. An (Ti)-based multifunctional platform for colorimetric detections of biomolecules and Hg2+. J. Mater. Chem. B 2020, 8, 114–124.
125. Guo, M.; Chi, J.; Li, Y.; Waterhouse, G.I.N.; Ai, S.; Hou, J.; Li, X. Fluorometric determination of mercury(II) based on dual-emission metal-organic frameworks incorporating carbon dots and gold nanoclusters. Microchim. Acta 2020, 187, 534.
126. Yang, Y.; Liu, W.; Cao, J.; Wu, Y. On-site, rapid and visual determination of Hg2+ and Cu2+ in red wine by ratiometric fluorescence sensor of metal-organic frameworks and CdTe QDs. Food Chem. 2020, 328, 127119.
127. Shellaiah, M.; Sun, K.W. Inorganic-Diverse Nanostructured Materials for Volatile Organic Compound Sensing. Sensors 2021, 21, 633.
128. Zhang, X.; Jiang, Y.; Zhu, M.; Xu, Y.; Guo, Z.; Shi, J.; Han, E.; Zou, X.; Wang, D. Electrochemical DNA sensor for inorganic mercury(II) ion at attomolar level in dairy product using Cu(II)-anchored metal-organic framework as mimetic catalyst. Chem. Eng. J. 2020, 383, 123182.

129. Salandari-Jolge, N.; Ensafi, A.A.; Rezaei, B. Ultra-sensitive electrochemical aptasensor based on zeolitic imidazolate framework-8 derived Ag/Au core-shell nanoparticles for mercury detection in water samples. Sensors Actuators B Chem. 2021, 331, 129426.
130. Zhang, X.; Zhu, M.; Jiang, Y.; Wang, X.; Guo, Z.; Shi, J.; Zou, X.; Han, E. Simple electrochemical sensing for mercury ions in dairy product using optimal Cu2+-based metal-organic frameworks as signal reporting. J. Hazard. Mater. 2020, 400, 123222.
131. Fu, L.; Xie, K.; Wang, A.; Lyu, F.; Ge, J.; Zhang, L.; Zhang, H.; Su, W.; Hou, Y.-L.; Zhou, C.; et al. High selective detection of mercury (II) ions by thioether side groups on metal-organic frameworks. Anal. Chim. Acta 2019, 1081, 51–58.
132. Qing, M.; Chen, S.; Xie, S.; Tang, Y.; Zhang, J.; Yuan, R. Encapsulation and Release of Recognition Probes Based on a Rigid Three-Dimensional DNA “Nanosafe-box” for Construction of a Electrochemical Biosensor. Anal. Chem. 2020, 92, 1811–1817.
133. Singh, S.; Numan, A.; Zhan, Y.; Singh, V.; Van Hung, T.; Nam, N.D. A novel highly efficient and ultrasensitive electro-chemical detection of toxic mercury (II) ions in canned tuna fish and tap water based on a copper metal-organic framework. J. Hazard. Mater. 2020, 399, 123042.
134. Kokkinos, C.; Economou, A.; Pournara, A.; Manos, M.; Spanopoulos, I.; Kanatzidis, M.; Tziotzi, T.; Petkov, V.; Margariti, A.; Oikonomopoulos, P.; et al. 3D-printed lab-in-a-syringe voltammetric cell based on a working electrode modified with a highly efficient Ca-MOF sorbent for the determination of Hg(II). Sens. Actuators B Chem. 2020, 321, 128508.
135. Zhang, L.; Feng, L.; Li, P.; Chen, X.; Jiang, J.; Zhang, S.; Zhang, C.; Zhang, A.; Chen, G.; Wang, H. Direct Z-scheme photocatalyst of hollow polyhedron constructed by ZIF-67-templated one-pot solvothermal route: A signal-on photoelectrochemical sensor for mercury (II). Chem. Eng. J. 2020, 395, 125072.
136. Chen, Y.; Bai, X.; Ye, Z. Recent Progress in Heavy Metal Ion Decontamination Based on Metal-Organic Frameworks. Nanomaterials 2020, 10, 1481.
137. Rezaei Kahkha, M.R.; Daliran, S.; Oveisi, A.R.; Kaykhaii, M.; Sepehri, Z. The Mesoporous Porphyrinic Zirconium Metal-Organic Framework for Pipette-Tip Solid-Phase Extraction of Mercury from Fish Samples Followed by Cold Vapor Atomic Absorption Spectrometric Determination. Food Anal. Methods 2017, 10, 2175–2184.
138. Hasankola, Z.S.; Rahimi, R.; Shayegan, H.; Moradi, E.; Safarifard, V. Removal of Hg2+ heavy metal ion using a highly stable mesoporous porphyrinic zirconium metal-organic framework. Inorg. Chim. Acta 2020, 501, 119264.
139. Li, J.; Li, X.; Alsaedi, A.; Hayat, T.; Chen, C. Synthesis of highly porous inorganic adsorbents derived from metal-organic frameworks and their application in efficient elimination of mercury(II). J. Colloid Interface Sci. 2018, 517, 61–71.

140. Leus, K.; Perez, J.P.H.; Folens, K.; Meledina, M.; Van Tendeloo, G.; Du Laing, G.; Van Der Voort, P. UiO-66-(SH)2 as stable, selective and regenerable adsorbent for the removal of mercury from water under environmentally-relevant conditions. Faraday Discuss. 2017, 201, 145–161.
141. Li, J.; Liu, Y.; Ai, Y.; Alsaedi, A.; Hayat, T.; Wang, X. Combined experimental and theoretical investigation on selective removal of mercury ions by metal organic frameworks modified with thiol groups. Chem. Eng. J. 2018, 354, 790–801.
142. Fu, L.; Wang, S.; Lin, G.; Zhang, L.; Liu, Q.; Fang, J.; Wei, C.; Liu, G. Post-functionalization of UiO-66-NH2 by 2,5-Dimercapto-1,3,4-thiadiazole for the high efficient removal of Hg(II) in water. J. Hazard. Mater. 2019, 368, 42–51.
143. Ding, L.; Luo, X.; Shao, P.; Yang, J.; Sun, D. Thiol-Functionalized Zr-Based Metal-Organic Framework for Capture of Hg(II) through a Proton Exchange Reaction. ACS Sustain. Chem. Eng. 2018, 6, 8494–8502.
144. Li, M.-Q.; Wong, Y.-L.; Lum, T.-S.; Leung, K.S.-Y.; Lam, P.K.S.; Xu, Z. Dense thiol arrays for metal–organic frameworks: Boiling water stability, Hg removal beyond 2 ppb and facile crosslinking. J. Mater. Chem. A 2018, 6, 14566–14570.
145. Yang, P.; Shu, Y.; Zhuang, Q.; Li, Y.; Gu, J. A robust MOF-based trap with high-density active alkyl thiol for the super-efficient capture of mercury. Chem. Commun. 2019, 55, 12972–12975.
146. Lin, D.; Liu, X.; Huang, R.; Qi, W.; Su, R.; He, Z. One-pot synthesis of mercapto functionalized Zr-MOFs for the enhanced removal of Hg2+ ions from water. Chem. Commun. 2019, 55, 6775–6778.
147. Zhao, M.; Huang, Z.; Wang, S.; Zhang, L.; Zhou, Y. Design of l-Cysteine Functionalized UiO-66 MOFs for Selective Adsorption of Hg(II) in Aqueous Medium. ACS Appl. Mater. Interfaces 2019, 11, 46973–46983.
148. Liu, F.; Xiong, W.; Feng, X.; Cheng, G.; Shi, L.; Chen, D.; Zhang, Y. Highly recyclable cysteamine-modified acid-resistant MOFs for enhancing Hg (II) removal from water. Environ. Technol. 2019, 41, 1–11.
149. He, Y.; Hou, Y.-L.; Wong, Y.-L.; Xiao, R.; Li, M.-Q.; Hao, Z.; Huang, J.; Wang, L.; Zeller, M.; He, J.; et al. Improving stability against desolvation and mercury removal performance of Zr(iv)-carboxylate frameworks by using bulky sulfur functions. J. Mater. Chem. A 2017, 6, 1648–1654.
150. Chen, S.; Feng, F.; Li, S.; Li, X.-X.; Shu, L. Metal-organic framework DUT-67 (Zr) for adsorptive removal of trace Hg2+ and CH3Hg+ in water. Chem. Speciat. Bioavailab. 2018, 30, 99–106.
151. Liu, Q.; Zhang, Q.; Liu, B.; Ma, J. A new synthesis and adsorption mechanism of ZrO2 based metal-organic frames for efficient removal of mercury ions from aqueous solution. Ceram. Int. 2019, 45, 15720–15724.

152. Xiong, Y.Y.; Li, J.Q.; Le Gong, L.; Feng, X.F.; Na Meng, L.; Zhang, L.; Meng, P.P.; Luo, M.B.; Luo, F. Using MOF-74 for Hg2+ removal from ultra-low concentration aqueous solution. J. Solid State Chem. 2017, 246, 16–22.
153. Wang, C.-M.; Lin, Y.-J.; Pan, M.-F.; Su, C.-K.; Lin, T.-Y. A Highly Stable Framework of Crystalline Zinc Phosphite with Selective Removal, Recovery, and Turn-On Sensing Abilities for Mercury Cations in Aqueous Solutions. Chem. Eur. J. 2018, 24, 9729–9734.
154. Esrafili, L.; Gharib, M.; Morsali, A. The targeted design of dual-functional metal–organic frameworks (DF-MOFs) as highly efficient adsorbents for Hg2+ ions: Synthesis for purpose. Dalton Trans. 2019, 48, 17831–17839.
155. Wu, Y.; Xu, G.; Wei, F.; Song, Q.; Tang, T.; Wang, X.; Hu, Q. Determination of Hg (II) in tea and mushroom samples based on metal-organic frameworks as solid phase extraction sorbents. Microporous Mesoporous Mater. 2016, 235, 204–210.
156. Mon, M.; Qu, X.; Ferrando-Soria, J.; Pellicer-Carreño, I.; Sepúlveda-Escribano, A.; Ramos-Fernandez, E.V.; Jansen, J.C.; Armentano, D.; Pardo, E. Fine-tuning of the confined space in microporous metal–organic frameworks for efficient mercury removal. J. Mater. Chem. A 2017, 5, 20120–20125.
157. Yazdi, M.N.; Yamini, Y.; Asiabi, H.; Alizadeh, A. A metal organic framework prepared from benzene-1,3,5-tricarboxylic acid and copper(II), and functionalized with various polysulfides as a sorbent for selective sorption of trace amounts of heavy metal ions. Microchim. Acta 2018, 185, 525.
158. Xu, W.-Q.; Lin, C.-C.; Qiu, Y.-X.; He, S.; Jiang, T.; Liu, X.-J.; Xie, L.-J.; Fuhr, O.; Fenske, D.; Jiang, J.-J. A Recoverable Complex with Nitrogen-Rich Double Rings for Hg(II) Sorption. ChemistrySelect 2018, 3, 7592–7595.
159. Xu, W.-Q.; He, S.; Liu, S.-J.; Liu, X.-H.; Qiu, Y.-X.; Liu, W.-T.; Jiang, L.-C.; Jiang, J.-J. Post-synthetic modification of a metal-organic framework based on 5-aminoisophthalic acid for mercury sorption. Inorg. Chem. Commun. 2019, 108, 107515.
160. Liang, L.; Chen, Q.; Jiang, F.; Yuan, D.; Qian, J.; Lv, G.; Xue, H.; Liu, L.; Jiang, H.-L.; Hong, M. In situ large-scale construction of sulfur-functionalized metal–organic framework and its efficient removal of Hg(ii) from water. J. Mater. Chem. A 2016, 4, 15370–15374.
161. Jiang, S.-Y.; He, W.-W.; Li, S.-L.; Su, Z.-M.; Lan, Y.-Q. Introduction of Molecular Building Blocks to Improve the Stability of Metal–Organic Frameworks for Efficient Mercury Removal. Inorg. Chem. 2018, 57, 6118–6123.
162. Wang, C.; He, C.; Luo, Y.-H.; Su, S.; Wang, J.-Y.; Hong, D.-L.; He, X.-T.; Chen, C.; Sun, B.-W. Efficient mercury chloride capture by ultrathin 2D metal-organic framework nanosheets. Chem. Eng. J. 2020, 379, 122337.

163. Tian, J.; Shi, C.; Xiao, C.; Jiang, F.; Yuan, D.; Chen, Q.; Hong, M. Introduction of Flexibility into a Metal-Organic Framework to Promote Hg(II) Capture through Adaptive Deformation. Inorg. Chem. 2020, 59, 18264–18275.
164. Halder, S.; Mondal, J.; Ortega-Castro, J.; Frontera, A.; Roy, P. A Ni-based MOF for selective detection and removal of Hg2+ in aqueous medium: A facile strategy. Dalton Trans. 2017, 46, 1943–1950.
165. Li, G.-P.; Zhang, K.; Zhang, P.-F.; Liu, W.-N.; Tong, W.-Q.; Hou, L.; Wang, Y.-Y. Thiol-Functionalized Pores via Post-Synthesis Modification in a Metal-Organic Framework with Selective Removal of Hg(II) in Water. Inorg. Chem. 2019, 58, 3409–3415.
166. Li, K.; Li, J.-J.; Zhao, N.; Xie, T.-T.; Di, B.; Xu, L.-L. Thioether-based recyclable metal-organic frameworks for selective and efficient removal of Hg2+ from water. Dalton Trans. 2019, 48, 17800–17809.
167. Han, Y.; Zheng, H.; Liu, K.; Wang, H.; Huang, H.; Xie, L.-H.; Wang, L.; Li, J.-R. In-Situ Ligand Formation-Driven Preparation of a Heterometallic Metal-Organic Framework for Highly Selective Separation of Light Hydrocarbons and Efficient Mercury Adsorption. ACS Appl. Mater. Interfaces 2016, 8, 23331–23337.
168. Mon, M.; Lloret, F.; Ferrando-Soria, J.; Martí-Gastaldo, C.; Armentano, D.; Pardo, E. Selective and Efficient Removal of Mercury from Aqueous Media with the Highly Flexible Arms of a BioMOF. Angew. Chem. Int. Ed. 2016, 55, 11167–11172.
169. Saleem, H.; Rafique, U.; Davies, R.P. Investigations on post-synthetically modified UiO-66-NH2 for the adsorptive removal of heavy metal ions from aqueous solution. Microporous Mesoporous Mater. 2016, 221, 238–244.
170. Wu, J.; Zhou, J.; Zhang, S.; Alsaedi, A.; Hayat, T.; Li, J.; Song, Y. Efficient removal of metal contaminants by EDTA modified MOF from aqueous solutions. J. Colloid Interface Sci. 2019, 555, 403–412.
171. Rouhani, F.; Morsali, A. Fast and Selective Heavy Metal Removal by a Novel Metal-Organic Framework Designed with In-Situ Ligand Building Block Fabrication Bearing Free Nitrogen. Chem. A Eur. J. 2018, 24, 5529–5537.
172. Hakimifar, A.; Morsali, A. Urea-Based Metal-Organic Frameworks as High and Fast Adsorbent for Hg2+ and Pb2+ Removal from Water. Inorg. Chem. 2019, 58, 180–187.
173. Mon, M.; Bruno, R.; Tiburcio, E.; Viciano-Chumillas, M.; Kalinke, L.H.G.; Ferrando-Soria, J.; Armentano, D.; Pardo, E. Multivariate Metal-Organic Frameworks for the Simultaneous Capture of Organic and Inorganic Contaminants from Water. J. Am. Chem. Soc. 2019, 141, 13601–13609.
174. Ru, J.; Wang, X.; Wang, F.; Cui, X.; Du, X.; Lu, X. UiO series of metal-organic frameworks composites as advanced sorbents for the removal of heavy metal ions: Synthesis, applications

and adsorption mechanism. Ecotoxicol. Environ. Saf. 2021, 208, 111577.

175. Li, H.; Liu, H.; Zhang, J.; Cheng, Y.; Zhang, C.; Fei, X.; Xian, Y. Platinum Nanoparticle Encapsulated Metal-Organic Frameworks for Colorimetric Measurement and Facile Removal of Mercury(II). ACS Appl. Mater. Interfaces 2017, 9, 40716–40725.
176. Shi, M.; Lin, D.; Huang, R.; Qi, W.; Su, R.; He, Z. Construction of a Mercapto-Functionalized Zr-MOF/Melamine Sponge Composite for the Efficient Removal of Oils and Heavy Metal Ions from Water. Ind. Eng. Chem. Res. 2020, 59, 13220–13227.
177. Liu, F.; Xiong, W.; Feng, X.; Shi, L.; Chen, D.; Zhang, Y. A novel monolith ZnS-ZIF-8 adsorption material for ultraeffective Hg (II) capture from wastewater. J. Hazard. Mater. 2019, 367, 381–389.
178. Nosike, E.I.; Jiang, Z.; Miao, L.; Akakuru, O.U.; Yuan, B.; Wu, S.; Zhang, Y.; Zhang, Y.; Wu, A. A novel hybrid nanoadsorbent for effective Hg2+ adsorption based on zeolitic imidazolate framework (ZIF-90) assembled onto poly acrylic acid capped Fe3O4 nanoparticles and cysteine. J. Hazard. Mater. 2020, 392, 122288.
179. Huang, L.; He, M.; Chen, B.; Hu, B. A designable magnetic MOF composite and facile coordination-based post-synthetic strategy for the enhanced removal of Hg2+ from water. J. Mater. Chem. A 2015, 3, 11587–11595.
180. Liang, L.; Liu, L.; Jiang, F.; Liu, C.; Yuan, D.; Chen, Q.; Wu, D.; Jiang, H.-L.; Hong, M. Incorporation of In2S3 Nanoparticles into a Metal-Organic Framework for Ultrafast Removal of Hg from Water. Inorg. Chem. 2018, 57, 4891–4897.
181. Ke, F.; Jiang, J.; Li, Y.; Wan, X.; Ko, S. Highly selective removal of Hg 2+ and Pb2+ by thiol-functionalized Fe3O4@metal-organic framework core-shell magnetic microspheres. Appl. Surf. Sci. 2017, 413, 266–274.
182. Sun, D.T.; Peng, L.; Reeder, W.S.; Moosavi, S.M.; Tiana, D.; Britt, D.K.; Oveisi, E.; Queen, W.L. Rapid, Selective Heavy Metal Removal from Water by a Metal-Organic Framework/Polydopamine Composite. ACS Cent. Sci. 2018, 4, 349–356.
183. Abdollahi, N.; Akbar Razavi, S.A.; Morsali, A.; Hu, M.-L. High capacity Hg(II) and Pb(II) removal using MOF-based nanocomposite: Cooperative effects of pore functionalization and surface-charge modulation. J. Hazard. Mater. 2020, 387, 121667.
184. Liu, Y.; Li, H.; Liu, J. Theoretical prediction the removal of mercury from flue gas by MOFs. Fuel 2016, 184, 474–480.
185. Tang, H.; Fang, H.; Duan, Y.; Sholl, D.S. Predictions of Hg0 and HgCl2 Adsorption Properties in UiO-66 from Flue Gas Using Molecular Simulations. J. Phys. Chem. C 2019, 123, 5972–5979.
186. Zhao, S.; Mei, J.; Xu, H.; Liu, W.; Qu, Z.; Cui, Y.; Yan, N. Research of mercury removal from sintering flue gas of iron and steel by the open metal site of Mil-101(Cr). J. Hazard. Mater. 2018,

351, 301–307.

187. Dong, L.; Huang, Y.; Liu, L.; Liu, C.; Xu, L.; Zha, J.; Chen, H.; Liu, H. Investigation of Elemental Mercury Removal from Coal-Fired Boiler Flue Gas over MIL101-Cr. Energy Fuels 2019, 33, 8864–8875.
188. Chen, D.; Zhao, S.; Qu, Z.; Yan, N. Cu-BTC as a novel material for elemental mercury removal from sintering gas. Fuel 2018, 217, 297–305.
189. Zhou, J.; Cao, L.; Wang, Q.; Tariq, M.; Xue, Y.; Zhou, Z.; Sun, W.; Yang, J. Enhanced Hg0 removal via α-MnO2 anchored to MIL-96(Al). Appl. Surf. Sci. 2019, 483, 252–259.
190. Zhang, X.; Shi, Q.; Shen, B.; Hu, Z. MIL-100(Fe) supported Mn-based catalyst and its behavior in Hg0 removal from flue gas. J. Hazard. Mater. 2020, 381, 121003.
191. Yang, Z.; Li, H.; Yang, J.; Feng, S.; Liu, X.; Zhao, J.; Qu, W.; Li, P.; Feng, Y.; Lee, P.-H.; et al. Nanosized Copper Selenide Functionalized Zeolitic Imidazolate Framework-8 (CuSe/ZIF-8) for Efficient Immobilization of Gas-Phase Elemental Mercury. Adv. Funct. Mater. 2019, 29, 1807191.
192. Yang, J.; Zhu, W.; Qu, W.; Yang, Z.; Wang, J.; Zhang, M.; Li, H. Selenium Functionalized Metal–Organic Framework MIL-101 for Efficient and Permanent Sequestration of Mercury. Environ. Sci. Technol. 2019, 53, 2260–2268.
193. Zhao, S.; Chen, D.; Xu, H.; Mei, J.; Qu, Z.; Liu, P.; Cui, Y.; Yan, N. Combined effects of Ag and UiO-66 for removal of elemental mercury from flue gas. Chemosphere 2018, 197, 65–72.
194. Zhang, X.; Shen, B.; Shen, F.; Si, M.; Yuan, P. The behavior of the manganese-cerium loaded metal-organic framework in elemental mercury and NO removal from flue gas. Chem. Eng. J. 2017, 326, 551–560.
195. Rudd, N.D.; Wang, H.; Fuentes-Fernandez, E.M.A.; Teat, S.J.; Chen, F.; Hall, G.; Chabal, Y.J.; Li, J. Highly Efficient Luminescent Metal-Organic Framework for the Simultaneous Detection and Removal of Heavy Metals from Water. ACS Appl. Mater. Interfaces 2016, 8, 30294–30303.
196. Zhang, L.; Wang, J.; Du, T.; Zhang, W.; Zhu, W.; Yang, C.; Yue, T.; Sun, J.; Li, T.; Wang, J. NH2-MIL-53(Al) Metal–Organic Framework as the Smart Platform for Simultaneous High-Performance Detection and Removal of Hg2+. Inorg. Chem. 2019, 58, 12573–12581.
197. Radwan, A.; El-Sewify, I.M.; Shahat, A.; Azzazy, H.M.E.; Khalil, M.M.H.; El-Shahat, M.F. Multiuse Al-MOF Chemosensors for Visual Detection and Removal of Mercury Ions in Water and Skin-Whitening Cosmetics. ACS Sustain. Chem. Eng. 2020, 8, 15097–15107.
198. Shahat, A.; Elsalam, S.A.; Herrero-Martínez, J.M.; Simó-Alfonso, E.F.; Ramis-Ramos, G. Optical recognition and removal of Hg(II) using a new self-chemosensor based on a modified amino-functionalized Al-MOF. Sens. Actuators B Chem. 2017, 253, 164–172.

199. Esrafili, L.; Gharib, M.; Morsali, A. Selective detection and removal of mercury ions by dual-functionalized metal-organic frameworks: Design-for-purpose. New J. Chem. 2019, 43, 18079–18091.
200. Xiong, Y.; Su, L.; Yang, H.; Ye, F.; Zhang, P. Fabrication of copper sulfide using a Cu-based metal organic framework for the colorimetric determination and the efficient removal of Hg2+ in aqueous solutions. New J. Chem. 2015, 39, 9221–9227.
201. Moradi, E.; Rahimi, R.; Safarifard, V. Porphyrinic zirconium-based MOF with exposed pyrrole Lewis base site as an efficient fluorescence sensing for Hg2+ ions, DMF small molecule, and adsorption of Hg2+ ions from water solution. J. Solid State Chem. 2020, 286, 121277.
202. Yang, H.; Peng, C.; Han, J.; Song, Y.; Wang, L. Three-dimensional macroporous Carbon/Zr-2,5-dimercaptoterephthalic acid metal-organic frameworks nanocomposites for removal and detection of Hg(II). Sens. Actuators B Chem. 2020, 320, 128447.
203. Shellaiah, M.; Thirumalaivasan, N.; Sun, K.W.; Wu, S.-P. A pH cooperative strategy for enhanced colorimetric sensing of Cr(III) ions using biocompatible L-glutamic acid stabilized gold nanoparticles. Microchem. J. 2021, 160, 105754.
204. Shellaiah, M.; Simon, T.; Thirumalaivasan, N.; Sun, K.W.; Ko, F.-H.; Wu, S.-P. Cysteamine-capped gold-copper nanoclusters for fluorometric determination and imaging of chromium(VI) and dopamine. Microchim. Acta 2019, 186, 788.
205. Shellaiah, M.; Chen, Y.-C.; Simon, T.; Li, L.-C.; Sun, K.W.; Ko, F.-H. Effect of Metal Ions on Hybrid Graphite-Diamond Nanowire Growth: Conductivity Measurements from a Single Nanowire Device. Nanomaterials 2019, 9, 415.
206. Shellaiah, M.; Sun, K.W. Review on Nanomaterial-Based Melamine Detection. Chemosensors 2019, 7, 9.
207. He, J.; Wu, X.; Long, Z.; Hou, X. Fast and sensitive fluorescent and visual sensing of cysteine using Hg-metalated PCN-222. Microchem. J. 2019, 145, 68–73.

Retrieved from https://encyclopedia.pub/entry/history/show/27211